Cape Peninsula
University of Technology

STRUCTURAL OPTIMISATION OF A LOWER LIMB EXOSKELETON FOR HUMAN LOCOMOTION ASSISTANCE

by

NICLA KABILA

Thesis 100% research project submitted in fulfilment of the requirements for the degree

Master of Engineering: Mechanical Engineering

in the Faculty of Engineering and the Built Environment

at the Cape Peninsula University of Technology

Supervisor: Mr Michael Petersen

Co-supervisor: Prof. Graeme Oliver

Bellville
3 December 2025

DECLARATION

I, Nicla Kabila, declare that the contents of this thesis represent my own unaided work, and that the thesis has not previously been submitted for academic examination towards any qualification. Furthermore, it represents my own opinions and not necessarily those of the Cape Peninsula University of Technology.

Signed  **Date** 3 March 2026

ABSTRACT

This thesis looks at the structural optimisation of a Lower Limb Exoskeleton (LLE) used for human locomotion assistance. An LLE is a wearable robotic device used to assist individuals with mobility impairment to walk, particularly individuals suffering from lower limb paraplegia due to strokes, spinal cord injury, etc. Research shows that LLEs are relatively heavy and as a result, are inefficient and not easy to transport. A high cost is also associated with designing, testing and manufacturing an LLE. Consequently, only a few LLEs have been commercialised, and wheelchairs remain the most efficient and affordable form of locomotion. This paper aims to optimise an LLE structure by reducing its weight while maintaining structural integrity. The thesis focuses on investigating alternative materials with a high strength-to-weight ratio and optimum structural design and profile. This will be done through the simulation of 3D models using the different forces acting on the structure at various phases of gait. This paper provides a background to the problem, followed by research questions, objectives, delineation of the research, significance of research and expected outcomes. The literature review explores the general design of existing LLE, materials, topology, manufacturing processes and structural analysis methods for LLE structures. Thereafter, methodologies are presented, along with the results and their discussions. The paper finishes with conclusions and future recommendations.

ACKNOWLEDGEMENTS

I want to thank my supervisor, Mr Petersen, for his patience and continued support over the years. Thank you for believing in me when I strongly doubted myself.

Thank you to my co-supervisor, Prof Oliver, CPUT and the Mechanical Engineering department.

To my friends Jessica Shihlomulo and Valery Mukengere, thank you for always encouraging me.

À ma mère Nana Kabila-Nkulu, mes sœurs et à toute ma famille, je vous aime profondément.

To God be the Glory.

CONTENTS

DECLARATION 2
ABSTRACT 3
ACKNOWLEDGEMENTS 4
CONTENTS 5
LIST OF FIGURES 8
LIST OF TABLES 10
LIST OF ABBREVIATIONS AND ACRONYMS 11
GLOSSARY 11
KEY WORDS 11
1. INTRODUCTION 12
1.1. Background 12
1.2. Problem Statement 14
1.3. Research Question 14
1.4. Research Objectives 15
1.5. Delineation of research 15
1.6. Significance of research 16
1.7. Expected outcomes 16
1.8. Chapter Outline 17
2. LITERATURE REVIEW 18
2.1. General Design 18
2.1.1. Gait support 19
2.1.2. Joints and Actuator 20
2.1.3. Performance and Evaluation 21
2.1.4. Safety 22
2.2. Materials 25
2.2.1. Aluminium 26
2.2.2. Titanium 27

2.2.3. Magnesium 28
2.2.4. Composite Materials 30
2.2.5. Polymers 31
2.3. Topology 34
2.4. Manufacturing Processes 37
2.4.1. Subtractive Manufacturing 37
2.4.2. Additive manufacturing 38
2.4.3. Manufacturing Process of Existing LLEs 38
2.5. Structural Analysis and Evaluations 39
2.5.1. Lower Limb Fitness Exoskeleton 41
2.5.2. Modular Wearable LLE Rehabilitation Robot 43
2.6. Summary of Findings 45
3. METHODOLOGY 46
3.1. Current Structure Design 47
3.2. Input Forces 50
3.2.1. Stance Phase Analysis 52
3.2.2. Swing phase analysis 57
3.3. Material Selection 60
3.3.1. Identifying Candidate Materials 61
3.3.2. Material Performance Index 61
3.4. Stress Analysis 65
3.4.1. FEA Model 65
3.5. Topology Optimisation 73
3.5.1. FEA Model 73
3.5.2. Topology Refinement 75
3.6. Manufacturing Process 75
3.6.1. Carbon Reinforced Fibre Composite 76
3.6.2. Aluminium 77

3.6.3. Titanium 79
4. RESULTS 82
4.1. Stress Analysis 82
4.1.1. Waist Bracket 83
4.1.2. Thigh Link 84
4.1.3. Shank Link 86
4.2. Topology Optimisation 87
4.2.1. Thigh Link 88
4.2.2. Shank Link 90
4.2.3. Topology Refinement 92
4.3. New Weight and Gait Force Results 95
5. DISCUSSION 97
5.1. Thigh Link ..... **Error! Bookmark not defined.**
5.2. Shank Link ..... **Error! Bookmark not defined.**
5.3. Refined Topology 98
5.4. Manufacturing Process 99
5.5. Carbon Fibre Reinforced Composites ..... **Error! Bookmark not defined.**
6. CONCLUSION 102
7. RECOMMENDATIONS 103
8. REFERENCES 105
Appendix A: FEA Model Set Up 113
Appendix B: Topology optimisation model set up 122
Appendix C: Current LLE Structure 124
Appendix D: Optimised and Refined Links 126

LIST OF FIGURES

Figure 1: ATALANTE exoskeleton at the Paris 2024 Olympics (Nelson, 2024) 18
Figure 2: Rex exoskeleton (Rupal, et al., 2017)..... 20
Figure 3: Ekso exoskeletons; ReWalk exoskeletons (Rupal, et al., 2017) 23
Figure 4: HAL-ML05 exoskeleton (Rupal, et al., 2017)..... 26
Figure 5: Mindwalker exoskeleton (Wang, 2015)..... 28
Figure 6: Indego exoskeleton (Rupal, et al., 2017)..... 31
Figure 7:Initial custom fit LLE structure design (Liu, et al., 2021) 35
Figure 8: Thigh Link topology optimisation remodelling (Liu, et al., 2021)..... 35
Figure 9: Lower Limb fitness exoskeleton device (Duan, et al., 2023)..... 41
Figure 10: Angular motion vs time graph; Force vs time graph of knee joint (Duan, et al., 2023) 42
Figure 11: Modular wearable lower limb exoskeleton rehabilitation robot (Liang, et al., 2025) 43
Figure 12: Length adjustable thigh link (Liang, et al., 2025) 43
Figure 13: Load application on robot structure during gait phase posture (Liang, et al., 2025) 44
Figure 14: FEA stress and strain results could map (Liang, et al., 2025)..... 44
Figure 15: Methodology layout..... 46
Figure 16: Initial Lower Limb Exoskeleton design..... 47
Figure 17: Initial Shank Link Design..... 48
Figure 18: Initial Thigh Link Design..... 48
Figure 19: Waist bracket design..... 49
Figure 20: Human Transverse, Frontal & Sagittal plane (Vaughan et al., 1992) 50
Figure 21: Gait cycle phases (Vaughan et al., 1992)..... 52
Figure 22: Ground reaction X, Y and Z forces (Vaverka et al., 2015) 53
Figure 23: Vertical Ground Reaction Force vs. Gait Cycle (Al-Hayali et al., 2021)..... 54
Figure 24: Vertical Ground Reaction Force as body weight percentage (Barela et al., 2014) 54
Figure 25: Graph of vertical ground reaction input forces through stance phase 56
Figure 26: Double pendulum free body diagram (Assencio, 2014)..... 57
Figure 27: Graph of input torque through swing phase..... 59
Figure 28: Strength vs Density (Ashby, 2020)..... 61
Figure 29: Waist bracket, thigh and shank link reference point location 68
Figure 30:Waist bracket, thigh and shank link fixed boundary condition location..... 69
Figure 31:Waist bracket, thigh and shank link load application..... 69

Figure 32: Amplitude load set up for Shank Link 71
Figure 33: Amplitude load set up for Waist Bracket and Thigh Link 71
Figure 34: FEA model mesh 72
Figure 35: Waist Bracket Material FEA Results 83
Figure 36: Thigh Link FEA Results 85
Figure 37: Shank Link FEA Results 86
Figure 38: Thigh Link Aluminium Topology Optimisation Results 88
Figure 39:Thigh Link Titanium Topology Optimisation Results 89
Figure 40: Shank Link Aluminium Topology Optimisation Results 90
Figure 41: Shank Link Titanium Topology Optimisation Results 91
Figure 42: Topology Optimisation Incomplete Features 93
Figure 43:Refined Topology Optimisation 93
Figure 44: Refined Model FEA Results 94
Figure 45: Force vs swing phase graph 96
Figure 46: Force Through Stance Phase graph 97
Figure 47: Abaqus material property set up 113
Figure 48: Abaqus material section set up 114
Figure 49: Abaqus interaction 114
Figure 50: Abaqus boundary conditions 115
Figure 51: Abaqus loads 116
Figure 52: Abaqus seeding 117
Figure 53: Abaqus mesh controls 117
Figure 54: Abaqus element type 118
Figure 55: Thigh link meshing 119
Figure 56: Waist bracket mesh 120
Figure 57: Shank link meshing 121
Figure 58: Optimisation task 122
Figure 59: Abaqus design response 122
Figure 60: Abaqus objective function 123
Figure 61: Abaqus constraint 123
Figure 62: Current LLE 3D CAD drawing 124
Figure 63: 2D drawing of the original LLE structure 125
Figure 64: 3D CAD drawing of optimised and refined thigh link 126
Figure 65: 3D CAD drawing of optimised and refined thigh link 127
Figure 66: 3D drawing of optimised and refined shank link 128
Figure 67: 2D drawing of optimised and refined shank link 129

LIST OF TABLES

Table 1: Popular Lower limb exoskeleton specs (Hussain et al., 2021) (Rupal et al., 2017) (Arunkumar et al., 2024) 24
Table 2: Popular lower limb Exoskeleton Design Features (Arunkumar et al., 2024) (Hussain et al., 2021) (Rupal et al., 2017) 36
Table 3: Weight of current LLE structure 49
Table 4: Stance phase ground reaction input forces 55
Table 5: Swing phase analysis input data 58
Table 6: Swing phase input forces per joint 59
Table 7: Material performance matrix 63
Table 8: Material Specs 67
Table 9: Step Settings 67
Table 10: Structure weight change 92
Table 11: Weight Reduction Results 95

LIST OF ABBREVIATIONS AND ACRONYMS

LLE	(Abbreviation) Lower Limb Exoskeleton.
SCI	(Abbreviation) Spinal Cord Injury
PI	(Abbreviation) Performance Indicator
SAQA	(Acronym) South African Quadriplegia Association
FDA	(Abbreviation) Food and Drug Administration (USA)
DOF	(Abbreviation) Degrees of freedom
CFRC	(Abbreviation) Carbon Fibre Reinforced Composites

GLOSSARY

Lower Limb Exoskeleton:	A wearable robotic device used to assist individuals with mobility impairment to walk, and or augment the strength of healthy individuals to perform load-bearing tasks.
Locomotion assistance:	To aid an individual with walking and other related activities, such as sitting, standing, etc.
Exoskeleton structure:	The frame of a lower limb robot, commonly composed of thigh and shank segments, and a joint mechanism. The structure is responsible for transmitting forces from the actuators to the interface attachment components of the exoskeleton.
Gait:	The manner or rhythm of walking.
Soft exoskeleton:	A wearable robotic device which makes use of “soft”/flexible materials to interface with the wearer’s body.

KEY WORDS

Lower Limb Exoskeleton, Human locomotion assistance, Lower Limb Exoskeleton structure, Gait, Specific strength, Structure design, Mechanical design, Topology Optimisation, Material Selection, Weight reduction

1. INTRODUCTION

This thesis aims to optimise a locomotion assistance lower limb exoskeleton (LLE) through weight reduction of its structure/frame. This will be done through material selection, which entails investigating high-specific-strength materials and running stress analysis. Topology optimisation will be used to obtain the optimum shape and profile of the structure, which allows for increased strength using minimum material.

1.1. Background

The South African province of Gauteng has one of the highest rates of trauma-induced spinal cord injuries (SCI) due to assault. SCI is a condition where the spinal cord is damaged, destroying the patient's motor and sensory function, leaving them with some form of paralysis/mobility impairment. SCI can be induced by trauma or disease, which is known as traumatic SCI (TSCI) or non-traumatic SCI (NTSCI). A study by Alves (2023) found that gunshot wounds and motor vehicle accidents were the leading causes of TSCI in Gauteng. The number one cause of NTSCI was infectious diseases, among which HIV played a significant role. In 2009, the Quadriplegia Association of South Africa (QASA) represented approximately 50,000 individuals who suffered mobility disorders (Joseph et al., 2017). Globally, incidences of TSCI are estimated between 10.5 and 23 cases per 100,000 population. NTSCI incidences are estimated to range between 0.6 and 6.8 per 100,000 (Alves et al., 2023).

Individuals with mobility disorders struggle to access public facilities such as public transport and recreational services. This excludes them from the job market and promotes social separation (Joseph et al., 2017). Being restricted to a sedentary lifestyle and lack of physical activity causes patients to develop severe secondary health conditions, such as depression, muscle atrophy, cardiovascular complications, and bowel/bladder dysfunction. This can further reduce the patients' life expectancy (Rodriguez-Fernandez et al., 2021). 69% of SCI patients in South Africa are from previously disadvantaged backgrounds. They also often face discrimination within their communities, which has a further negative impact on their standard of living and mental health (Alves et al., 2023). A study by Joseph (2017) found that some of the core needs of patients with SCI are to be seen as equals in society, to contribute to society, and have rights and responsibilities in their communities.

Over the past few decades, the field of wearable exoskeletons has made significant progress in supporting the walking function for individuals with neuromuscular impairments (Rodriguez-Fernandez et al., 2021). A Lower Limb Exoskeleton (LLE) is a wearable robotic device which helps humans perform specific tasks. These devices can be categorised into two groups, i.e.

medical and non-medical. Non-medical exoskeletons perform the function of strength augmentation by assisting able-bodied individuals to perform heavy lifting tasks or activities that require a high amount of human strength (Rupal et al., 2017). Such LLEs are commonly used in the military, for emergency workers such as firefighters, and industrial labourers who perform heavy lifting tasks (Flora-Unda et al., 2023).

Medical exoskeletons can be subdivided into two groups, namely gait rehabilitation or locomotion assistance. Gait rehabilitation LLEs are designed to aid the rehabilitation process of patients with mobility disorders caused by strokes, accidents or other ailments. Mainly used in medical facilities, these LLEs assist patients in regaining lower limb motor function and walking abilities (Rupal et al., 2017). This also releases the heavy burden on therapists and professional healthcare workers from traditional physical therapy (Chen et al., 2016).

This paper will focus on the Locomotion Assistance LLE, a device designed to assist paraplegic patients who have lost lower limb motor function due to spinal cord injury, stroke, cerebral palsy or other neurological disorders (Sanchez-Villamañan et al., 2019). Paraplegic patients suffer from lower limb paralysis, which is an inability in the sensory-motor functionality of the lower limbs, inhibiting normal motion. The purpose of this wearable robot is to help such patients walk and do other basic activities, such as sit, stand, and climb stairs. Locomotion assistance exoskeletons can improve the user's quality of life and provide a greater sense of independence than that which comes from the use of a wheelchair. Wheelchairs fail to provide full motion autonomy and therefore have limited use (Rupal et al., 2017). Although there is still no cure for SCI, wearable exoskeletons offer patients the opportunity for increased social and environmental engagement, which improves quality of life. Participating in physical activity through regular use of a LLE can improve blood circulation, bowel and bladder function and prevent muscle atrophy. There are also many psychological and social benefits associated with standing, including improved self-image and reduced depression. All this aids in reducing the risk of secondary health conditions (Rodriguez-Fernandez et al., 2021).

Although significant developments have been made in the design of locomotion assistance LLEs, there are still many shortcomings:

- Most developed locomotion assistance LLE structures are large and bulky, which makes them difficult to transport (Huo et al., 2016)
- Large power sources and electric actuators are required to power both the patient and the robot. Consequently, the devices are relatively heavy, inefficient and can only operate for a few hours at a time (Zouh et al., 2025)
- Balance capabilities of wearable exoskeletons still require much development to ensure user safety and reliability (Rodriguez-Fernandez et al., 2021).

- The complexity of these mechanical structures generally requires a team to support fitting into, as well as turning the device on and off (Annon, 2016).
- Wearable exoskeletons are intended to be used as assistive devices in daily living activities such as climbing stairs, walking on different surfaces, entering cars and side stepping; however, these functions are poorly covered by current exoskeletons. Most LLE can only support simple forward walking on flat surfaces (Pinto-Fernandez et al., 2020).
- Additionally, joint misalignment is still an issue in current exoskeletons, which may increase metabolic cost and discomfort for the wearer, leading to skin abrasions, ulcers and an increased risk of fractures (Yang et al., 2024)
- Finally, the cost of wearable exoskeletons for personal use must be reduced. Their exorbitant price makes them inaccessible to the general population (Rupal et al., 2017).

1.2. Problem Statement

Modern locomotion assistance LLEs are inefficient and difficult to transport (Chen et al., 2016) The structures are mostly made of standard aluminium alloy profiles and are relatively heavy, weighing up to 80kg. (Liu et al., 2021) (Hussain et al., 2021). Consequently, large power packs and high motor torque are required to drive the structure (Rupal et al., 2017) and battery life is limited to one to two hours, reducing the level of independence the patient has (Zouh et al., 2025) (Sanchez-Villamañan et al., 2019).

1.3. Research Question

- What impact will the weight reduction of an LLE have on the maximum motor torque requirement, strength, deflection and factor of safety?
- Which materials can be used for the structure to provide a good weight-to-strength ratio?
- Will reducing the overall weight of an LLE structure reduce the required motor torque to operate it.
- How can the design of LLE structures be modified to reduce weight while maintaining structural integrity?

1.4. Research Objectives

- Design an LLE, using a 3D drawing software.
- Determine suitable alternative materials for the structure of the LLE.
- Select the most suitable material.
- Optimise the shape/profile of the structure and establish the optimum geometry.
- Conduct stress analysis simulations of the structure under the different external loads.

1.5. Delineation of research

- This research will only look at the weight reduction of a locomotion assistance lower limb exoskeleton. Other types of exoskeletons, such as gait rehabilitation and strength augmentation, will not be considered.
- The paper will look at straight line forward walking only. Other activities such as sitting, climbing stairs or squatting, will not be considered.
- Improving the stability and balance of LLEs will not be considered in this research.
- There will be no human participation in this research
- Only the structure of the LLE will be optimised. The power pack, actuation and control system will not be considered.
- All the work in this research will be computer simulation based. No physical prototype models will be built; therefore, no budget is required to complete this research.

1.6. Significance of research

Much work has been put into making exoskeletons safer, more efficient and more affordable. Having access to an LLE can improve the standard of living for paraplegic patients. Regaining a degree of independence through walking with the aid of an exoskeleton can have a positive impact on their mental health. Traditionally, patients suffering from paraplegia make use of wheelchairs as a means of locomotion. Wheelchairs however come with their own advantages and disadvantages. One of the pros of wheelchairs is that they are affordable, commercialised and easily accessible. However, the disadvantages are that wheelchairs are only practical on relatively flat surfaces, limiting the mobility of the user to wheelchair friendly environments (Annon, 2016). There is a high financial cost associated with making an environment wheelchair accessible. Lastly, wheelchair usage results in prolonged sitting which negatively impacts health (Rupal et al., 2017).

This makes a well-functioning locomotion assistance LLE a more attractive solution. The exoskeleton requires less cost to adapt to the user's environment. It provides the user with mobility independence which is a big factor in improved mental health and quality of life. Lastly, the gait motion replicated is a form of exercise which can help prevent secondary illness (Rupal et al., 2017). Unfortunately, only a few LLEs have been commercialised, but even those robots are inefficient. They are heavy with large power packs and can only be used for 1 to 2 hours. This research paper aims to contribute to the robotics community with knowledge on how to manufacture a lighter weight LLE structure. This could assist researchers and institutions in manufacturing lighter robots, leading to lower energy requirements and improved efficiency.

1.7. Expected outcomes

From this research, the following can be expected: 3D model drawing of a lower limb exoskeleton structure with weights for each component. Force input data for FEA based on human gait analysis to determine the loads acting on the structure. Selection of the optimum material through stress analysis and the most suitable manufacturing method. Optimised, lighter LLE model topology using Abaqus topology optimisation feature.

1.8. Chapter Outline

Chapter 1 Introduction: This chapter introduces the subject of this thesis and motivation for the study, it outlines the research problem, objectives, research questions, and defines the scope and significance of the investigation.

Chapter 2 Literature Review: A comprehensive review of existing LLE designs, materials, manufacturing methods, and structural evaluation techniques. It highlights current limitations and identifies opportunities for weight reduction through material selection and topology optimisation.

Chapter 3 Methodology: Details the approach used to analyse and improve the structural design of the LLE. It includes the current design assessment, input force analysis, material selection criteria, and the setup of finite element analysis using Abaqus.

Chapter 4 Results: Presents the outcomes of simulations and analyses, including weight comparisons, stress distributions, and performance metrics. The results demonstrate the impact of material and design changes on structural performance.

Chapter 5 Discussion: Interprets the findings in relation to the research objectives. It discusses the implications of weight reduction on usability, performance and manufacturability. It evaluates the trade-offs involved in material and topology design choices.

Chapter 6 Conclusion & Recommendations: Summarises the key insights gained from the study, reflects on its contributions to the field, and offers recommendations for future research and development in lightweight exoskeleton design.

2. LITERATURE REVIEW

In this section, the general designs of existing LLEs are reviewed, followed by a discussion of materials suitable for the production of LLE structures. The topology of LLE structures and their manufacturing processes are analysed. Lastly, the structure analysis methods used to evaluate LLE frames are discussed. The focus is on seven of the most popular medical exoskeletons for paraplegic patients. Six of these devices have already been approved by the United States Food & Drug Administration (FDA) and are commercially available, i.e. Ekso, HAL, Indego, REX, ReWalk and ATALANTE.

2.1. General Design

Although many LLEs have been commercialised, many are still under development (Chang et al., 2015). The Vanderbilt Exoskeleton was developed and prototyped over a span of ten years at Vanderbilt University. It is now commercialised as Indego and was the second LLE to gain FDA approval. ReWalk, the first exoskeleton to gain FDA approval, was developed in Israel. The French-designed LLE, ATALANTE, recently made an appearance at the Paris 2024 Olympics, assisting paraplegic tennis player Kevin Piette carry the relay torch. Refer to Figure 1. (Nelson, 2024). In 2018, a nine-month-long clinical trial of the US developed Ekso suit was conducted at the University of Cape Town (Sicetsha, 2018). Japanese company Cyberdyne developed HAL-ML05, the first LLE to use bio-electric signals from the patient's skin to direct movement (Chang et al., 2015). New Zealand robot Rex was the first commercialised LLE to provide full-body support without the requirement for additional walking aids. Mindwalker, a European Union-commissioned project, is one of many LLEs yet to be commercialised (Rupal et al., 2017).

Figure 1: ATALANTE exoskeleton at the Paris 2024 Olympics (Nelson, 2024)

These autonomous bipedal exoskeletons all utilise rechargeable batteries to drive the hip and knee joint motors and were designed for patients with lower limb paralysis. They have compliant actuators and rigid structures, composed of mechanical links and transmission mechanisms placed in parallel with the user's limbs (Sanchez-Villamañan et al., 2019). It is important to note that these LLEs are expensive. ReWalk, the more affordable of the six commercialised LLEs, was retailing for ±$70k (± R1.27 million) while Rex LLE peaked at $150k (± R2.7 million) in 2017. HAL-ML05 provides a rental option for the device at ± $1950 per month (± R35k/month). This makes these devices inaccessible to most paraplegic patients (Rupal et al., 2017) (Annon, 2016).

From the locomotion assistance LLEs in Table 1, we obtain an average weight of 31kg. The heaviest of all LLEs is ATALANTE. This 80kg robot is exclusively used for SCI patients. Rex closely follows at 38kg. Indego weighs significantly less at only 12kg. Some notable contributing factors to the weight of an LLE are. The number of actuated joints and degrees of freedom, the type of battery/power source, the actuators being used, and the material and profile of the structure. Overall, there is a strong correlation between weight and the type of mobility impairments an LLE has been designed to cater to. Locomotion assistance exoskeletons used for SCI patients have the highest mean weight, compared to LLEs used for patients with other types of mobility impairments. The average weight of exoskeletons used by stroke patients and patients with other pathologies is 9kg. Note that added loads in the legs increase net metabolic cost (Rodriguez-Fernandez et al., 2021) (Annon, 2016).

2.1.1. Gait support

SCI lower limb paraplegia is associated with balance disorders, and despite immense technological advances, supervision from clinical staff is nearly always required as balance remains one of the key areas of development for LLEs. A common trend observed was that most locomotion assistance LLEs require walking aids, such as crutches, in conjunction with support from clinical staff (Shi et al., 2019). ReWalk, Ekso, Indego and HAL-ML05 all require the use of crutches to support gait. This limits the user's independence and mobility. Additionally, prolonged use of crutches may lead to shoulder pain. During ReWalk clinical trials, several participants emphasised the effort exerted with the arms while using the exoskeleton (Chang et al., 2015).

Aside from reducing the risk of falls, crutches can also serve as a feedback tool to guide motion (Sanchez-Villamañan et al., 2019). Sensors are placed on the crutches to detect motion and the intended direction of the user. These signals are sent back to the LLE robot, which subsequently moves in the signalled direction (Rodríguez-Fernández, 2021).

Mindwalker, on the other hand, utilises handrails to support the wearer. LLEs like ATALANTE and Rex have overcome the need for crutches as they have been designed to support patients with complete SCI. They can be operated from a simple handheld joystick. Refer to Figure 2. The downside to this full-body support system is that the robot requires a larger, bulkier, and significantly heavier structure than other LLEs. ATALANTE, for example, weighs almost four times more than its crutch-using counterparts. (Ning et al., 2016)

2.1.2. Joints and Actuator

Actuators contribute significantly to the weight of an LLE; hence, selecting the correct actuator is a key part of the design. An actuator with a high power-to-weight ratio is preferred. Electric actuators are approximately twice the weight of hydraulic actuators. Electric actuators are, however, 92% more effective than hydraulic ones. (Zouh et al., 2025) (Hussain et al., 2021).

The most common type of actuator used for LLE is the electric motor, as it is easy to control and exhibits high precision with high specific power. A study by Rodríguez Fernández (2021) found that 22 out of the 25 exoskeletons used electric actuators, and only three of the reviewed exoskeletons used hydraulic or pneumatic actuators. Pneumatic actuators are preferred for soft LLE and non-ambulatory gait rehabilitation LLEs (Tian et al., 2025) (Shi et al., 2019).

LLEs are commonly designed with one to three degrees of freedom (DOF) in the sagittal plane per leg; this excludes REX, which allows movement in the transverse and frontal planes. The most common number of DOF per leg is two. All 7 LLEs in Table 1 make use of electric actuators, and all but one exoskeleton (Rex) has two actuated joints per leg. A relationship exists between heavier LLE and an increased number of active joints and DOF (Arunkumar et al., 2024).

Figure 2: Rex exoskeleton (Rupal, et al., 2017)

Making use of the same actuator for different active DOF is common practice when designing LLEs. This modular application is cost-saving and simplifies the development and

manufacturing processes of LLEs. Although facilitating the mechanical design, this practice commonly yields oversized actuators, which negatively impact the overall weight and efficiency of the LLE. One promising solution is the application of modularity only on the actuation principle and optimising the actuator design for the operator's specific torque requirements for a particular joint. This means a more compact, customised and personalised actuator designed for the joint and patient-specific torque requirements. The result could be a more efficient and lightweight solution. (Sanchez-Villamañan et al., 2019).

Regarding the power supply, although the battery life of these devices varies between two and six hours, the robot's operating time is only between one and two continuous hours. The battery/power pack can account for anything between 6% and 20% of the LLE's weight. (Rodríguez-Fernández, 2021)

2.1.3. Performance and Evaluation

To determine if a modification made to the design of an LLE has a positive impact, one must be able to effectively evaluate its performance. Unfortunately, there is currently a lack of technical information and no formally agreed-upon standards, procedures or benchmarking methodology for performance evaluation in the LLE robotics community (Pinto-Fernandez et al., 2020). Common practice is to compare exoskeleton performance through competitions. Following a review of 187 publications, Pinto-Fernandez (2020) reveals that the two main factors to consider in the performance evaluation are the motor skill being evaluated and the performance indicator (PI).

Flat ground walking was the most evaluated motor skill, followed by sitting, standing and climbing stairs. The PIs most frequently used to assess different motor skills are, minimum motor task execution time and maximum distance covered when performing a task. In flat ground clinical trials, time is commonly measured by conducting a 10 meter walking test (10MWT) or 6 minute walking test (6MWT). These PIs alone are considered insufficient to validate or quantify the performance. Though a critical PI, stability has often been neglected in trials (Chang et al., 2015). Other common performance indicators used for evaluating LLEs are:

- Kinetics, a measure of global torques, global forces, global power and ground reaction forces (GRF) (Pinto-Fernandez et al., 2020).

- Metabolic cost, which refers to the amount of physical energy the wearer uses when performing a task. In this category, heart rate, oxygen consumption, and carbon dioxide production were common PIs (Arunkumar et al., 2024).

- Comfort: An important PI can be measured based on the user's perception of the human-robot interaction. User's subjective perception of comfort has unfortunately been excluded from evaluation studies (Sanchez-Villamañan et al., 2019). PIs found that the most relevant for comfort were pain scales, clinical questionnaires, and satisfaction scales, which are more challenging to measure in patients suffering from paraplegia. (Pinto-Fernandez et al., 2020).

Only a few studies have assessed physiological improvements or improvements related to secondary health conditions. For example, Baunsgaard (2017) was one of a few studies that analysed quality of life. They measured bowel/ bladder function as well as levels of depression. Some sources suggest that LLE developments should focus more on health benefits and preventing secondary health conditions than robot performance, as LLE usage will not result in improved patient gait. (Baunsgaard et al., 2017)

2.1.4. Safety

Safety is the primary criterion for any wearable robot, given the unavoidable physical contact between humans and robots. If safety is not evident, the performance of all other technical functions becomes irrelevant, and commercialisation is impossible. Ekso and ReWalk exoskeletons present the broadest range of injuries with the largest number of patients. This is because far more studies and clinical trials have been conducted on these robotic devices. Safety can be challenging to measure in paraplegic patients, hence common hazards associated with LLE are, falls, bruising or skin abrasions, and in some severe cases, damage to joints. (Rodríguez-Fernández, 2021) (Nasr et al., 2024)

Falling is a serious safety concern, and stability remains a big issue for LLEs. This is evident in clinical trials, highlighting the need for effective control programs and robust, sturdy structures. A strong structure manufactured from compliant materials provides a safe and ergonomic experience for the user. (Hussain et al., 2021). Although there is no set standard on factors of safety, ISO standard for lower limb prosthetics and wearable robotic devices are expected to carry well above it bearing load. Common practice among designers is working to a FOS between 2 and 4. (Thesleff, 2021)

Skin abrasion is a common issue associated with the prolonged use of an LLE, as well as crutches. An important symptom to look for as an indication of pain is not always clear. This is often addressed with padding around the user attachment components. It is also important that the robot structure is adjustable to the user's height and overall body proportions. In a study by Van Herpen (2019), the authors reported two cases of bone fractures that occurred

during training with LLEs. Mechanical lock mechanisms that prevent the robot's motion from exceeding the user's motion range are also critical. (Van Herpen et al., 2019)

Damage to joints can occur due to the close interaction between the exoskeleton and the wearer. Many exoskeletons have been designed with the principle of replicating the human lower limb structure as closely as possible. However, the mechanical designs of exoskeletons are relatively simple compared to the complex mechanics of human lower limbs, which results in a motion mismatch between the device and the wearer. This mismatch is mainly caused by misalignment between the joint axis of the LLE and that of the wearer's lower limbs. Furthermore, this could lead to serious injuries and augments the risk of bone fractures. (Shi et al., 2019) (Yang et al., 2024).

It is therefore necessary for exoskeletons to be adjustable and adapt to the wearer's anthropometry. A proposed solution to addressing the issue of axis misalignment is the simple concept of adding passive degrees of freedom into LLEs and by doing so, obtaining an axis alignment free design. According to Sanchez-Villamañan (2019) this is the most effective solutions. However, this solution increases the weight, friction and inertia of the device, which in turn increases metabolic cost of the wearer and can therefore not be worn for long periods of time. (Poggensee et al., 2024)

International safety regulation standards IEC SC62D and ISO TC299 JWG36 have been recently published for the design and function of LLEs. These aid designers meet standards which lead to commercialisation. These regulations are still shortcoming and require more development from the LLE community. It is crucial for researchers and industry to design and manufacture LLE robots that comply with these safety regulations to ensure successful commercialisation (Rupal et al., 2017).

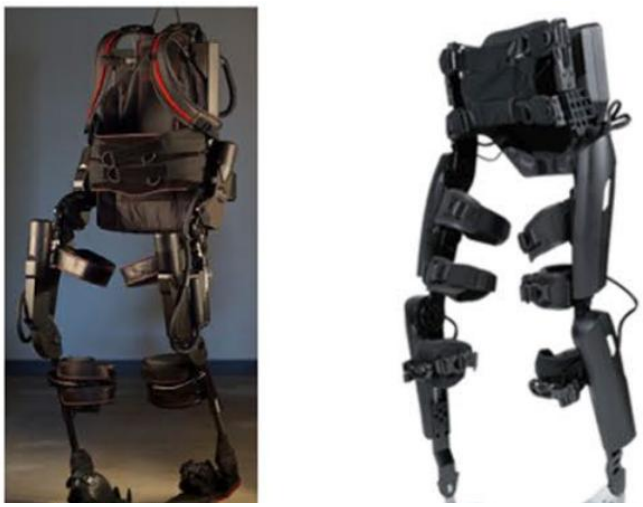

Figure 3: Ekso exoskeletons; ReWalk exoskeletons (Rupal, et al., 2017)

Table 1: Popular Lower limb exoskeleton specs *(Hussain et al., 2021) (Rupal et al., 2017) (Arunkumar et al., 2024)*

Name	**Origin**	**Medical Application**	**Device weight (kg)**	**Commercialisation**	**Unique feature**
ReWalk	ReWalk Ltd. (Israel)	Paraplegic patients	23.3kg	Exoskeleton has been commercialised and FDA approved for home use. Retails at about $70k	Must be used with the assistance of crutches.
Ekso	Ekso Bionics University of California	Paraplegic & stroke patients	20 to 23kg	Exoskeleton has been commercialised FDA for stroke patients. Retails at about $100k	
Indego/ Vanderbilt	Vanderbilt University.	Paraplegic & stroke patients	12kg	Exoskeleton has been commercialised and FDA approved for stroke patients. Retails at about $140k.	Lightest commercialised LLE
Rex	Rex Bionics (New Zealand)	Paraplegic patients	38kg	Exoskeleton has been commercialised and approved by the United States Food & Drug Administration. Retails at about $150k.	This LLE can be operated without the use of crutches. Rex makes use of a hand operated joystick and three-button keypad instead.
Mindwalker	European Commission	Paraplegic patients	30kg	Exoskeleton has not been commercialised	Under development and must be used in a controlled medical environment. Patients must make use of handrails while using.
ATALANTE	Wandercraft (France)	Paraplegic patients	80kg	Approved by the United States Food & Drug Administration.	
HAL-ML05	Cyberdyne Inc. (Japan)	Paraplegic patients	15kg	Exoskeleton has been commercialised and can be rented for $1950	Makes use of EMG (myoelectric signals) for control.

2.2. Materials

LLE devices should be lightweight and easy to transport. A substantial amount of research has gone into developing lightweight materials and their associated manufacturing processes. The goal is to make the exoskeletons lighter, more user-friendly and improve energy efficiency (Hasan et al., 2025). However, there is insufficient emphasis on the material properties and manufacturing processes used to develop these LLEs. There is a significant lack of data on the materials used in the manufacture of LLE, particularly commercialised LLE. (Hussain et al., 2021).

In order to utilise material selection as a production optimisation tool or weight reduction tool, it is important to establish an analytic material selection method. The focus of all material selection methods is centred around material properties alignment with the function of the product. Function looks at factors like load bearing and environmental interactions.

Najam (2018) present a material selection method that compares the performance index of candidate materials to select the most suitable. Performance index is calculated based on the core material properties. This is a quantitative method that sets priority on material property based on product application.

Another method is multi-criteria material selection method. This focus on considering at a broader list of material properties, performance requirement, cost, environment etc. However, this can lack to be quantitative. (Aires et al., 2022)

At present, there is a variety of robotic exoskeletons that use metals such as aluminium and its alloys or carbon fibre reinforced composites in their frame structures. HAL-ML05, for example, used hard and stiff metallic frames. ReWalk is constructed with a rigid metallic pelvic frame, along with pads, shoes, and waist belts to secure the user to the exoskeleton. Rigid metallic frames were also used in the design of the self-balancing robots, ATALANTE and Rex. (Hussain et al., 2021). More details on materials used can be found in Table 2 is a review of high-specific-strength materials that have been identified as suitable for the construction of LLE frames.

Figure 4: HAL-ML05 exoskeleton (Rupal, et al., 2017)

2.2.1. Aluminium

Favoured for its light weight, corrosion resistance and low cost, aluminium has a varied and extensive use. Its density ranges between 2600 and 2900 kg/m^3 and yield strength between 200Mpa to 600Mpa. Aluminium alloys can be categorised into 8 groups (numbered 1 to 8) depending on the predominant alloying element. Alloys in group 2XXX are strong and tough, specifically AA2014 & AA2024; however, they have relatively poor corrosion resistance. The 5XXX group, AA5052 also presents high strength, ductility as well as high corrosion resistance. In group 6XXX, AA6061 is one of the lightest alloys with relatively good strength. The strongest alloys are found in group 7XXX. With applications in the aerospace industry, AA7050, AA7068, and AA7075 all display good corrosion and fatigue/fracture resistance. AA7050 and AA7075 have already been used in the Lower Limb Exoskeleton application. Aluminium-Lithium (AL-Li) is a promising group 8 alloy which is being developed for use in the aerospace industry. It can be considered an advanced material with great fatigue resistance and the lightest aluminium alloy to date. (Danylenko, 2018) (Helmenstine, 2020)

Many LLE frames use aluminium or steel as the standard design material. Aluminium alloys are widely used to create links between the exoskeleton joints. Most commonly, rigid metal frames of aluminium are used in an exoskeleton that actuates multiple Degrees of Freedom (DOF) (Hussain et al., 2021) (Arunkumar et al., 2024).

A few LLEs that have made use of aluminium alloys for their structure are WPAL, CUHK-EXO28, Indego and Ekso. Walking Power-Assist Leg (WPAL) is a concept design LLE, manufactured using aluminium alloy for its structure, with the objective of achieving a

lightweight design. Wearable LLE robot CUHK-EXO28 was designed in Hong Kong for stroke patients. It utilises aluminium alloy 7075-T651 as the main manufacturing material. Additionally, steel was used for the transmission shaft, and high-density polyethene for the braces. Indego is also reported to make use of high-strength aluminium at the joints to enhance strength. Ekso robot also uses aluminium and titanium alloy for its mechanical structure (Annon, 2020).

2.2.2. Titanium

With a low density of 5060kg/m^3, titanium is a lightweight metal with exceptional strength. Despite being as strong as steel, Ti is about 40% lighter. Its extended benefits include excellent corrosion resistance and cavitation resistance (Bell, 2019).

Similar to aluminium, titanium is an essential structural material in the aerospace industry. Structural applications also extend to military hardware and sporting equipment fields. In addition, Ti's non-magnetic and biocompatible properties have increased its use in the medical industry. Ti has shown to have no negative impact on the human immune system and is therefore the chosen material for dental implants and prosthetics. The primary disadvantage of Ti is its high cost. This is due to the exorbitant price associated with the manufacturing methods. Titanium alloys can be categorised into three main groups, Alpha, Betha and Alpha-Betha (Bell, 2019) (Helmenstine, 2019).

Alpha alloys are pure titanium with a small quantity of alloying elements. This group of alloys has better wear resistance than pure titanium and strong oxidation resistance.
It also has the best machinability and weldability of all titanium alloys. Examples of these are Ti 5.8Al-4Sn-3.5Zr-0.7Nb-0.5Mo-0.35Si, which exhibits a high tensile strength of 1030 MPa (Choudhury, nd).

Betha alloys are strengthened by heat treatment that is followed by quenching and ageing. Of the three groups, Betha alloys display the worst machinability. These alloys can reach a strength of 1372 MPa to 1666 MPa at room temperature. For example, the ultimate tensile strength of high-strength titanium alloy TI-10V-2Fe-3Al is approximately 1200 MPa (Choudhury, nd) (Bell, 2019).

Alpha-Betha is the most used group of alloys. It exhibits good structural stability, toughness, plasticity, and high-temperature deformation properties, which can be further enhanced by hot-pressure processing followed by quenching and ageing. Grade 5 titanium, specifically Ti-6Al-

4V, is the most popular alpha + beta alloy. It makes up half of all titanium used globally. Ti-6Al-4V has a density of about 4,420 kg/m³. It is considerably stronger than commercially pure titanium. This alloy provides a great combination of strength, weldability, corrosion resistance, and ease of manufacturing. It is the preferred material for many applications, including aircraft turbines, engine parts, and aerospace structural elements. (Helmenstine, 2019) (Bell, 2019).

For the manufacture of LLE structures, titanium is preferred over aluminium in terms of strength-to-weight ratio. Its high price, however, limits its use. MINDWALKER is reportedly made of a combination of metallic and non-metallic materials for its structure. This includes the use of high-grade titanium rods, likely for their thin torque-transmitting thigh and shank links. Refer to Figure 5. Another LLE known to use titanium for its structure is ALEX III, a bilateral exoskeleton for gait rehabilitation developed at the University of Delaware. ALEX III employs high-strength titanium Ti6A1-4v, in combination with aluminium 7075 and steel AISI304 (Arunkumar et al., 2024).

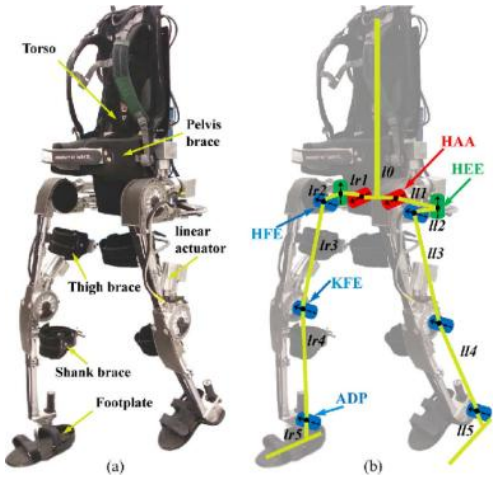

Figure 5: Mindwalker exoskeleton (Wang, 2015)

2.2.3. Magnesium

Magnesium is a lightweight metal with a low density of 1740kg/m^3 at room temperature. Although pure Mg is rarely used for structural applications, Mg alloys have significant benefits as structural materials. There are very few sources indicating the use of magnesium alloys for exoskeleton structures. However, this is an area that should be explored as magnesium alloys are lighter than both aluminium and titanium alloys, while still display good strength (Najam et al., 2018). Other beneficial properties of magnesium include high stiffness-to-weight ratio, castability and machinability. Some drawbacks of Mg alloys include low corrosion resistance and flammability; however, there are now many ways to mitigate these issues (McClements, 2025).

The application of structural Mg alloys ranges from the automotive, commercial and aerospace industries. In the medical field, Mg alloys are also being used in the manufacturing of sport wheelchairs where lightweight designs are crucial. Due to its excellent biocompatibility, bio-absorbability, and density and modulus of elasticity similar to those of human bones, this metal's use has been extended to surgical implants (Najam et al., 2018).

In recent years, Mg-lithium alloys have gained great interest as "ultra-light" structural materials. With Lithium possessing a low density of 530 kg/m^3, Mg-Li alloys are very ductile and formable, but with reduced strength. The manufacturing processes of Mg alloys include high-pressure die casting, sand casting, investment casting, and wrought production (McClements, 2025). A few notable Mg alloys, as per the ASTM standard:

Alloys that can be die-cast.

AZ91D - Good strength, popular die casting alloys with excellent corrosion resistance.
AM6OB - Good yield and tensile strength with excellent corrosion resistance.
AZ91E - General purpose alloy with good strength and excellent corrosion resistance.
QE21A, QE22A and QH21A all display high yield strength.
WE54A and ZK61A both exhibit exceptionally good strength; however, ZK61A alloy is prone to hot shortness cracks and is not weldable. (McClements, 2025)

Alloys used for Wrought products (extruded shapes, rods, sheets, plates and forgings).

AZ31B - A widely used alloy with moderate strength and good formability.
AZ31C - Is used for lightweight structural metal applications and has moderate corrosion resistance.
ZK60A - An alloy with both high strength and toughness. (McClements, 2025)

Although a strong candidate material, research indicates little use of magnesium alloys in LLE structures. Honda's third-generation humanoid robot, ASIMO, is reportedly made of a lightweight alloy, with its shell constructed from magnesium alloy (Annon, 2020).

Although magnesium alloys have been initially used in robots, a significant obstacle limiting their application in LLE parts is that the strength and toughness of current magnesium alloy grades are lower than those of steel and aluminium alloys. Therefore, developing high-performance magnesium alloys and their forming and processing technologies for manufacturing robot parts is very important. (Annon, 2020).

2.2.4. Composite Materials

Popular high-specific-strength composite materials to consider for the structures of exoskeletons and prosthetics are carbon fibre composites and Kevlar composites (Najam et al., 2018)

2.2.4.1. CFRC

Due to its high strength and stiffness, carbon fibre reinforced composites (CFRC) are being used in many engineering disciplines to replace structures previously constructed with steel or aluminium. CFRC can possess an ultimate tensile strength of up to ~3,500 MPa. Carbon fibre-reinforced plastics (CFRPs) can have a Young's modulus of up to ~150 GPa, significantly higher than aluminium alloys (~70 GPa) and steel (~200 GPa). CFRC have similar stiffness to traditional metals used in structures and machinery. CFRC can be manipulated based on the "lay up" of the sheets, fibre pattern, and resin matrix to generate desired material properties. (Annon, 2018) (Jones, 2023)

MINDWALKER is known to utilise CFRC and rubber. Ekso was also reported to make use of CFRC components. A less popular exoskeleton that also utilises CFRC in its design is the pneumatically operated robot knee-ankle-foot orthosis (KAFO). Developed by the University of Michigan, KAFO was designed on the concept of a lightweight mechanism (Hussain et al., 2021).

Shortcomings of CFRC include the difficulty of creating a desired complex shape compared to metals. Impact and fracture susceptibility, while CFRC is strong, it can be more prone to damage from sharp impacts or collisions (Oomi, 2024). This sudden, abrupt failure could be a safety concern for the LLE wear and needs to be considered in design.

CFRC materials present specific challenges at the joint level where the robot's torque is applied. The frequent rotational motion results in friction and rapid wear-and-tear of the joints. This yields delamination and reduced strength, leading to accelerated failure. This issue has been overcome by developing structures where the joint region is made of machined metal, and the non-friction-bearing links are manufactured from CFRC. This is a promising solution that the developers of Indego have implemented. Indego is composed of CFRC, while high-strength aluminium is utilised at the joints. This has helped reduce the weight of Indego to 12kg without compromising its strength, making it the lightest commercialised locomotive assistance LLE. MINDWALKER is also a successful example of such a combination. (Hussain et al., 2021)

Figure 6: Indego exoskeleton (Rupal, et al., 2017)

2.2.4.2. Kevlar

Kevlar composite is a proprietary material made only by the DuPont ™ chemical company. A fabric made of woven plastic originally developed as a lightweight replacement for steel bracing in vehicle tires. It is now best known for its use in bulletproof vests and knife proof body armour. With a strength five times greater than steel and specific tensile strength eight times greater than that of steel wire, its incredible properties are partly due to its internal structure and the tight knit of the fibres. Prolonged exposure to UV rays from sunlight results in some degradation of this material. Kevlar is used by itself as a fabric or as part of a composite material to provide added strength (Kiron, 2024).

Kevlar® and its composites have numerous applications in the automotive industry, including belts, brake pads, clutches, and gaskets. Kevlar® composite has been used in NASCAR™ car bodies, replacing fibreglass composite, as it doesn't shatter or leave debris on the race track after a crash. Its use also extends to the manufacture of lighter and more durable components for the marine and aircraft industries. The main drawback of Kevlar is its relatively poor compressive strength. Hence, its use as a primary structural component is limited. (Woodford, 2023)

2.2.5. Polymers

UHMWPE and PEEK are durable polymers with high strength-to-weight ratios. Below, their advantages and disadvantages are discussed as well as potential for use in LLE structures.

2.2.5.1. UHMWPE

Polyethylene is the most frequently used plastic globally. Ultra-high-molecular-weight polyethylene (UHMWPE) has been used in the manufacture of exoskeletons. It is a very tough subtype polyethylene with a specific strength 8-15 times greater than steel. Due to its many benefits, UHMWPE is used for a wide range of applications; this includes body armour, automotive industry, wire and cable applications, mining and mineral processing equipment, manufacturing equipment, transport-related applications, including truck trays, bins and hoppers. (Shippee, 2017)

The advantages of UHMWPE include light weight, excellent resistance to stress and cracking, 15 times greater abrasion resistance than carbon steel, self-lubricating with a very low coefficient of friction, exceptional chemical resistance and non-toxic. It has been FDA approved for use in food and medical applications. A few noteworthy disadvantages; compared to other popular polymers UHMWPE has a low melting point (297° to 305° F). Therefore, it's not suitable for high temperature applications. Its low coefficient of friction can be a drawback depending on the application. (Shippee, 2017)

2.2.5.2. PEEK

PEEK is a high-performance rigid plastic, and like UHMWPE, its use extends to the automotive, electronics and aerospace industry as it slowly replaces metals like aluminium in many applications.

This polymer is tough, lightweight, possesses great rigidity and high tensile strength. Additionally, PEEK displays excellent fatigue strength, high flame and chemical reaction resistance when compared to other thermoplastics. It exhibits good creep resistance, meaning it can withstand high loads for extended periods without incurring permanent deformation. Furthermore, its nontoxic properties make it suitable for use in the food industry and make it biocompatible for use in the medical industry (Jindal, 2023)

PEEK is relatively manufacture-friendly, suitable for processes like injection moulding, extrusion moulding, compression moulding and 3D printing. This also makes it ideal for producing complex custom components. To achieve maximum benefits, PEEK is often reinforced with carbon fibre or fibreglass. Doing so increases its creep, fatigue resistance and thermal conductivity. However, the relatively high cost of PEEK limits its use to special applications. It is also considered to have a low resistance to UV damage. (Annon, 2025).

Polymers often used for the manufacture of exoskeletons are PEEK and UHMWPE (Najam, 2018). HAL-ML05's metallic frame is fixed to the wearer's legs with the use of moulded plastic bands. CUHK-EXO28, which is manufactured with aluminium alloy and steel frame, incorporates high-density polyethylene for the braces. ReWalk is reported to use polymers for its 3D printed casing, which houses the motors and actuator on the structure. The use of polymers for structural applications of an LLE is limited. (Hussain et al., 2021).

2.3. Topology

Topology optimisation involves a computer program-based optimisation algorithm, a process that is run repeatedly by comparing different solutions until an optimal or satisfactory one is achieved. This has been proven to be an effective tool which saves on the time and cost associated with trials and prototyping. Topology optimisation looks at optimising the shape, size, and 2nd moment of inertia of a component. To put it simply, it looks at removing material where it is not needed and adding material where it is needed. (Yadav, 2019). An effective way of measuring topology optimisation is by quantitatively measuring the strength to weight ratio before and after the change. This is the overall of a product divided by the yield strength it is made from. (Avialasha et al., 2025)

There is limited information available regarding the shape and profile of commercialised LLE structures. Many conceptual uncommercialised LLEs make use of standard profile aluminium channels for their torque transmission components. It is known that MINDWALKER utilises titanium rods for this purpose. (Hussain et al., 2021)

A great space saving and weight reduction design is presented by Mu Jiamin (2019). For a lighter weight LLE structure, the thighs of the exoskeletons are made of hollow tubes. Two electric motor actuators as well as encoders are located inside each hollow thigh tube. The two motors are placed on opposite ends, with one of the motors connected to a spiral bevel gear, which transfers power to the hip joint, and the other is connected to a bevel gear which transfers power to the knee joint. (Jiamin et al., 2019)

The use of topology optimisation for the design of LLEs is limited in literature. However, Liu (2021) presents an integrated approach for designing custom-fit and lightweight LLEs. Structural optimisation is achieved through finite element analysis and topology optimisation, ensuring the exoskeleton meets required strength standards while minimising weight. Iterative design techniques help construct a lattice framework. (Liu et al., 2021)

Liu (2021) proposes designing an LLE structure by 3D scanning the lower limbs of a patient and, from that, creating a custom fit design from 5mm thick aluminium plates which closely curve around the patient's limbs. See Figure 7. Finite element analysis is then conducted on the organically shaped LLE links to achieve topology optimisation. Boundary conditions are set as well as simple vertical static mechanical loads in the model to simulate the full body weight of the patient on the structure.

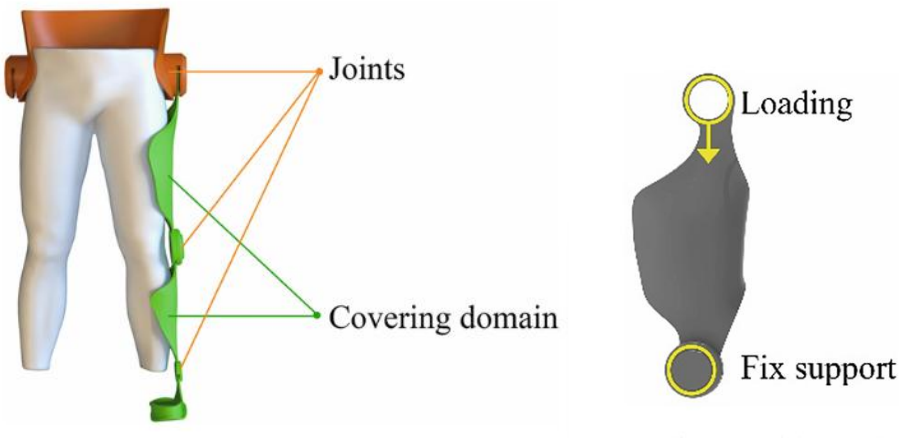

Figure 7:Initial custom fit LLE structure design (Liu, et al., 2021)

An iterative conventional topology optimisation method, namely solid isotropic material with a penalty (SIMP), was used for initial optimisation. SIMP is an element density-based optimisation method, making a density approach to a specific range. (Liu et al., 2021)

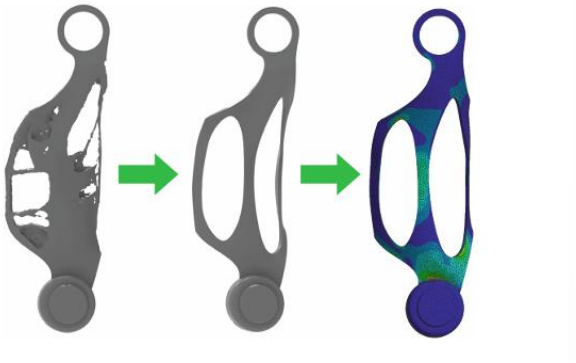

Figure 8: Thigh Link topology optimisation remodelling (Liu, et al., 2021)

To ensure that the lightweight result is consistent with the scientific and accurate analysis, the strength of the trimmed result was analysed under the same vertical static load. The maximum stress experienced was the yield strength of aluminium. This offers an effective framework for lightweight optimisation using a lattice structure. (Liu et al., 2021)

Table 2: Popular lower limb Exoskeleton Design Features *(Arunkumar et al., 2024) (Hussain et al., 2021) (Rupal et al., 2017)*

Exoskeleton	**Joints**	**Actuator type**	**User max weight (kg)**	**Battery life**	**Operation time**	**Structure material**	**Manufacturing process**	**Gait initiation mode**
Rewalk	Hip-Actuated Knee-Actuated Ankle-Passive	Electric	100	2 hours 40min	2 hours	Metals	3D printing	Weight shifts CoM (body tilt)
Ekso	Hip-Actuated Knee-Actuated Ankle-Passive	Electric	100	6 hours	1 hour	Carbon fibre and metals	3D printing of individual parts	Weight shift button
Indego / Vanderbilt	Hip-Actuated Knee-Actuated Ankle-Passive	Electric	113	1hour	1,5 hours	Carbon fibre and metals	3D printing and CNC machining	COP (Body tilt)
Rex	Hip-Actuated Knee-Actuated Ankle-Actuated	Electric	100	2 hours	1 hours	Metals	No data	Joystick
Mindwalker	No data	Electric	No data	No data	No data	Carbon fibre & high-grade titanium	3D printing and extrusion	No data
ATALANTE	No data	Electric	No data	3-hours	No data	No data	No data	No data
HAL-ML05	Hip-Actuated Knee-Actuated Ankle-Passive	Electric	100	2 hours 40min	1,5 hours	Metals	No data	EMG Weight shifts

2.4. Manufacturing Processes

The selection of an appropriate manufacturing method ensures that the exoskeleton structure meets the required strength and functional capabilities at the links and joints as per the design. The durability of the robot's structure is ensured by the manufacturing method. Manufacturing methods are generally selected after the material and the profile have been finalised. These methods vary depending on the chosen material. (Hussain et al., 2021). Often, more than one manufacturing method is required to produce the end product (Munro, 2023). Manufacturing processes can be grouped into two groups. Subtractive and additive. This section reviews the possible manufacturing processes required to produce an LLE structure based on selected material and profile.

2.4.1. Subtractive Manufacturing

Subtractive manufacturing processes, such as computer numerical control (CNC) machining, are commonly used to manufacture LLE frames in combination with other conventional processes, such as extrusion and casting. Refer to Table 2 for manufacturing processes employed for existing LLEs. (Hussain et al., 2021)

The frames of exoskeleton robots Chuk-Exo and ATALANTE were manufactured with extruded and CNC-machined components, indicating that their structure could make use of metal rods or standard continuous profile channels. Several other LLEs have been manufactured using conventional methods such as casting and extrusion, which are combined with subtractive manufacturing such as drilling and CNC machining. (Hussain et al., 2021)

Welding and fastening have been key processes in assembling fabricated modular components. WPAL exoskeleton was produced through extrusion followed by welding of the extruded aluminium parts. CNC machining of complex shapes is well suited for prototyping but is relatively expensive. Conventional techniques like extrusion and metal casting face challenges such as ensuring uniform wall thickness and limited accuracy in the final design and shape. (Hussain et al., 2021).

2.4.2. Additive manufacturing

For manufacturing topology optimised components, additive manufacturing (AM) techniques are considered the most effective manufacturing method. This is due to its capability to produce complex-shaped, lightweight structures, with minimal waste and high precision. This is applicable for both metallic and non-metallic structures. Methods such as selective laser melting (SLM), selective laser sintering (SLS), and fused deposition modelling (FDM) are particularly suitable for creating the intricate geometries often resulting from topology optimisation (Okorie et al., 2023). Of these manufacturing processes, 3D printing was utilised to produce several LLE components. This is because of its advantages over traditional manufacturing methods. Ref Table 2. (Hussain et al., 2021).

3D printing is an additive manufacturing process that utilises three-dimensional (3D) model data to produce components layer by layer. It has strong capabilities for producing complex geometries. This process was originally commonly used for polymers; however, it has now been expanded in the manufacture of metal components. (Hussain et al., 2021).

2.4.3. Manufacturing Process of Existing LLEs

Indego uses a combination of 3D-printed carbon fibre composite components and CNC-machined metallic components. Lokomat also utilises CNC-machining to produce components for its structural frame and 3D-printed polymeric casings that covered the device's mechanical components. (Hussain et al., 2021)

Metallic 3D printed components are joined by means of welding. A heat bonding process joins the 3D printed polymer parts. However, the strength between 3D printed LLE structures and those produced by traditional machining processes remains unexplored. (Hussain et al., 2021). Nonetheless, Churchwell (2016) designed and built the Joint Torque Augmentation Robot (JTAR), a hip exoskeleton whose key structural components were initially manufactured from CNC-machined aluminium and later replaced with 3D-printed polylactic acid. The 3D-printed parts underwent destructive testing to validate the design requirements. The average force required to destroy the part was 2500 N. This level of strength provided a safety factor of more than four times the expected load. A significant reduction in weight and manufacturing time was achieved with the 3D printing method as compared to the conventional CNC-machined aluminium exoskeleton (Churchwell et al., 2016).

Although there are many benefits to 3D printing, its components are found to be less durable than their metallic counterparts (Batkuldinova et al., 2021). Research indicates that 3D printing has been more commonly used to custom make braces or cuffs. This is achieved using a model obtained from a 3D scanner. Scanning patients' limbs for the manufacture of 3D printed braces is a promising, low-cost solution (Sanchez-Villamañan et al., 2019). Interest in 3D printing LLE structures is rapidly growing. To gain commercial success, research needs to focus on the study of materials, their mechanical properties, 3D printers and 3D printing software. (Batkuldinova et al., 2021)

Furthermore, hybrid manufacturing methods that combine additive and subtractive techniques enhance performance by allowing optimised shapes while refining surface quality and adding material selectively for enhanced durability. Other traditional methods like casting and injection moulding are also applied in cases where optimised shapes are simpler or when mass production is essential. They however come with more limitations in design complexity compared to AM (Okorie et al., 2023).

2.5. Structural Analysis and Evaluations

To design and evaluate an LLE structure, one must understand the motion and forces it experiences during walking. It is essential to start by understanding human gait (Shi et al., 2019). In a floating-base open-chain robotic system, such as a lower limb exoskeleton, kinematics and dynamics can be used to study the motion, forces, and torques of gait. Forward kinematics of a robot refers to the calculation of the position and orientation of its end-effector frame from its joint coordinates. In LLE research, the end effector is the "foot" of the exoskeleton. The inputs for these calculations are gait patterns of a healthy individual, taking into account the main factors that influence gait, such as step length, width, and speed. In patients with paraplegia, gait data must be collected from healthy individuals. (Shi et al., 2019).

$$x = L_1 \cos\theta_1 + L_2 \cos(\theta_1 + \theta_2) + L_3 \cos(\theta_1 + \theta_2 + \theta_3) \quad (1)$$

Equation 1: X coordinate

$$y = L_1 \sin\theta_1 + L_2 \sin(\theta_1 + \theta_2) + L_3 \sin(\theta_1 + \theta_2 + \theta_3) \quad (2)$$

Equation 2: Y coordinate

$$\emptyset = \theta_1 + \theta_2 + \theta_3 \quad (3)$$

Equation 3: Angle of link end effector

Equations 1,2, and 3 are used to calculate the position/location of the end effector in terms of x, y and Θ. L_1, L_2 and L_3 I represent the length of the thigh, shank, and foot links/elements. This is the process of position prediction, velocity, and acceleration once a design is specified. (Lynch et al., 2017).

Robot dynamics is the study of motion, focusing on the forces and torques that drive it. Forward dynamics is used to calculate the acceleration of the robot when the position and joint forces and torques are given, as shown in Equation 4. (Lynch et al., 2017)

$$\ddot{\theta} = M^{-1}(\theta)(\tau - h(\theta, \dot{\theta})) \quad (4)$$

Equation 4: Acceleration equation

Inverse dynamics on the other hand, is used for determining the joint forces and torques corresponding to the robot's state/position and given acceleration, using Equation 5. (Lynch et al., 2017)

$$\tau = M(\theta)\ddot{\theta} + h(\theta, \dot{\theta}) \quad (5)$$

Equation 5: Torque equation

With Ӫ representing the accelerations at the relevant joint and τ representing the Torque. A robot's dynamic equations are typically derived in one of two ways, by a direct application of Newton's and Euler's dynamic equations, or by the Lagrangian dynamics formulation derived from the kinetic and potential energy of the robot. This is particularly important for understanding the kind of loads and stress a structure withstands. (Lynch et al., 2017).

In LLE design, the torque is useful input for FEA simulations to analyse the structure. Research shows that simulation-based optimisation of LLE structure is a practical tool to reduce weight without compromising mechanical properties (Sanchez-Villamañan et al., 2019). LLE developers have employed various methods to assess the structural strength of LLEs. Below are some of the methods developers have taken to design and evaluate their LLE structures.

2.5.1. Lower Limb Fitness Exoskeleton

Lan Duan (2023) designed a lower limb fitness exoskeleton to assist individuals in exercising their lower limb muscles (see Figure 9). First, the degrees of freedom for each joint were selected. Thereafter, the range of motion for each joint is set based on the average range of motion of a healthy adult during walking and exercise. A material is then selected for the LLE. (Duan et al., 2023)

Figure 9: Lower Limb fitness exoskeleton device (Duan, et al., 2023)

The shape and profile of the thigh and shank links were selected by comparing a round tube against a rectangular tube of common material and wall thickness. The authors determined that the LLE is likely subjected to damping forces and bending stresses. Equations 6 and 7 were used to calculate the maximum bending stress the round and rectangular tube would experience when subjected to predicted gait input forces. F_{max} is the maximum expected load that would act on the structure, L is the length of each link, and d, h, b and y are the cross-sectional dimensions of the two rods. Calculation results indicated that the maximum bending stress of the rectangular tube was lower than that of the round tube under the same force. The rectangular tube was therefore selected for the thigh and shank link. (Duan et al., 2023).

$$\sigma_{max1} = \frac{F_{max} \times L}{\frac{I_{z1}}{y_{max1}}} = \frac{F_{max} \times L}{\frac{b_{outer}h_{outer}^3 - b_{inner}h_{inner}^3}{12}} \times \frac{2}{h}$$

$$= 2.16 \times 10^{-3} F_{max} \times L \quad (6)$$

Equation 6: Bending stress of rectangular tube *(Duan et al., 2023)*

$$\sigma_{max2} = \frac{F_{max} \times L}{\frac{I_{z2}}{y_{max2}}} = \frac{F_{max} \times L}{\frac{\pi d_{outer}^4 - \pi d_{inner}^4}{64}} \times \frac{2}{d}$$

$$= 3.70 \times 10^{-3} F_{max} \times L \quad (7)$$

Equation 7: Bending stress of round tube *(Duan et al., 2023)*

A SolidWorks 3D model of the structure with rectangular tubes for the shank and thigh links was imported into *Adams*. To simplify analysis, every component/part was defined with the same material. The model was then simplified into 8 modules and the belt or waist bracket was connected to the world frame (Duan et al., 2023)

Inputs to the model include damping forces, frictional forces, angular displacements at the joints over a set period (as per the established walking range for healthy human gait), and gravitational forces. From this, the software produced two sets of graphs for the knee and ankle joints, a sine graph of angular displacement vs time and a force vs time graph for the X, Y, and Z-axis (ref Figure 10) (Duan et al., 2023).

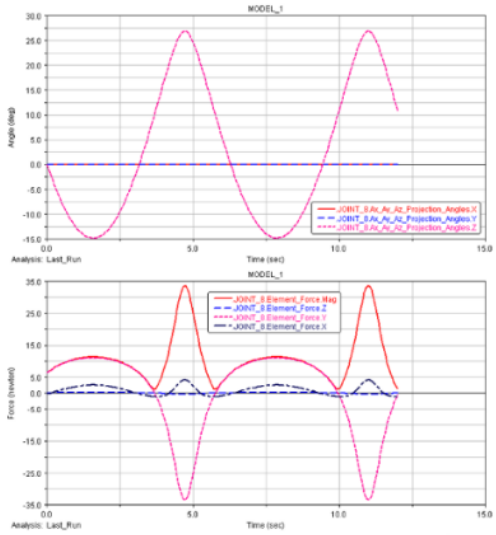

Figure 10: Angular motion vs time graph; Force vs time graph of knee joint (Duan, et al., 2023)

Lan Duan et. al. then used the maximum force value to calculate the maximum stress in the thigh and shank links. The stress value in each link was compared to the yield stress of the selected material. A significantly lower stress in the links compared to the selected material's yield stress was an indication that the strength requirement was satisfied. (Duan et al., 2023).

2.5.2. Modular Wearable LLE Rehabilitation Robot

Liang (2025) designed and evaluated a modular wearable LLE rehabilitation robot (ref Figure 11). They began by selecting the number of degrees of freedom, using only the minimum necessary to achieve walking motion, thereby reducing the mechanism's complexity. Similar to most LLEs, this bipedal robot was designed to mimic human anatomy. It consisted of three joints, namely, the hip, knee, and ankle. The thigh and shank links were made of rectangular components with a length-adjusting feature (see Figure 12). SolidWorks was used to create a 3D model of the structure, and an aluminium alloy was selected for the material. To verify whether the structural strength and stiffness of the exoskeleton robot meet the requirements, the following Finite Element Analysis were conducted on Ansys Workbench (Liang et al., 2025).

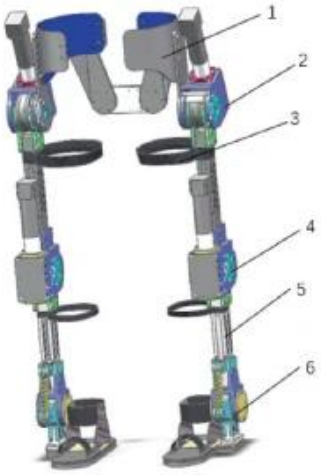

Figure 11: Modular wearable lower limb exoskeleton rehabilitation robot (Liang, et al., 2025)

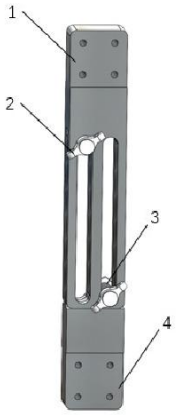

Figure 12: Length adjustable thigh link (Liang, et al., 2025)

Material selection was verified through static analysis at four stages of the gait cycle, standing, swinging, single-leg support, and double-leg support. A full robot analysis was run for each gait phase with a different corresponding posture. Static loads were applied vertically to each leg and the waist bracket. The force magnitude and robot position/posture varied across gait stages (the author does not provide details on how these forces were selected/calculated). The simulation algorithms involved calculating the stress and strain of the structure under the static loads, as shown in Figure 13. Across the four gait postures, the stress cloud maps were blue, indicating low stress values. The maximum stress magnitude was identified to be within the allowable stress of the selected material. This confirmed the structural safety of the design. The same was done for the strain value (Liang et al., 2025).

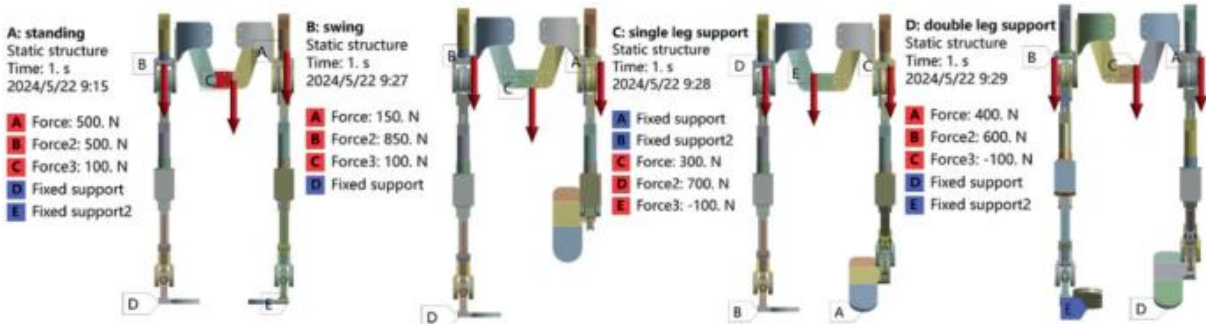

Figure 13: Load application on robot structure during gait phase posture (Liang, et al., 2025)

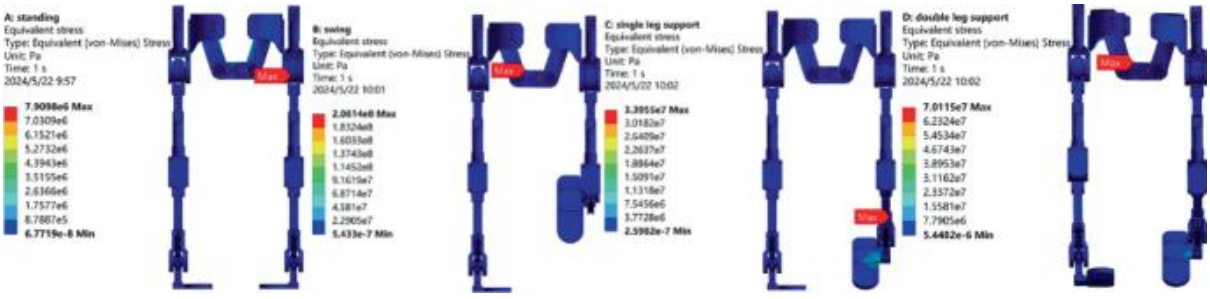

Figure 14: FEA stress and strain results could map (Liang, et al., 2025)

Because the robot structure endures cycling loading, vibrations from the electric components and ground reaction forces, the LLE model was tested for resonance. Simulations were run to determine the vibrational characteristics of the structures, and the results showed no risk of resonance at the LLE's operating frequencies in all gait phases. (Liang et al., 2025).

2.6. Summary of Research Gaps

Globally, only six LLEs for paraplegic patients have been commercialised with FDA approval. There are still many drawbacks, including the fact that LLEs are relatively heavy and inefficient. The seven most popular locomotion LLEs reviewed weigh between 80 kg and 12 kg. Major contributing factors are the number of actuated joints, degrees of freedom, battery/power source, actuators, and the material and profile of the structure. Locomotion assistance LLEs, more specifically, fully body support robots, weigh the most. Most LLEs utilise electric actuators due to their superior efficiency, although they weigh about twice as much as hydraulic actuators. The battery/power pack contribute between 6% and 20% of the LLE's weight, but devices can typically operate for only one to two continuous hours. (Rodriguez-Fernandez et al., 2021) (Shi et al., 2019)

Given the continued importance of stability, robust structures have been highlighted as critical. Research emphasises the need to utilise materials with high specific strength. The most common materials used to manufacture LLE structures are metals, more commonly aluminium alloys. Titanium alloys have also been employed in some commercialised LLEs. Other materials, such as magnesium alloys, carbon fibre-reinforced composites, PEEK, and UHMWPE, have not been used for structural purposes in LLEs; however, they have promising potential. The employment of topology optimisation for the design of LLEs structures is limited in literature. (Annon, 2020) (Arunkumar et al., 2024)

Most LLEs utilise standard continuous profile channels such as rods or tubing. Subtractive manufacturing processes, like CNC machining, are commonly used to fabricate structures; however, additive manufacturing processes are well suited for prototyping complex geometries typical of topology optimisation. The structural evaluation process for LLEs often includes using human gait forces in FEA studies to validate the strength and suitability of a candidate material. (Hussain et al., 2021)

3. METHODOLOGY

Optimisation through weight reduction has become an important factor in design. Globally, industries are looking to weight reduction optimisation as an effective way to reduce cost and improve efficiency while not compromising on performance (Yadav, 2019) (George, 2014). There are several ways to effectively reduce the weight of a structure or component. Figure 15 illustrates the methodology for optimising the LLE structure. This section begins by examining the current design of the LLE to be optimised, followed by an analysis of the input forces acting on the LLE. Thereafter, the material selection method and topology optimisation method are presented. This section ends with a review of the manufacturing process to be used for producing the new design structure.

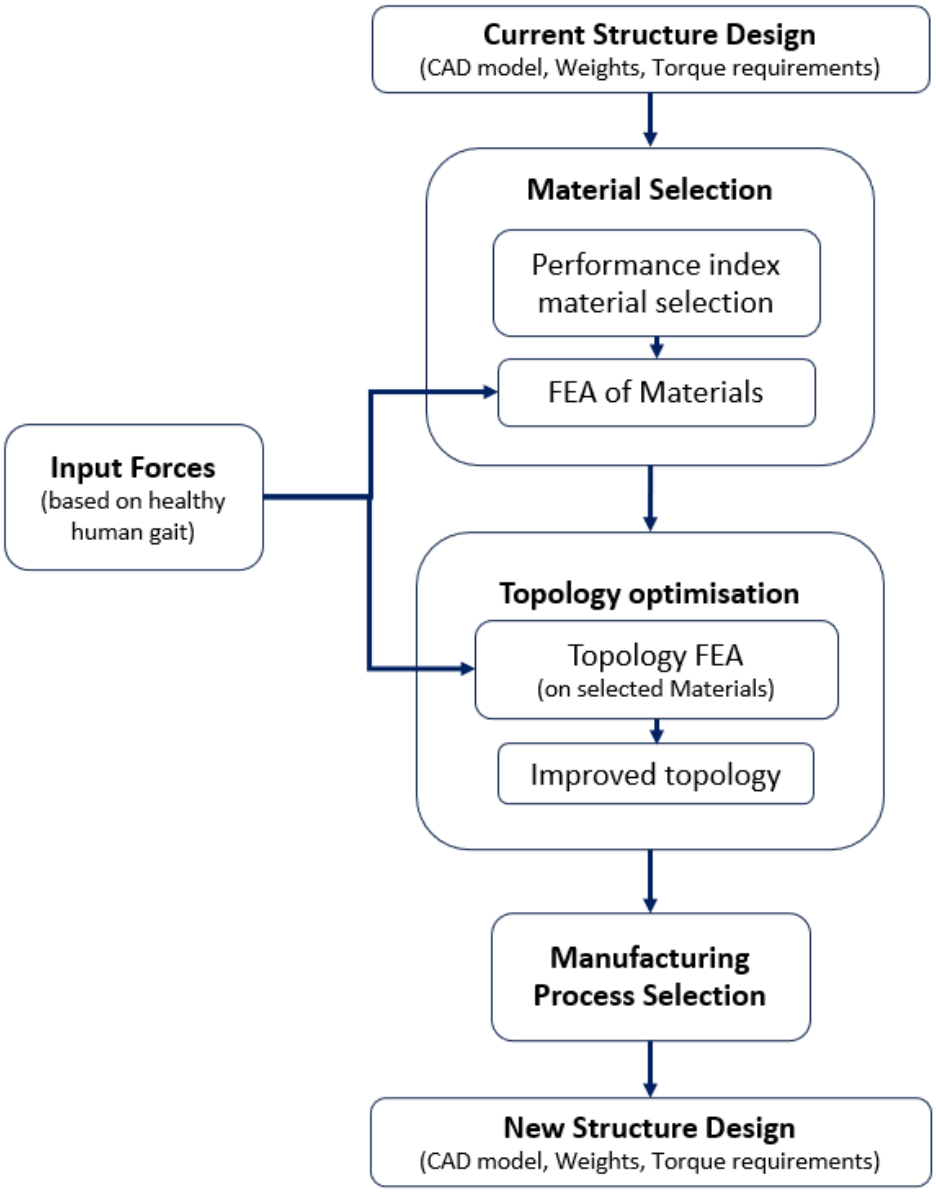

Figure 15: Methodology layout

3.1. Current Structure Design

This thesis focuses on the optimisation of an existing design of a Lower Limb Exoskeleton. An image of the structure design is shown in Figure 15. The structure can be subdivided into four categories: two shank links, two thigh links, two foot supports and a waist bracket. This LLE is designed to be actuated at the hip and knee joints via electric motors. The ankle joint is a passive (unactuated) joint. (See more details in Appendix C, Figures 62 and 63)

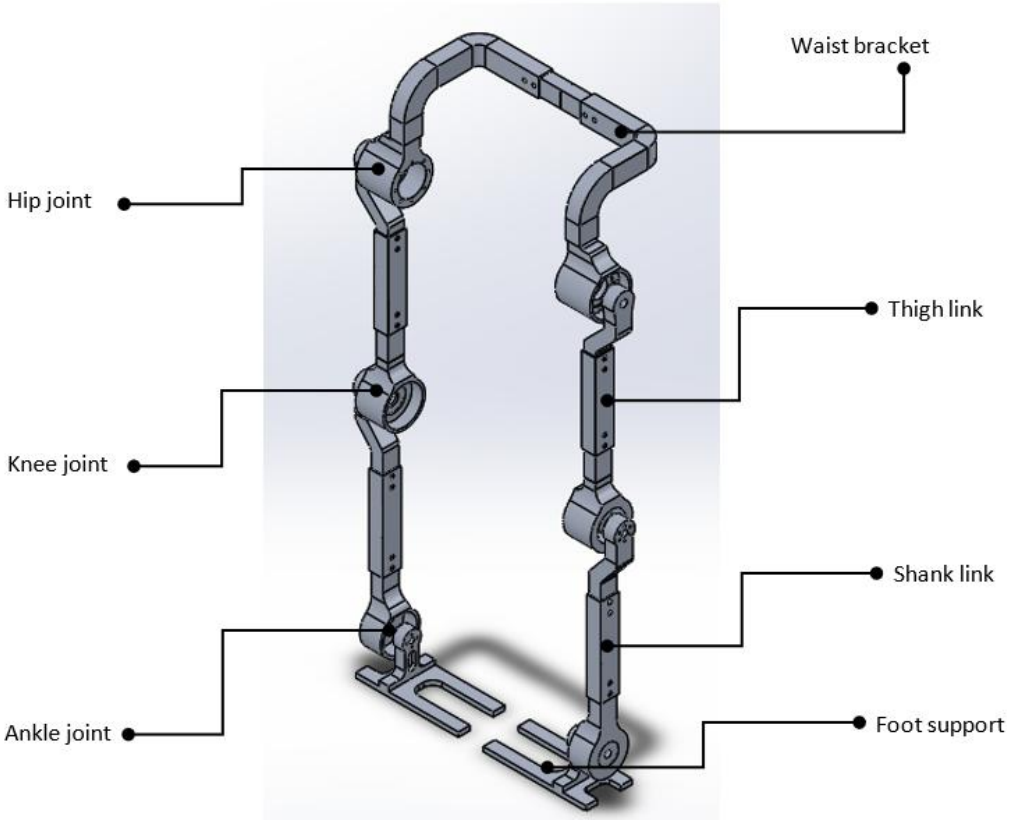

Figure 16: Initial Lower Limb Exoskeleton design

Taking a closer look at the structure, the thigh and shank links are similar in design (see Figures 16 and 17). They are both made up of three subcomponents: the top link which is connected to the above joint from the exterior, the bottom link which connects to the lower joint and has a round hollow shape to house the electric motor and actuator. The middle link is a channel that connects the top and bottom links. It contains bolt holes which allow for length adjustments of the thigh and shank. This design feature is to cater to individuals of varying heights. The waist bracket holds the two limbs together. Its two ends protrude into the housing for the hip joint. It also has a length adjustment feature catering to a wider range of individuals.

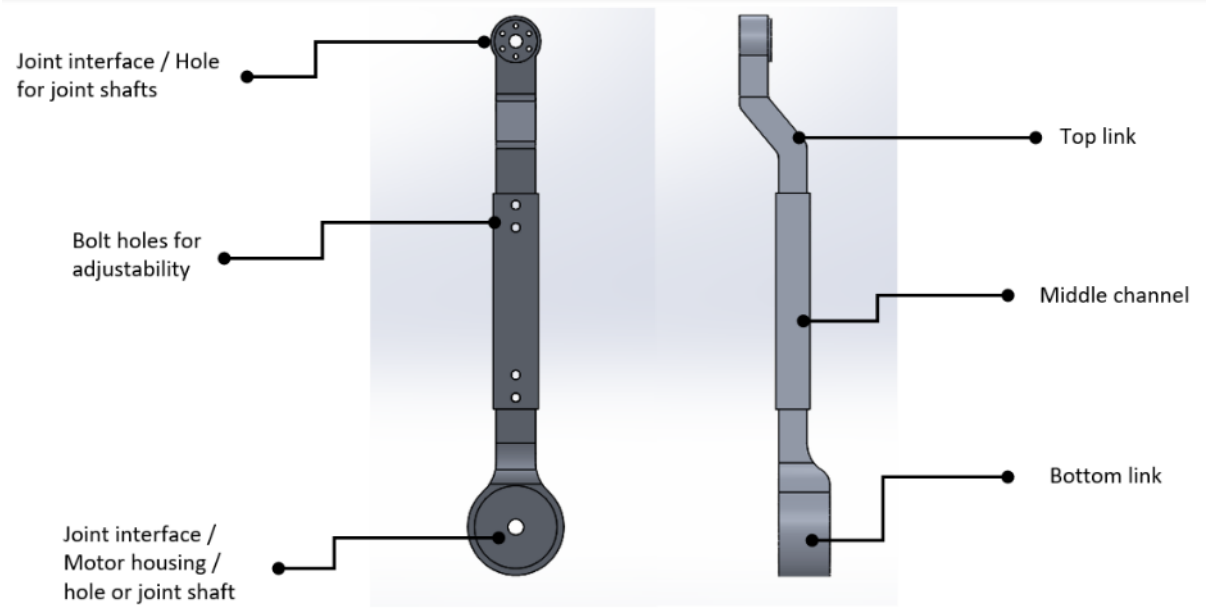

Figure 17: Initial Shank Link Design

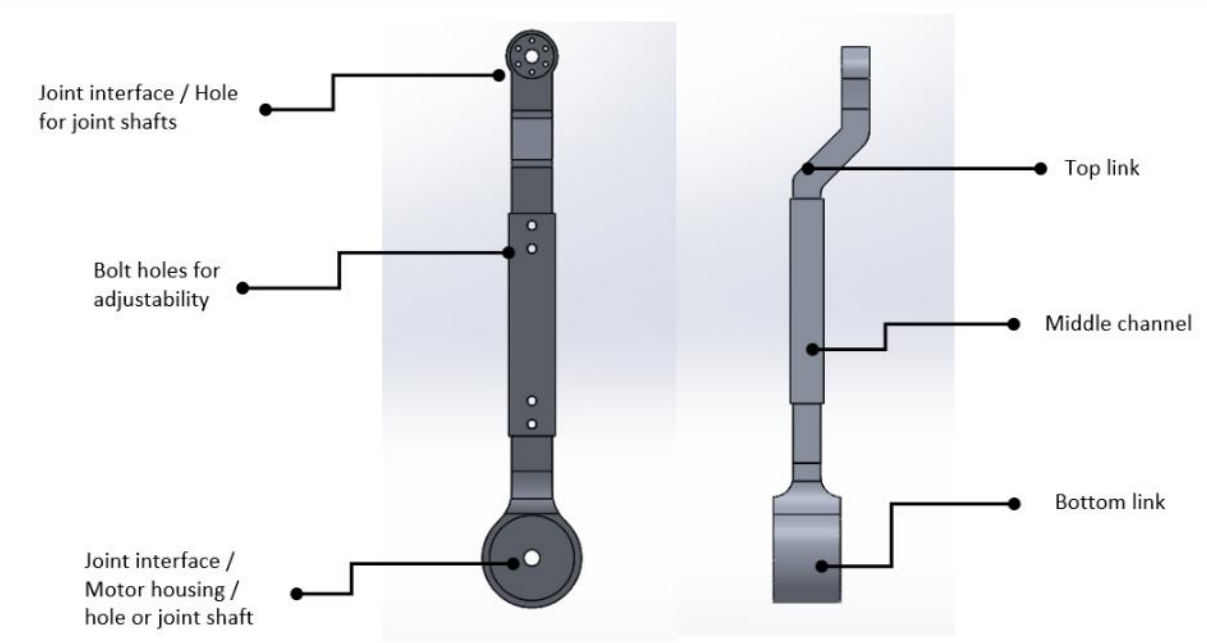

Figure 18: Initial Thigh Link Design

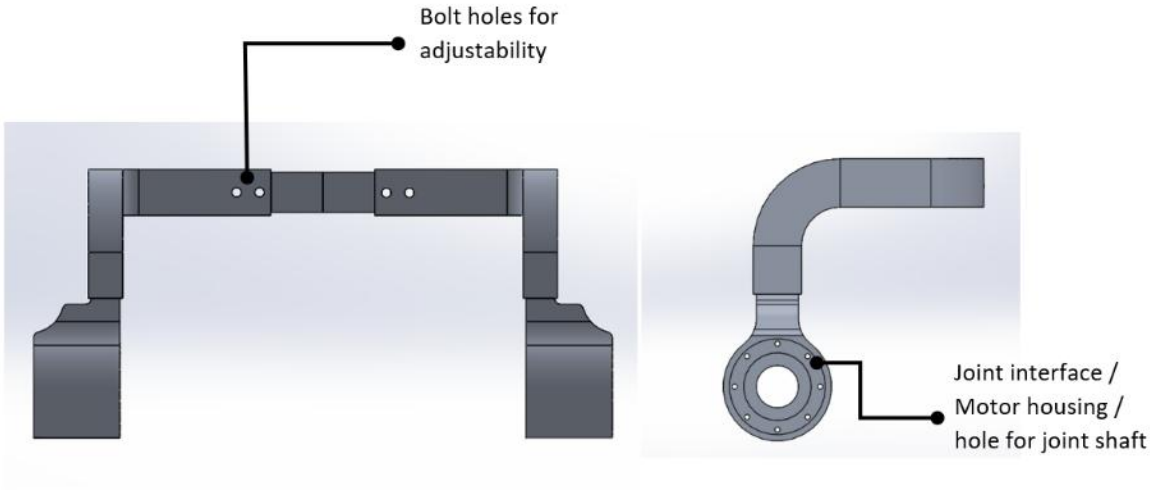

Figure 19: Waist bracket design

For the initial design, the material for all components listed in table 3 was aluminium alloy Al7075. The overall weight of the structure is 9.73kg. The LLE included a power pack which would be attached to the waist bracket. With Al7075 having a yield strength of 467Mpa the overall strength-to-weight ratio of this structure is 48Mpa. Electric motors are used to actuate the hip and knee joint, leaving the ankle joint passive. This LLE was designed to be used with crutches for extra support.

Table 3: Weight of current LLE structure

	Original Design Weight (kg)	Material
Waist connector	2,809	Al7075
Thigh link	1,549	Al7075
Shank Link	1,347	Al7075
Foot	0,563	Al7075
Total (for whole structure)	**9,727**	
Strength to weight ratio	**48Mpa/kg**	

3.2. Input Forces

To understand the loads acting on the LLE structure, it is necessary to comprehend the biomechanics of human gait. Gait is the period of motion that occurs when a person walks, otherwise stated as the cyclic series of motion of each foot from one position of support to the next. A single human gait cycle commences when the heel of one foot strikes the ground and ends when that same foot hits the ground once more. It is essential to note that although the lower limbs do most of the work during gait, full-body participation is required for successful execution. Cooperative motion from the spine, pelvis and arms all aid in the forward propulsion (Vaughan et al., 1992) (Gruijicic, 2023).

The analysis of human gait should be three-dimensional. If the human body is divided into three segments, as seen in Figure 19. Most of the gait motion takes place in the sagittal plane. However, to have a full picture, the motion and forces in the transverse and frontal planes should be analysed (Vaughan et al., 1992). In research and medical practice, gait analysis is done through inverse dynamics studies, which calculate the forces and torques occurring at every joint based on inputs like mass, velocity and displacements. Another means of analysing gait is Electromyography (EMG), which involves the use of muscle sensors placed on the skin. Last and most common is the analysis of ground reaction forces (GRF) applied through the feet to support the body while making use of a force plate (Derlatka et al., 2023). (Al-Hayali et al., 2021) (Vaverka et al., 2015)

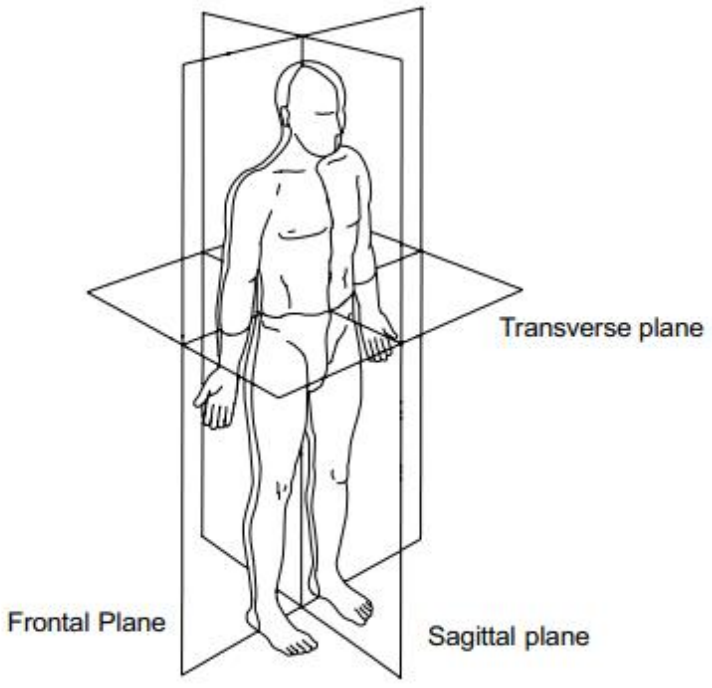

Figure 20: Human Transverse, Frontal & Sagittal plane *(Vaughan et al., 1992)*

The gait cycle observes the motion of only one leg. It can be divided into two phases, stance phase and swing phase. As can be seen in Figure 20, the stance phase, which makes up ±60% of a healthy adult gait cycle, is the period of the cycle when the observed foot is on the ground. Stance is also known as the load bearing phase, which commences with heel strike and ends with toe off. The swing phase, which makes up ±40% of a healthy adult's gait cycle, is the period when the foot is off the ground. The swing phase starts after toe off and ends just before the heel strikes the ground again (Gruijicic, 2023).

Stance phase is subdivided into the following five phases:

1. Heel strike is universally considered the first subphase of gait. During this step, the observed leg (which is also the forward/front leg) makes initial contact with the ground through the heel.
2. During foot flat, the foot drops forward until the full plantar is in contact with the ground. The body weight is shifting to the observed leg.
3. Midstance, the entire body is supported only by the observed leg while the opposite leg is in swing phase.
4. Heel off, the body weight now begins to shift back to the opposite leg while the heel of the observed leg leaves the ground.
5. Toe off is the final stance phase. In this phase, the toes are pushed toward the ground, generating a forward push in preparation for the swing phase. (Gruijicic, 2023).

Swing phase is subdivided into the following three phases:

6. Early swing, or acceleration, is the beginning of swing phase and follows right after toe off. The observed foot is lifted from the ground in an accelerated motion.
7. Mid-swing, the leg swings forward, directly beneath the torso, moving past the opposite weight bearing leg.
8. Late swing, or deceleration, is the final phase of gait, taking place when the foot is once again extended in front of the body, decelerating in preparation for heel strike and a new stance phase. (Gruijicic, 2023)

At any given time, the gait cycle of each leg is in different overlapping phases. For example, when the right leg is in the midstance phase, the left leg is most likely in its mid-swing phase. Although the phases may differ from one leg to the other, in a healthy human gait, the periodic patterns and corresponding GRF per respective phase are very close to identical (Vaughan et al., 1992).

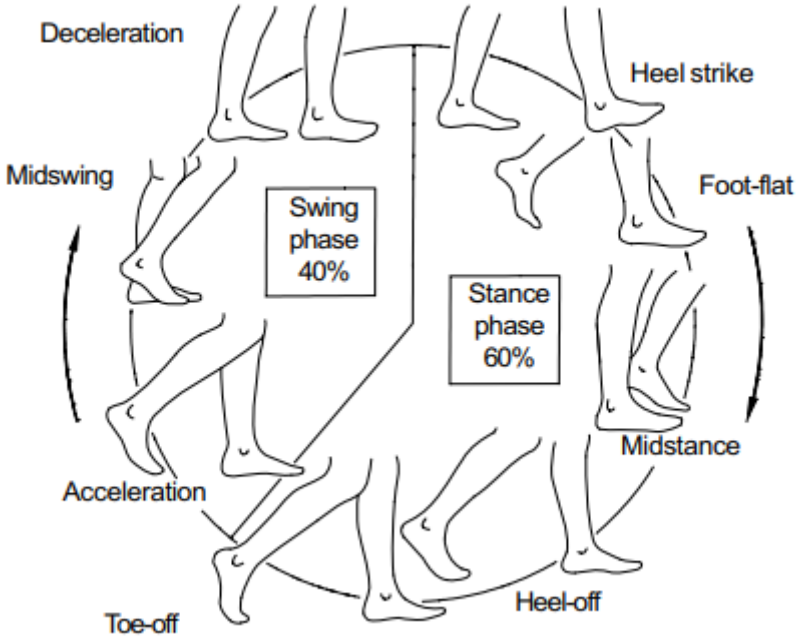

Figure 21: Gait cycle phases *(Vaughan et al., 1992)*

3.2.1. Stance Phase Analysis

Different methods must be employed to analyse human gait during stance and swing phases. Research shows that stance phase is most commonly analysed through the study of ground reaction force (GRF). Particularly through the use of data obtained from a force plate. This is easy to understand as stance is the load-bearing phase, and GRF readings can be obtained as the reaction force to the load of the foot (Derlatka et al., 2023).

Because gait is a three-dimensional activity, GRF is a resultant force with three component forces in the X, Y, and Z directions. Looking at Figure 21, Fx, the mediolateral (ML) GRF component is active in the frontal and transverse planes, acting perpendicular to the sagittal plane. These forces are responsible for balance during gait. Fy, anteroposterior (AP) GRF component would be seen in the sagittal and transverse planes, perpendicular to the frontal plane. This is where most of the motion happens. Fy is responsible for acceleration and deceleration in gait. Lastly, the Fz, vertical GRF component, acts perpendicular to the ground against gravity. Fz forces have the largest magnitude of the three components.

Figure 21 shows periodic force graphs of the mediolateral, anteroposterior and vertical component forces through the different subphases of gait. These readings were taken from individuals walking over a force plate. It can be assumed that the patterns of these GRF graphs

remain the same across different healthy individuals; changes occur mostly in magnitude and time values based on the individuals' weight and walking speed. (Vaverka et al., 2015).

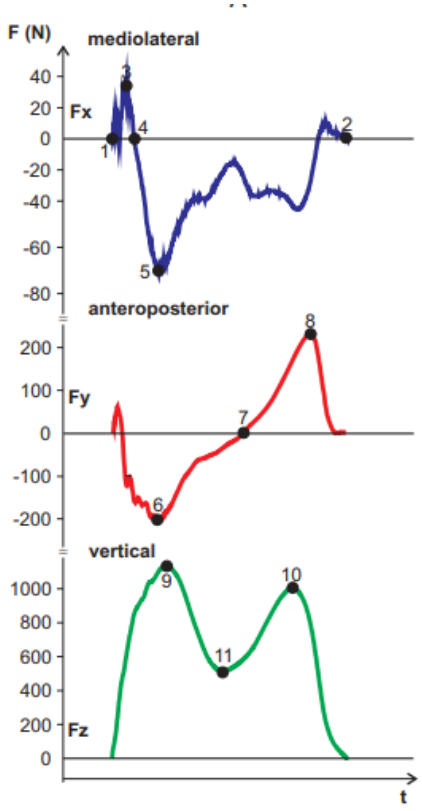

Figure 22: Ground reaction X, Y and Z forces *(Vaverka et al., 2015)*

The vertical ground reaction force (Fz) is the largest component of the GRF in gait and therefore receives the most focus during gait analysis. From Figures 21 and 22 it can be seen that the Fz vs time graph forms an "m" shape consisting of two peaks. The first peak is representative of the foot-flat phase, the valley is a result of midstance, and the second peak reflects the heel-off phase. Toe off, the final stance phase, can be seen as the point just before the graph hyphenates. Figure 22 shows a typical vertical GRF graph where force is given in terms of body weight (BW) percentage, measured at different gait phase percentages instead of time. (Al-Hayali et al., 2021) (Vaverka et al., 2015)

The pace at which a person walks affects the magnitude of the vertical GRF. This is explained through Newton's second law of motion, F=Ma. Although the walker's body weight remains the same, an increase in acceleration results in an increase in Fz values. This can be seen in the graph in Figure 23 where the GRF at the two peaks are greater than 100% of the walker's body weight.

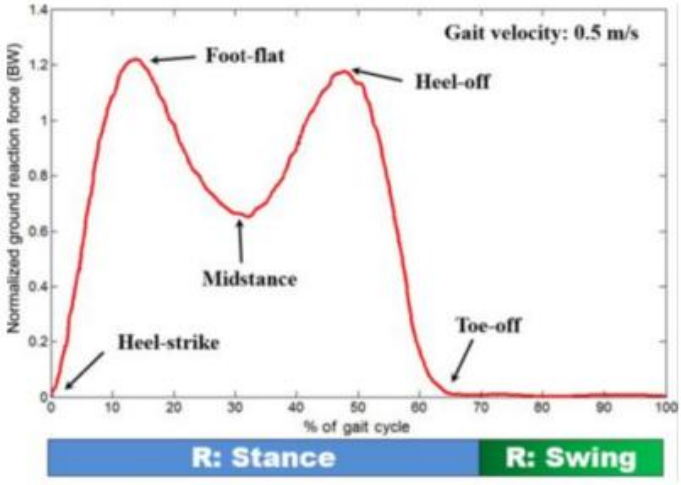

Figure 23: Vertical Ground Reaction Force vs. Gait Cycle *(Al-Hayali et al., 2021)*

A study of eighteen healthy young adults (27±4 years old) walking across a force plate to record vertical GRF was conducted by Barela (2014). From that study, the table in Figure 24 shows the average Fz in BW percentage during the different stance phases. Note that this study was focused on seeing the impact of body weight support for rehabilitation. Therefore, this thesis will only focus on the results for no body weight support (0% BWS) (Barela et al., 2014). These will be used for input load calculations for stance phase. To simplify the analysis, the Fx and Fy forces, which are minor in comparison to Fz, will be excluded in this study.

Variables	Leg	0% BWS	15% BWS	30% BWS
Vertical component				
1st peak (% BW)	Right	104 (4.65)[a,b]	86 (6.77)[a,c]	73 (7.01)[b,c]
	Left	104 (5.98)	87 (8.06)	75 (7.71)
2nd peak (% BW)	Right	93 (4.33)[a,b] 95	76 (4.69)[a,c]	66 (4.88)[b,c]
	Left	(5.08)	76 (5.61)	67 (5.67)
Valley (% BW)	Right	76 (5.87)[a,b] 75	67 (3.78)[a,c]	60 (4.82)[b,c]
	Left	(6.31)	67 (5.57)	60 (5.13)
Weight acceptance	Right	5.78 (1.27)	5.72 (1.90)	5.82 (2.05)
rate (BW/s)	Left	6.07 (1.57)	6.05 (1.99)	5.81 (1.91)
Push-off rate	Right	4.66 (0.70)[a,b]	3.20 (0.89)[a,c]	2.33 (0.52)[b,c]
(BW/s)	Left	4.86 (0.87)	2.89 (0.78)	2.31 (0.53)
Anterior-posterior component				
Deceleration peak	Right	−12.3 (3.33)[a,b]	−8.2 (3.08)[a,c]	−5.5 (2.14)[b,c]
(% BW)*	Left	−12.9 (3.01)	−9.1 (3.91)	−6.8 (2.59)
Acceleration peak	Right	12.7 (1.43)[a,b]	8.9 (1.56)[a,c]	7.3 (1.44)[b,c]

Figure 24: Vertical Ground Reaction Force as body weight percentage *(Barela et al., 2014)*

The vertical ground reaction force is based on the full weight of the robot and user. It is important to note that in practice, the robot would not support the full weight of the user, as this LLE was designed to be used with crutches. In this case, however, to test the design, the ground reaction forces will be based on the full weight of both robot and user.

$$F_z = 9.81(m_{structure} + m_{user})BWS \quad (8)$$

Equation 8: Fz (during stance phase)

Equation 8 was used to calculate the Fz values at the different stages of stance phase. $m_{strucure}$ symbolises the mass of the structure, m_{user} is the mass of the user. BWS is the body weight percentage with zero support taken from the table in Figure 23. For the user, a mass of 70kg was used, which is the average body mass of a healthy adult male (Fryar et al., 2021). Results are shown in Table 4.

Table 4: Stance phase ground reaction input forces

	Heel Strike (weight acceptance)	**Foot flat (1st peak)**	**Mid Stance**	**Heel off (2nd peak)**	**Toe off (Push off)**
$m_{structure}$ (kg)	9,164	9,164	9,164	9,164	9,164
m_{user} (kg)	70	70	70	70	70
0%BWS	0.0578	1.04	0.76	0.98	0.0466
Force (N)	**45**	**808**	**590**	**722**	**36**

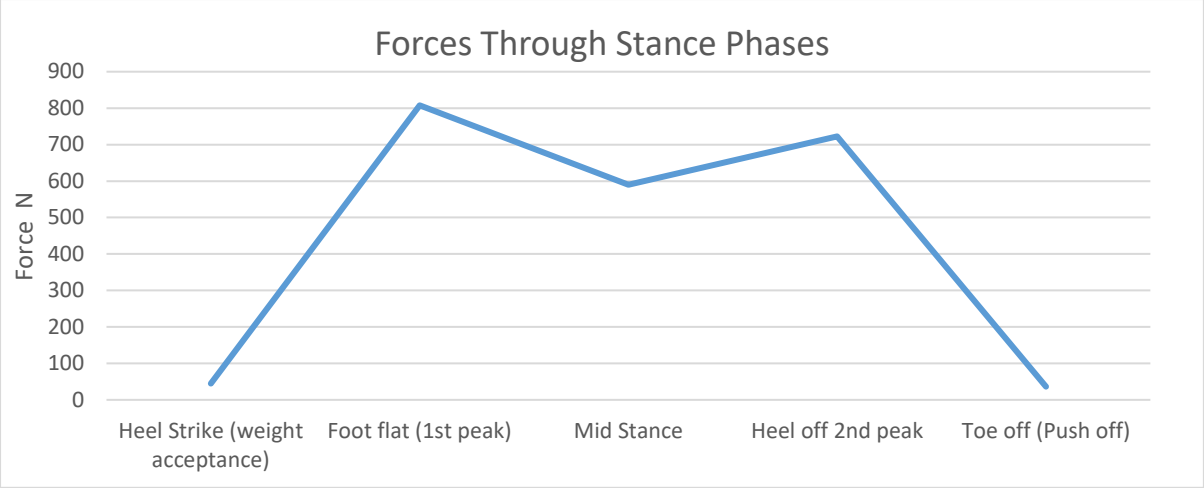

Figure 25: Graph of vertical ground reaction input forces through stance phase

The maximum force of 807N is experienced during foot flat stage. The data in Table 4 was used to create the force vs stance phase graph in Figure 25, which shows a typical m-shaped Fz GRF graph. These forces will be used as input data for FEAs required for material selection and topology optimisation. As these are the loads the LLE would experience during the stance phase of gait.

3.2.2. Swing phase analysis

Swing phase analysis helps to understand the forces and torques acting through the legs during swing, as well as the torque required from a motor at the joints to lift the legs. For this analysis, inverse dynamics calculations or electromyography (EMG) using muscle sensors are used. For this thesis, inverse dynamics calculations will be employed. This starts by looking at the robot legs during the swing phase as an open chain two-dimensional planar double pendulum.

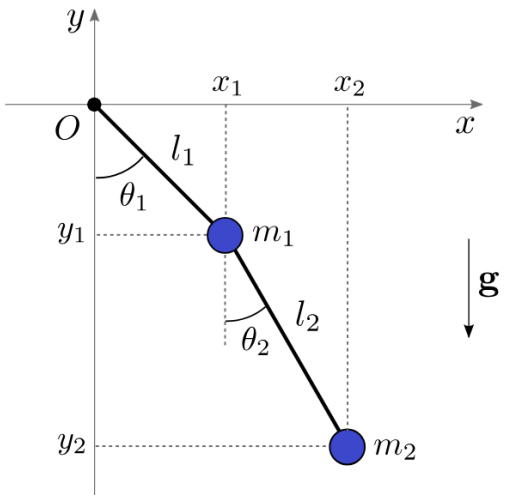

Figure 26: Double pendulum free body diagram *(Assencio, 2014)*

Consider the double pendulum shown in Figure 26. Each pendulum consists of a mass at the joint connected to a massless rigid link that only moves along a vertical plane. The pivot of the first pendulum is fixed to a point. To simplify the analysis all motion is considered as frictionless. The fixed point, which is the hip to waist bracket / hip joint, will be taken as the origin of a cartesian coordinate system. Θ_1 and Θ_2 are angles that the thigh and shank links make with the vertical direction, respectively. The following parameters are used:

l_1: Length of thigh link.

l_2: Length of shank link.

m_1: Mass of thigh link plus mass of human thigh for the average male adult.

m_2: Mass of shank link and foot support, plus mass of human shank and foot, for the average male adult.

Θ_1: The angle between the thigh link and the vertical. This varies at different stages of swing phase. Refer to the table in Figure 26.

Θ_2: The angle between the shank link and the vertical. This varies at different stages of swing phase. Refer to the table in Figure 26.

Table 5: Swing phase analysis input data

	Swing Phase:			
	Early Swing (acceleration):	**Mid Swing:**	**Late Swing (deceleration):**	**Source**
Hip Θ1	20° of flexion	30° of extension	30° of flexion	(Kapelovich, nd) (Tang et al., 2022)
L1 (m)	0,406	0,406	0,406	Refer to Table 3
m1 - Thigh link (kg)	1,549	1,549	1,549	Refer to Table 3
m1 - Thigh (kg)	9,912	9,912	9,912	(de Leva, 1996)
Knee Θ2	60° of flexion	30° of flexion	0° of flexion	(Kapelovich, nd) (Tang et al., 2022)
L2 (m)	0,432	0,432	0,432	Refer to Table 3
m2 - Shank link (kg)	1,347	1,347	1,347	(de Leva, 1996)
m2 - Shank (kg)	3,031	3,031	3,031	(de Leva, 1996)
m2 - Foot support (kg)	0,563	0,563	0,563	Refer to Table 3
m2 - Foot (kg)	9,408	9,408	9,408	(de Leva, 1996)

From the data in Table 5, the torque acting at the hip and knee joints at the three stages of swing phase, T, can be calculated using the Lagrangian inverse dynamics formula. In equation 9, L is the Lagrangian and $\dot{\theta}$ is the angular velocity.

$$\tau = \frac{d}{dt}\frac{\delta L}{\delta \dot{\theta}} - \frac{\delta L}{\delta \theta} \quad (9)$$

Equation 9: Inverse Dynamics Torque Formula

The Lagrangian can be calculated as the difference of the kinetic (T) and potential energy (V).

$$L = T - V = \frac{1}{2}m\dot{x}^2 + mgx \quad (10)$$

Equation 10: Lagrangian energy formula

Torque / force results from these calculations are shown in Table 6. Figure 27 shows the force vs swing phase graph. These values represent the torque required from the motor to move the links. The negative torque values indicate the direction of motion.

Table 6: Swing phase input forces per joint

	Early swing	Mid swing	Late swing
Theta	-15	2	20
Knee joint – Force N	-105	138	144
Hip joint – Force N	-369	508	515

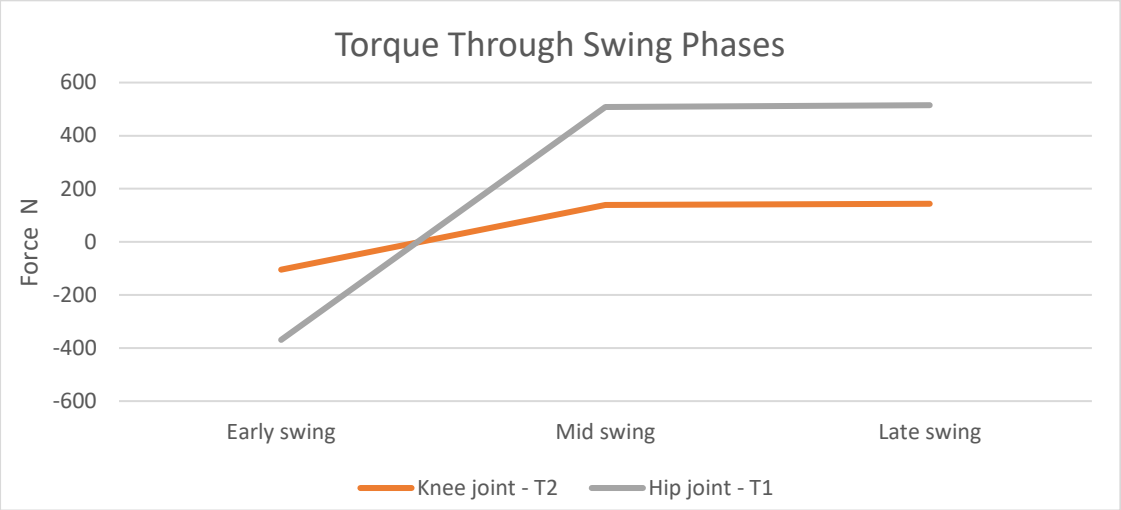

Figure 27: Graph of input torque through swing phase

The torque required at the hip joint to move the thigh link is more than double the torque required at the knee joint to swing the shank link. The greatest torque for both joints occurs at late swing. This data will be used as input for FEA simulations for material selection and topology optimisation. As these are the loads the LLE structure will experience during the swing phase of gait.

3.3. Material Selection

Proper material selection can allow for a lighter design without compromising on performance. There are thousands of engineering materials to choose from; to select the most suitable material, the required material properties/characteristics of the component must be determined (Najam et al., 2018). These material properties/characteristics can be grouped into two categories, key primary characteristics and secondary characteristics. Primary characteristics are the most critical “non-negotiable” properties. These can be determined by understanding the performance requirements of the component: “What does the part need to do?”. “What kind of load will it bear?”. As well as the kind of environment it will be exposed to. This will provide a good indication of the primary characteristics the candidate material should possess. Secondary characteristics are not necessarily crucial to the performance of the component, but are important characteristics to consider, for example, affordability and manufacturability (George, 2014).

The exoskeleton structure experiences axial loading and cyclical loading in an atmospheric environment. It operates in close contact with the human body. The following material properties have been identified as primary characteristics:

- Bending and compressive strength – During the stance and swing phases of gait, the structure experiences bending and compression forces.
- Lightweight – As the goal of this project is to reduce weight and thereby improve the design.
- Fatigue resistance – Gait imposes repetitive cyclical loading on the structure.
- Stiffness – A structure that bends or flexes excessively can compromise the stability and the safety of the wearer.
- Biocompatibility – The structure operates in close contact with the wearer; therefore, it must be nontoxic and hypoallergenic.

The following material properties were identified as secondary characteristics:

- Affordability – LLEs are exorbitantly priced and unaffordable for the average patient. The cost of manufacturing the structure should remain low to encourage overall cost reduction of the LLE.
- Machineability – The material selected should be easily formed into the desired finished product.

3.3.1. Identifying Candidate Materials

The first step of material screening is conducted using the Ashby Strength vs Density chart (ref. Figure 28). Based on the requirements stated, only materials that are lighter than steel, have a minimum tensile strength of 100 MPa and perform well under cyclical loading will be considered

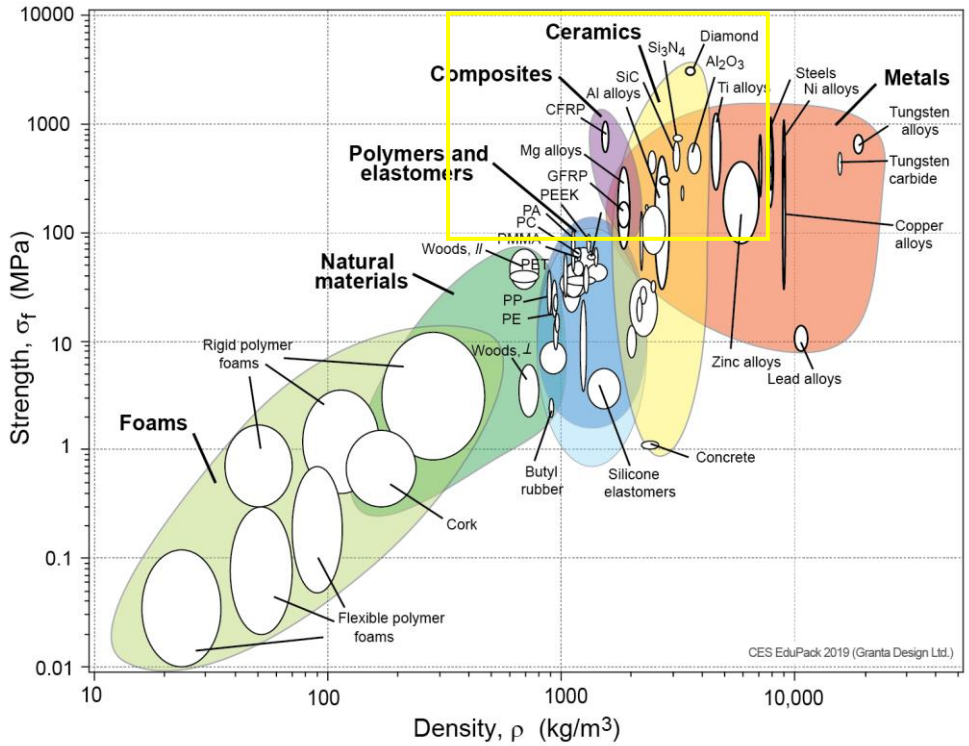

Figure 28: Strength vs Density (Ashby, 2020)

This narrows the search down to five groups of materials, titanium alloys, aluminium alloys, magnesium alloys, composite materials and polymers. These have been identified for their high specific strength. The lightest and strongest alloys/grades in these three groups will be analysed further.

3.3.2. Material Performance Index

Najam (2018) employs a material selection method that compares the performance index of candidate materials to select the most suitable. Performance index is calculated based on the core material properties (George, 2014). For the structure, the performance indices are compression strength, bending strength/stiffness and fatigue strength. Because the focus of this material selection is weight reduction, these material properties will be looked at in terms

of “weight ratios”. Secondary factors such as cost and manufacturability are of high importance and will be looked at in the manufacturing section.

The most important material property to consider is the strength-to-weight ratio (specific strength). A high specific strength means a lighter / smaller quantity of a material can provide a high amount of strength. This ratio is calculated using Equation 11, where the density of the material is ρ and σ is the yield strength of the material. *y* is the factor for volume and can be considered as 1 when comparing identical components.

$$M_1 = \frac{\sigma y}{\rho} \quad (11)$$

Equation 11: Strength to weight ratio

The second most important material property to consider is the stiffness to weight ratio. A high stiffness to weight ratio means that not only is the material strong and less likely to fracture under load, but it is also less likely to bend or buckle. This ratio is shown in Equation 12, where E is the Young’s Modulus of the material:

$$M_2 = \frac{E^{0.5}}{\rho} \quad (12)$$

Equation 12: Stiffness to weight ratio

Lastly is material fatigue strength. A high fatigue strength-to-weight ratio means the material is likely to have high fatigue life and can undergo many cycles before fracture occurs. In In Equation 13, K_{1c} is the fracture toughness of the material.

$$M_3 = \frac{K_{1c}}{\rho} \quad (13)$$

Equation 13: Fatigue strength to weight ratio

The performance index is the sum of the three ratios listed. Each property ratio will first be multiplied by a “priority number”, which magnifies the level of importance of that property in the material selection, with 3 being the most important and 1 being the least. In this case, compression strength takes first property, followed by bending strength and fatigue strength (Najam et al., 2018) (George, 2014). Performance index (Z) is then calculated in the manner:

$$Z = 3M_1 + 2M_2 + 1M_3 \quad (14)$$

Equation 14: Performance index equation

Table 7: Material performance matrix

Material	Density (g/cm³)	Yield Strength (MPa)	Young's Modulus (GPa)	Fatigue Strength (MPa)	M1	M2	M3	Performance Index
Aluminium AA7075	2,81	460	71	160	163,70	3,00	56,94	554,04
Aluminium AA6061	2,7	240	68,9	96	88,89	3,07	35,56	308,37
Aluminium AA7050	2,82	460	72	200	163,12	3,01	70,92	566,30
Aluminium AA7068	2,79	480	73	159	172,04	3,06	56,99	579,24
Magnesium AZ31C	1,78	130	45	70	73,03	3,77	39,33	265,96
Magnesium ZK60A	1,83	290	45	120	158,47	3,67	65,57	548,31
Magnesium WE54A	1,83	180	44,4	98 - 130	98,36	3,64	62,30	364,66
Magnesium ZK61A	1,81	290	45	120 - 140	160,22	3,71	71,82	559,90
Magnesium AZ91D	1,81	200	45	90	110,50	3,71	49,72	388,63
Ti-6Al-4V (Grade 5) Titanium	4,43	900	110	350	203,16	2,37	79,01	693,22
Ti-3Al-2.5V (Grade 9) Titanium	4,48	830	110	350	185,27	2,34	78,13	638,61
KetaSpire KT 820CF30 PEEK	1,3	100	3,6	50 - 150	76,92	1,46	76,92	310,61
Victrex PEEK 450 CA30	1,52	100	3,5	50 - 150	65,79	1,23	65,79	265,62
Carbon Fibre Reinforced Composite	1,50	2500	230	100 -300	1428,57	8,67	114,29	5153,55
UHMWPE	0,93	20-40	0,6-1,3	15-30	32,26	1,05	24,19	123,1

In Table 7, the performance index of 16 different candidate materials was calculated. carbon fibre composites had by far the greatest performance index, nearly 6 times greater than its closest counterparts, titanium. Ti-6Al-4V yielded the highest PI of the titanium alloys. In fifth place, AA7068 proved to be the best aluminium alloy, outperforming AA7050 and AA7075. Magnesium ZK61A closely followed the aluminium alloys. The polymers presented the lowest PI, nearly half that of magnesium. The top-performing materials of the top three groups will

undergo further FEA analysis, namely, carbon fibre reinforced composite, titanium Ti-6Al-4V and aluminium AA7068.

3.3.2.1. Carbon Fibre Reinforced Composite

Although having by far the highest PI, it is important to note that its performance index is a "best case scenario" or a representation of the potential of CFRC. The material properties of composite parts, such as CFRC, cannot be directly compared to those of other materials, like steel, aluminium, or plastic. These materials are homogeneous and isotropic, with properties that are the same at all points and along all axes. CFRC parts are neither homogeneous nor isotropic but anisotropic in nature. CFRC performs poorly in multi-directional load bearing, easily failing to carry loads applied across the fibres, but performs exceptionally well in carrying loads along the direction of the fibres (Anon, 2025). Being an anisotropic, CFRC's performance index would vary drastically based on the construction of the component and the direction the load is applied. (Lindsey et al., 2023). It is also important to note that, unlike metals, CRFC lacks significant plastic deformation before fracture, which means it often fails abruptly and without warning (Oomi, 2024).

However, CFRC can be manipulated to produce more favourable and reliable results. Employing quasi-isotropic layup to manufacture the components would increase in-plane isotropic behaviour. As well as aligning the fibres with the direction of the applied loads (swing / GRF loads). More specifically, the quasi-isotropic laminates are layered in the xy-plane, and the swing load is acting along the x-axis, and the GRF load is acting along the y-axis. This would also require that the forces in the z-axis are negligible or non-existent. laminate is balanced and symmetric with evenly distributed fibre angles (e.g., 0/+45/-45/90 with thin plies), and the structure is loaded primarily in-plane, an effective isotropic modulus can approximate global stress distribution. Under these conditions, the risk of directional failure is reduced compared to a highly anisotropic laminate.

3.3.2.2. Aluminium AA7068

Exhibits exceptional mechanical properties due to its high zinc content. AA7068 stands as the strongest commercially available aluminium alloy, initially developed for military applications, and is now undergoing evaluation for adoption in diverse markets, including aerospace and automotive industries. This alloy was specifically formulated to offer superior strength and serve as a high-strength replacement for AA7075. (Karthikeyan et al., 2024)

3.3.2.3. Titanium Ti-6Al-4V

Known for its excellent fatigue resistance, titanium Ti-6Al-4V is a popular choice for aerospace and medical applications. It performs well under cyclical loading due to its high strength and

toughness. The alloy typically has a fine microstructure, which contributes to its good fatigue properties (Morrissey et al., 2005). It is also biocompatible; with extensive application it is well suited for close home contact. Although considered expensive, it is a widely available material with vast global usage. (Jaynes, 2024)

3.4. Stress Analysis

Finite element analysis simulations were conducted using Abaqus to establish the Von Mises stress and displacement that occurs in each component across the three candidate materials. This is done when the working loads or gait forces obtained in section 3.2. for stance and swing phase are applied.

The waist bracket, thigh and shank links experience complex dynamic cyclic loads. The loads are multi-directional and fluctuate from phase to phase. Swing loads act horizontally in the x-axis, and GRF act vertically in the y-axis. This results in bending, compression and possibly torsional stresses in the components. The Von Mises stress is chosen as the stress criterion in this study, because of the isotropic and ductile nature of the chosen materials, aluminium and titanium. Von Mises will provide an equivalent stress for the bending, compression and torsional stresses the components experience.

CFRC is neither ductile nor isotropic. However, under ideal manufacturing and loading conditions (such as quasi-isotropic laminate layup and load application along the length of the fibres), the risk of directional failure is reduced compared to a highly anisotropic laminate, and CFRC would behave more isotropically. However, this is still an oversimplification of the material properties and behaviour of CFRC.

The purpose of this is to evaluate the candidate materials' yield stress to the Von Mises stress, which aids in determining if a material is strong enough to carry the load and establishing the factor of safety (FOS). Max displacement is important for understanding the amount of deflection that can occur under the applied loads. Minimal deflection, which is a reflection of high stiffness in a material, is critical in the design of LLE structures and ensures sturdiness and stability.

3.4.1. FEA Model

Below is the step-by-step setup of the Abaqus model used to run the stress analysis on the three components. Refer to Appendix A for more details. Multiple simulations were run in this section, with the waist bracket, thigh link, and shank link all tested in three different candidate materials.

3.4.1.1. Geometry

- To simplify the model, changes were made from the original design. Certain features that were relatively not critical for the overall outcome of the FEA were removed. This is to reduce meshing complexity and processing time.
- All bolt holes were removed, with the exception of the main joint holes along the rotating axis. Small noncritical steps and grooves were removed along the actuator housing, and joint holes were removed. This was done to simplify meshing.
- The length adjustment / telescopic features were removed, and models were redrawn as one solid feature instead of two sub-assemblies (refer to Figures 17, 18, 19 and 29). Modelling sub-assemblies requires the introduction of contact pairing and surface interactions, which increases computational complexity.
- The connecting channels which were hollow, were filled out so that components, were solid uniform models. Solid geometries produce more stable, and uniform mesh, than hollow geometries. This improves convergence and accuracy during finite element analysis. Hollow shapes with thin walls, sharp internal features can lead to mesh distortion, stress singularities, or numerical instability.
- Drawings were made on SolidWorks and imported as Step files into Abaqus using Abaqus Standard, Explicit Model solver on.

3.4.1.2. Material Properties

- As mentioned above, the following three materials were used across the three models: aluminium AA 7068, titanium Ti-6Al-4V and CFRC.
- The materials were all set up with inputs of density, elastic properties, modulus of elasticity and Poisson's ratio. Note that all three materials were set as isotropic, although CFRC is anisotropic. This was done to simplify the simulation, as anisotropic materials are required to be built layer by layer, which amplifies the computational complexity of the model. (Refer to Figure 47).

  Modelling CFRC as an isotropic material in Abaqus assumes that the mechanical properties of CFRC are the same in all directions, which is an over-simplification (Djadoudi, 2025). This means Abaqus would employ the same Young's Modulus and Poisson's Ratio for all directions of the material, which eliminates critical behaviours like delamination and shear failure. (Sineri et al., 2015)

Although this type of modelling oversimplifies CFRC's anisotropic nature, it is a start toward understanding the approximate potential of CFRC under ideal conditions. (Anon, 2025)

Table 8: Material Specs

Material Property	**Aluminium AA 7068**	**Titanium Ti-6Al-4V**	**Carbon Fibre Composite (CFRC)**
Density kg/m^3	2850	4430	1550
Modulus of elasticity GPa	73	110	150
Poisson's Ratio	0,33	0,34	0,28

3.4.1.3. Assembly

- Create a part independent instance for each model.

3.4.1.4. Step Definition

- One Static General step is created, which is the "Loading Step". The total time for the step is one second, which is representative of one gait cycle. NIgeom is turned on. Automatic incrementation set as follows:

Table 9: Step Settings

Max number of increments	Increment size Initial	Increment size Minimum	Increment size Maximum
1000	0.01	1,00E+15	0.1

- Field Output Request domain is set to the whole model, and selected output variables are:
    - S, Stress components and variants
    - E, Total strain components
    - PE, Plastic strain components
    - U, Translations and Rotations
    - RF, Reaction forces and moments

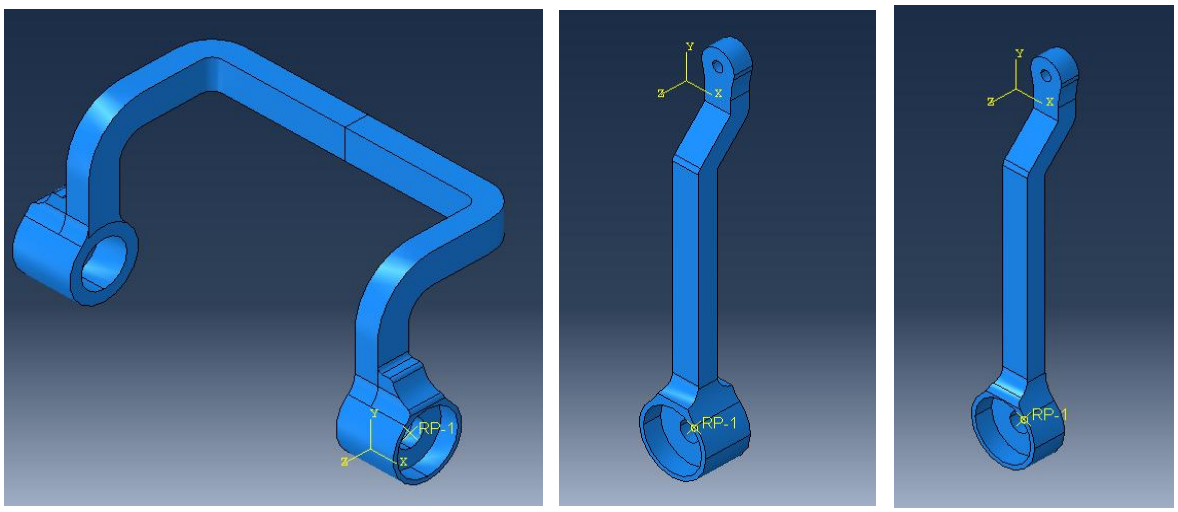

Figure 29: Waist bracket, thigh and shank link reference point location

3.4.1.5. Interaction Properties

A reference point (RP) is created at the axis of rotation of every joint where the forces are to be applied. The reference point is constrained to the inner surface of the joint hole via a rigid body coupling constraint, selecting the Pin (nodes) region type. (Refer to Figure 49)

3.4.1.6. Boundary Conditions and Loads

• One mechanical *Encastre* boundary condition is applied to each model on the opposite end to the load application point / created reference point. The boundary condition is applied to the joint hole inner surface and set to *Encastre*. This prevents movement or rotation in any direction. The boundary condition is set active in both the Initial and created Loading step. (Refer to Figures 50 and 51). This is to globally fix the component. As per Newton's first law of motion, without and *Encaster* boundary condition set in every step the object will move when a load is applied without experiencing any stress of plastic deformation.

- Two concentrated force loads, namely Ground Reaction Force (GRF) and Swing Force, are created on every model and are both applied to the reference point. Amplitude loading is used for both these concentrated loads to simulate cyclic loading.

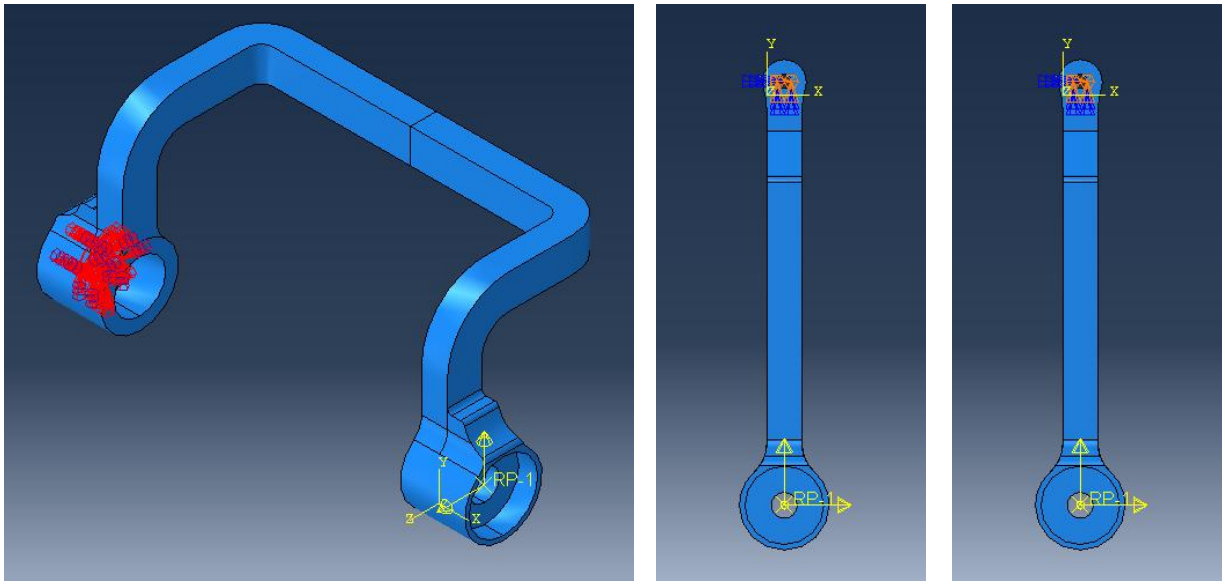

Figure 30:Waist bracket, thigh and shank link fixed boundary condition location

- The GRF load replicates the vertical component ground reaction forces experienced during stance phase gait, this replicates the ground reaction to the weight of the robot and the user. For each model, the force is acting along the Y axis, hence CF2 is set to 1 (CF1 and CF3 are set to zero). A tabular amplitude is created for load GRF, and the gait data is input here.

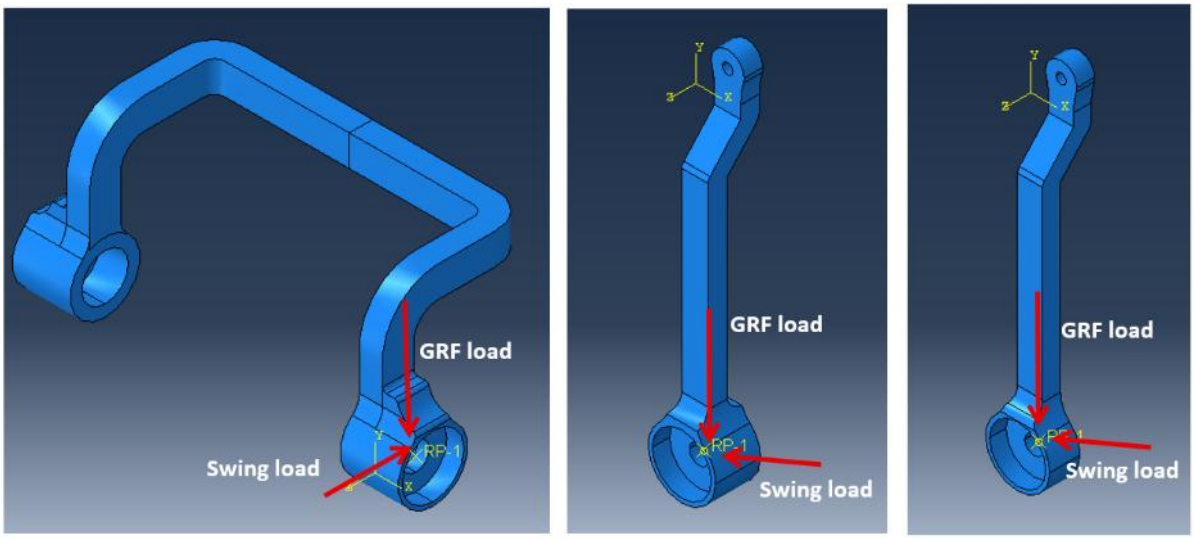

Figure 31:Waist bracket, thigh and shank link load application

- The swing load replicates the load experienced due to the motor's applied torque. This is to create the motion of lifting the leg during swing phase. This motion is angular and happens in a direction from the vertical position of the leg towards a horizonal position of the leg. Because the swing component force is in the horizontal axis, the X axis

(CF1) is set to 1 (CF2 and CF3 are set to zero) for the thigh Link and Shank model only. The global axis of the waist bracket is different, simply because of the orientation in which it was drawn. The Z- axis (CF3) is set to 1 (CF1 and CF2 are set to zero).

- A tabular amplitude is created for Swing loads with the gait data calculated.
- One second has been set as the time period for one full gait cycle, hence the time for each phase, of which there are eight (GRF and Swing combined) amplitudes increments of 0.125seconds. The step alternate in the same manner, the five varying loads experienced in stance phase, followed by the 3 varying swing loads.
- The GRF and Swing load are both only active in the created Loading step
- The Knee and hip joint experience different swing loads, refer to Figures 32 and 33

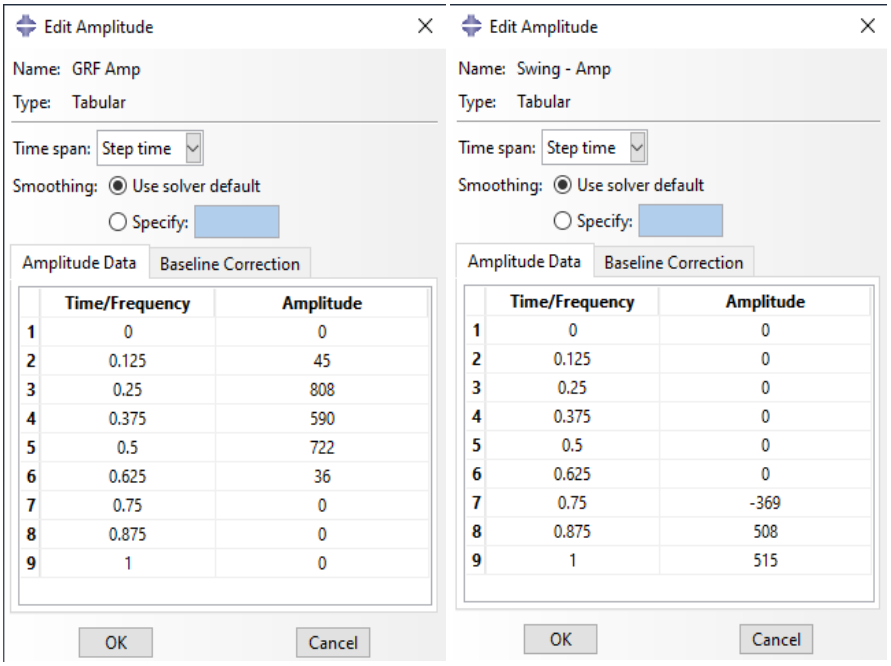

Figure 332: Amplitude load set up for Waist Bracket and Thigh Link

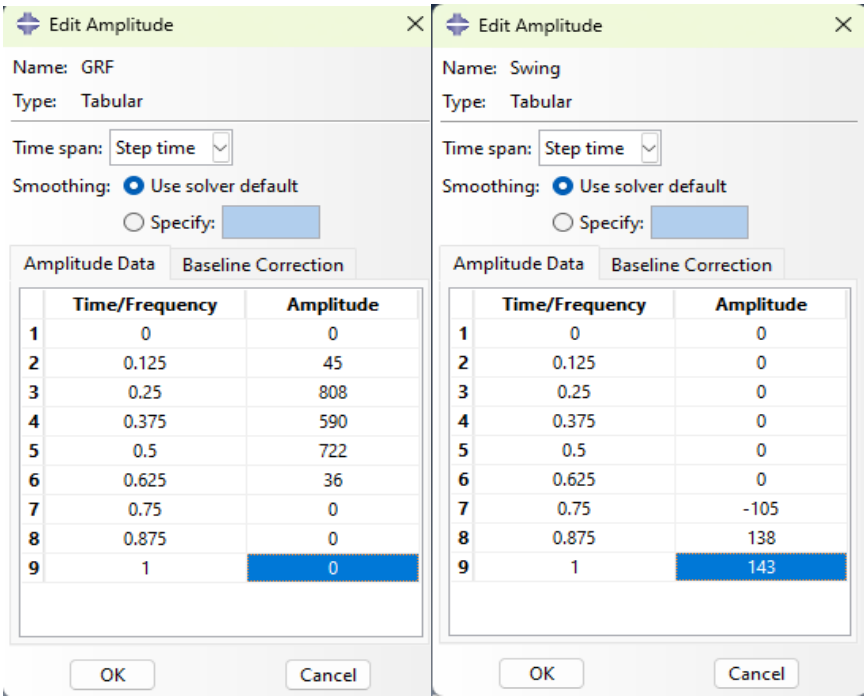

Figure 323: Amplitude load set up for Shank Link

3.4.1.7. Meshing

- All models were seeded with an approximate global size of 0.005, with curvature control maximum deviation factor set to 0.1. The mesh element shape was set to tetrahedral with the default algorithm for the whole model. Element type, standard element library used and quadratic geometric order. (Refer to Figures 52, 53 and 54 for more details)

- To find the optimum mesh for each model mesh conversion was conducted. Although a simulation may run successfully, fine mesh provides more accurate or reliable results than course mesh very fine mesh can significantly increase computational time. For these simulations, computation time varied from 1hour to 48 hours. However, only tetrahedral mesh was successfully meshing the part due to the complexity of the geometries. Partitioning wash helpful in achieving a hex-dominate mesh, however simulations would fail immediately due to distorted nodes.

- The simplification of the geometrical adjustments mentioned in section 3.3.1 made the three models' meshing process significantly simpler. No partitioning or special edge seeding was required on any of the models. (Refer to Figures 55, 56 and 57 for more details)

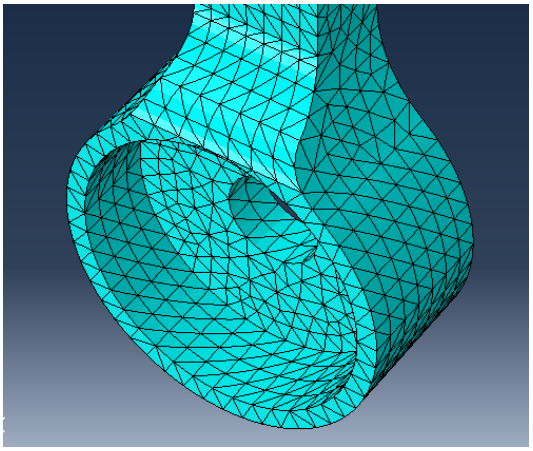

Figure 34: FEA model mesh

3.5. Topology Optimisation

In this section topology optimisation FEA models are set up on Abaqus with the goal of reducing the component weights while maintaining structural integrity. Similar to the stress analysis simulation set up. The criterion are Von Mises stress, displacement and percentage volume reduction.

The geometric changes made are particularly important for the topology optimisation. When conducting topology optimisation to reduce the weight of a structure, starting with a simple solid shape is beneficial because it provides the algorithm with maximum design freedom. A solid domain allows the optimiser to explore the full material space and remove unnecessary regions without being constrained by pre-existing voids. This approach improves numerical stability, ensures better load distribution, and avoids biasing the solution with premature design assumptions. Ultimately, beginning with a solid shape enables the discovery of more efficient and innovative structural configurations that might not emerge from a hollow starting geometry.

3.5.1. FEA Model

Making use of the same model as, all steps remain the same, and an optimisation task was created prior to running the optimisation job. Below are the steps taken to create a FEA topology optimisation model on Abaqus. (Refer to Appendix B)

3.5.1.1. Boundary condition

A secondary boundary condition was introduced on each model on the axis of the rotation hole, in the same location where the load is applied. This boundary condition is created to “freeze” this zone during the topology optimisation; otherwise, the system will remove the radial hole completely. Inform the program that the key areas in each model are the axial hole where the load is applied and the axial hole with the fixed boundary condition. In other words, the system can be told not to remove material in the regions where boundary conditions exist.

This is a mechanical displacement/rotation boundary condition made active only in the created loading step. Once the surface area is selected, U3 (Z-axis) is set to a value of one and U1, U2, UR1, UR2, and UR3 are all set to zero. This has no impact on the loads applied to the model as motion does not take place in the z-axis.

3.5.1.2. Optimisation task

- A topology optimisation task was created, selecting the whole model and freezing the load region and boundary condition region. This is to inform the system that these are critical surfaces and not to remove material in these regions. (see Figure 58)

3.5.1.3. Design responses

- Two single term design responses were created, one for volume and the other for strain energy. Volume represents the amount of material used in the design space. By minimising volume, the weight of the model will be reduced. Strain energy represents how the structure stores and distributes mechanical energy under load. Maximising strain energy ensures that the remaining material has enough stiffness and load-bearing capacity. Without the volume design response, the system may not remove material with the goal of reducing weight. Without the strain energy design response, the system could remove too much mass, neglecting the structural strength requirements. (see Figure 59)

- The whole model was selected for both design responses so that volume/weight reduction and maximising the strain energy are applicable throughout the whole model.

3.5.1.4. Objective Function

- An objective function was then created with a set target of “minimise design response values”; the volume design response was then selected. Thereafter, a second objective function is created for the strain energy and set to “minimise design response value”. (see Figure 60)

- An optimisation constraint was created, and the volume design response was selected. The constraint was set to “*A fraction of the initial value <= 0.5*”. This means that the volume should be reduced to less than 50% of the model’s original volume.

- Several iterations were run, each time reducing the constraint of the volume design response to less than 40%, 30% and then 20%. This is to understand how much volume can be reduced before the model fails.

3.5.1.5. Optimisation Process Job

Under the job module, an optimisation process was created. The maximum number of cycles was set to 50 and “data save” was set to “last”. The process was then submitted.

3.5.2. Topology Refinement

The Abaqus topology optimisation is likely to produce an organic/complex geometry model which includes rough surface, sharp transitions. This is due to its element-based process, where the mesh size influences the output geometry. Although weight reduction would be achieved, some aspects of the geometry could be impractical and costly to manufacture (Junk et al., 2019).

Refinement is required to ensure cost effective manufacturability, compatibility for assembling and ensure all design requirements are met. Therefore, the material will be refined/redrawn on SolidWorks, and a third Abaqus simulation will be run using the same input loads. This is to ensure the refined structure still retains structural integrity. This may result in a slightly heavier model than the raw-optimised model.

3.6. Manufacturing Process

This section looks at the manufacturing processes required to produce the designed structure based on the selected material and optimised topology. Selecting the correct manufacturing process is key to producing a quality product that meets performance requirements and keeping production costs low (Munro, 2023). Often, more than one manufacturing process is required to manufacture the end product. The key influencing factors to consider when determining the best process are:

- **Material**: The material used is an extremely important factor, as certain materials only allow for certain manufacturing processes. For example, steel cannot be injection moulded (Munro, 2023). Some manufacturing processes alter the mechanical properties of the material

- **Geometry**: Methods to produce complex shaped structures will differ from simple structures (Junk et al., 2019).

- **Manufacturing cost:** This is often comprised of the cost of equipment/machinery, special tooling, manning (is special skills required) and other resources such as electricity. This also includes waste production that the process allows, which is an

indication of how much input material is required to produce the end product. (Rasheed, 2022)

- **Volume and time**: Processing time looks at how quickly the product can be produced. Some processes are better suited for large volume production, whereas some are only practical for low volume prototyping (Rasheed, 2022).

- **Precision and tolerances:** Certain manufacturing processes can achieve tighter tolerances than others (Rasheed, 2022).

The three different candidate materials and their suitable manufacturing processes are reviewed.

3.6.1. Carbon Reinforced Fibre Composite

In a CFRC, strength resides along the axis of the fibres, and thus fibre density and orientation greatly impact mechanical properties (Anon, 2025). It is possible to manufacture organic-shaped components using CFRC that can support complex loads, including cyclical loading (Anon, 2018). This has been achieved through components such as medical prosthetics, aircraft wings, and chassis. For the manufacture of complex/organic shaped CFRC only one manufacturing method is suitable, namely lay-up, and more specifically quasi-isotropic layup.

The first step would be to select a suitable fibre and resin for the composite product. Carbon fibre reinforcements come in a variety of weaves, braids, and other formats, such as tow and unidirectional. These are combined with various resins to produce carbon fibre-reinforced composites in a wide range of shapes and fibre patterns (Anon, 2025). High-quality moulds are created, typically from materials like aluminium or steel, to shape the carbon fibre (Zhang, 2024).

Lay-up Process: the most important step in the manufacturing process. Layup ensures that the component can carry multidirectional loads by layering pre-resin impregnated carbon fibre fabric and orienting the fibres in specific directions to optimise performance. This is a task meticulously done by hand into or around a mould to ensure proper fibre orientation and resin distribution (Anon, 2018)

The mould is placed in an autoclave or oven to cure the resin, bonding the carbon fibre layers together. This process involves carefully controlled temperature, pressure, and time to achieve optimal results (Anon, 2018). Developing reliable and cost-effective joining techniques is

crucial, especially when dealing with multi-axis loads. Techniques such as adhesive bonding, mechanical fastening, and hybrid joining methods are commonly used (Yadav et al., 2025). This is because there are many risks that come with conventional joining methods. Drilling holes for fasteners for can cause delamination of layers of carbon fibre, leading to separation and weakening the structure (Olliges, 2018).

After curing, the component is removed from the mould and undergoes additional finishing touches such as sanding, trimming, and coating. Carbon fibre can degrade over time when exposed to UV radiation and moisture. Protective coatings are often needed to mitigate these effects (Annon, 2018).

- **Geometry:** A Lay-up manufacturing process allows for the creation of lightweight, strong, and durable CFRC components with relatively complex shapes, suitable for structural applications.
- **Manufacturing Cost**: CFRC is more expensive to produce than traditional materials like steel or aluminium due to the complexity of the manufacturing processes. This could increase the already high cost of manufacturing a Lower limb exoskeleton (Oomi, 2024).
- **Time and volume:** The process is also time consuming and not suitable for high-speed mass production (Oomi, 2024).
- **Precision and tolerances:** Precision is relatively lower with CFRC lay-up compared to the precision which can be achieved through metallic manufacturing processes (Hussain et al., 2021).

3.6.2. Aluminium

The most effective manufacturing methods for producing complex shaped aluminium components include Selective Laser Melting (SLM), casting and machining (Junk et al., 2019).

SLM: An additive manufacturing method, useful for its ability to create intricate, lightweight structures that traditional methods like casting or machining cannot achieve effectively. Although Selective Laser Melting (SLM) is an ideal additive manufacturing method for aluminium structures, it also presents many disadvantages. The largest setback, however, is that not all alloys are suitable for SLM. SLM favours alloys like Al-Si10Mg due to their weldability. High-strength alloys, such as AA7068, are prone to cracking during SLM. This defeats the primary purpose of producing an optimum high-strength, lightweight, organic-

shaped structure. SLM-fabricated aluminium parts may present defects such as porosity and surface irregularities caused by suboptimal process parameters or material properties. This may reduce the mechanical strength and surface quality of the end product. Research and advancements in SLM technology continue with the aim of reducing these challenges and making it more viable for diverse applications (Fereiduni et al., 2020).

- **Geometry**: SLM allows for the production of complex geometries that are often required by topology optimisation algorithms to minimise material usage while maintaining structural integrity (Junk et al., 2019).
- **Manufacturing Cost**: SLM is a meticulous process, and a lot of precision is taken to minimise defects. To achieve optimal results, expensive high-purity powders and precise calibration of process parameters are required (Fereiduni et al., 2020).
- **Precision and tolerances:** Relatively good precision can be achieved at lower levels when compared to machining (Fereiduni et al., 2020).
- **Time and Volume:** The layer-by-layer fabrication approach makes it a slow process, not suitable for large volume high-speed production (Fereiduni et al., 2020)

Casting: Like SLM, casting is prone to producing defects, such as porosity, which can act as stress concentrators and reduce fatigue life (Hong et al., 2023). Lastly, high strength aluminium alloys such as AA7075 and AA7068 may experience hot tearing and other defects during casting. Proper process optimisation is necessary to minimise these issues (Thorat, nd).

- **Geometry:** This process allows for the production of complex, intricate shapes, including internal cavities and is suitable for a wide range of aluminium alloys, including AA7068 and AA7075. (Thorat, nd)
- **Manufacturing Cost:** Can be a far more affordable process compared to SLM and machining. (Thorat, nd)
- **Time and Volume:** High speed process, ideal for large volume production. (Thorat, nd)
- **Precision and tolerances:** Lower levels of precision are achieved compared to machining (Thorat, nd)

Machining: A subtractive manufacturing process. Idea for high-strength aluminium alloys. Due to the fine, uniform microstructure and minimal defects, machined aluminium components typically exhibit the best resistance to fatigue failure, compared to SLM and casting (Hong et al., 2023).

- **Geometry**: Machining allows for the production of very complex geometries and smooth finishes. (Hong et al., 2023).
- **Manufacturing Cost:** This process is relatively affordable for rapid prototyping, which is often the need for LLE. (Hong et al., 2023).
- **Time and Volume:** Low volume, slow speed, ideal for rapid prototyping (Hong et al., 2023).
- **Precision and tolerances:** Very high precision and tight tolerances can be achieved with machining of aluminium alloys. (Hong et al., 2023).

3.6.3. Titanium

For manufacturing complex shaped titanium components, Laser Powder Bed Fusion (LPBF) and Electron Beam Melting (EBM) are among the best additive manufacturing techniques, along with Directed Energy Deposition (DED). Other traditional techniques include casting and machining.

LPBF and EBM: This method is particularly effective for titanium alloys, such as Ti-6Al-4V. The LPBF process uses a laser to melt titanium powder layer by layer, allowing for precise control over the material distribution, which is essential for implementing topology optimisation (Orme et al., 2017). Electron Beam Melting (EBM) is another effective method, especially for producing larger titanium components. EBM utilises an electron beam instead of a laser, which is more effective in dealing with titanium's high melting point. This AM method is often used to produce titanium components for the aerospace industry. Additive manufacturing methods like LPBF and EBM for producing complex titanium structures come with several disadvantages. Similar to SLM, methods like LPBF and EBM are likely to produce porosity due to incomplete melting of the powder or improper fusion of melt tracks. This can lead to reduced mechanical properties, limiting the material's performance. The layer-by-layer manufacturing method results in anisotropic properties, where mechanical strength and fatigue resistance vary with the build orientation. This can complicate the design process and may require post-manufacturing rigorous testing. (Fereiduni et al., 2020)

- **Geometry**: Both techniques allow for the production of parts with intricate, organic shapes that are optimised for strength and weight reduction (Orme et al., 2017)

- **Manufacturing Cost:** Titanium is an expensive material, and the specific titanium powder suitable for these AM processes is even more expensive. LPBF and DMLS are energy-intensive processes, which further increase production (Saboori et al., 2017). Unfortunately, though effective, both Electronic Beam Melting and Laser Powder Bed Fusion are relatively expensive processes.
- **Time and Volume:** The build volumes of LPBF and DMLS machines are generally constrained to 1meter wide, making it difficult to produce large titanium structures without segmenting and assembling components (Anon, 2022)
- **Precision and tolerances:** Relatively good precision can be achieved with these AM, with LPBF producing the tightest tolerances for an AM. (Balasubramani et al., 2025)

DED: DED uses either titanium powder or wire and a high-powered energy source, such as a laser, to build up material layer by layer. This technique is often more cost-effective due to its relatively high deposition rate and the ability to work with larger volumes of material compared to other additive methods. Additionally, Hybrid Manufacturing methods, which combine additive processes like DED with traditional subtractive manufacturing (such as milling), offer a promising way to reduce costs while still achieving complex geometries. This hybrid approach can help refine the final part after it is initially built, offering high precision at lower costs. However, this process still involves a combination of technologies, which may limit its affordability compared to purely subtractive methods. (Saboori et al., 2017)

- **Geometry**: It also allows for complex shapes and functionally graded parts, making it a good fit for topology-optimised designs. (Balasubramani et al., 2025)
- **Manufacturing Cost:** Although high cost, DED is **a** more affordable AM method, an alternative to the more expensive powder-bed fusion methods, LPBF and EBM. (Saboori et al., 2017)
- **Time and Volume:** A much faster manufacturing process than LPBF and EBM (Balasubramani et al., 2025)
- **Precision and tolerances:** DED cannot achieve the tight tolerances of LPBF and EBM. Additional machining processes are often required to achieve tighter specs. (Balasubramani et al., 2025)

Casting: Investment casting is commonly used for titanium. For certain titanium components, casting is considered a more traditional and cost-effective method, as it remains more affordable than additive manufacturing. However, similar to AM processes, porosity and inclusions may occur, resulting in lower mechanical properties than wrought material. Casted titanium components also display better resistance to fatigue failure than LPBF (Orme et al., 2017).

- **Geometry**: Although casting works well for producing internal cavities, it can be limited in producing highly complex geometries. Casting methods like investment casting for titanium alloys could be useful for simpler, optimised shapes. (Wong, 2025)
- **Manufacturing Cost:** Far more affordable than AM processes. It could be more cost-effective than machining when producing larger volumes.
- **Time and Volume:** Fast manufacturing process. Suitable for medium- to high-volume production.
- **Precision and tolerances:** Moderate precision; a secondary machining process may be required to achieve tight tolerances.

Machining: Unlike aluminium, titanium alloy Ti-6Al-4V exhibits poor machinability because of its low thermal conductivity and high strength. This is often displayed as tool wear and a damaged workpiece. Although challenging, machining Ti-6Al-4V can be achieved through the proper selection of tools, lubricants, and cutting speeds. Another shortfall of this subtractive manufacturing process is the waste of material, which can be very costly for Ti-6Al-4V. (Abdulgadir et al., 2019)

- **Geometry**: Can produce very complex shaped components.
- **Manufacturing Cost:** Machining Ti-6Al-4V can be very costly due to high tool wear, expensive raw material waste, and its labour-intensive nature. It can be more cost-effective than casting when producing low-volume prototyping
- **Time and Volume:** This is a slow process most suited for prototyping.
- **Precision and tolerances:** Achieves very high precision and tight tolerances.

4. RESULTS

In this section, the results of the stress analysis and topology optimisation for the three components, waist bracket, thigh link and shank link are presented. For the stress analysis, the focus is on the Von Mises stress due to compression and bending stresses, as well as the maximum strain/displacement. For the topology optimisation, the focus is on percentage volume reduction, as well as the Von Mises stress and displacement at the reduced volume. Lastly, the FEA results for the refined topology are reviewed as well as force impact during the phases of gait.

4.1. Stress Analysis

Multiple FEA simulations were run of the three components, in the three candidate materials, aluminium AA7068, titanium Ti-6Al-4V and CFRC. The maximum Von Mises stress is expected to vary slightly across the three materials. A greater variation in max deflection and factor of safety is expected. Results are presented, refer to Figures 35, 36, and 37.

4.1.1. Waist Bracket

Table 10: Waist Bracket FEA Results

Waist Bracket	Aluminium AA7068	Titanium Ti-6Al-4V	CFRC
Max Von Mises Stress	68.83 Mpa	68.84 Mpa	69.52 Mpa
Max Deflection	$7.458e^{-3}$ mm	$4.970e^{-3}$ mm	$3.589e^{-3}$ mm
Factor of safety (FOS)	7	12	36

Across all three materials, the location of the maximum stress appears along the sharp 90° corner created by the rectangular frame. Refer to Figure 35. The FOS, as seen in Table 10 is 7 for aluminium and peaks at 32 for CFRC. This is based on the maximum Von Mises stress and the material yield stress (refer to Table 7). Little to no stress was found around the motor/actuator housing. All the stress appears to be on one side of the bracket, more specifically on the applied load side, opposite to the fixed boundary condition end. This shows signs of torsion and shear stress. In real world applications, because each leg alternates in producing the same motion, this type of stress would be symmetrical.

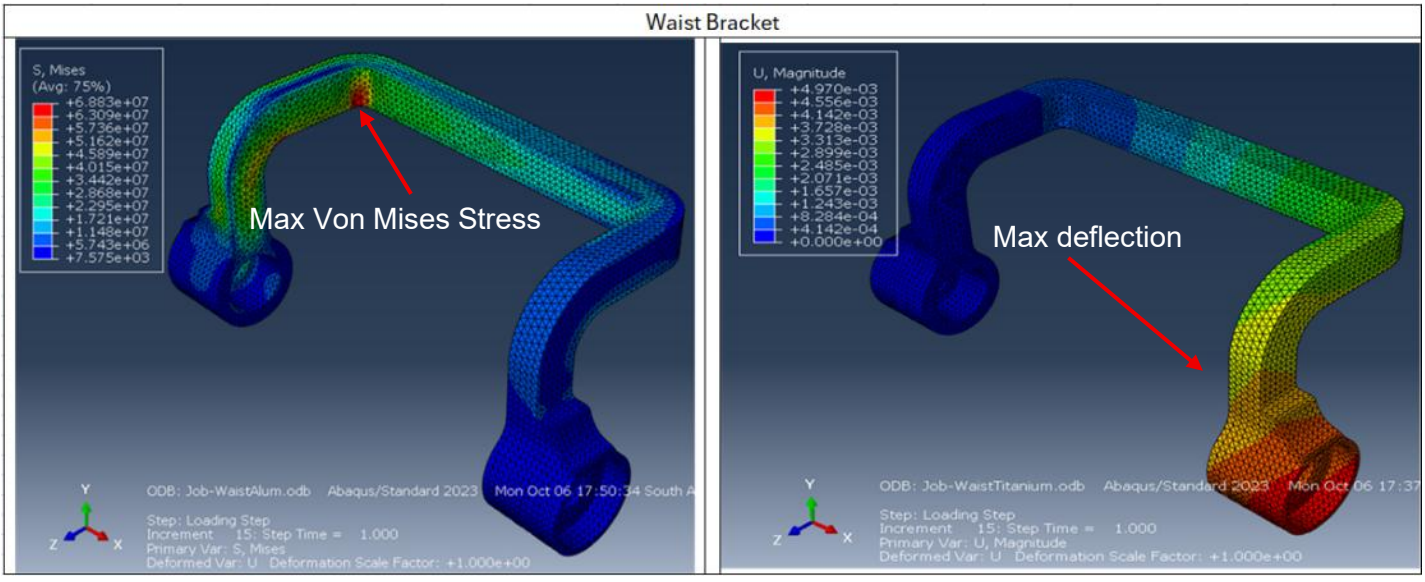

Figure 35: Waist Bracket Material FEA Results

4.1.2. Thigh Link

Table 11: Thigh Link FEA Results

Thigh Link	**Aluminium AA7068**	**Titanium Ti-6Al-4V**	**CFRC**
Max Von Mises Stress	21.24 Mpa	21.22 Mpa	21.29 Mpa
Max Deflection	$0.801e^{-3}$ mm	$0.533e^{-3}$ mm	$0.3867e^{-3}$ mm
Factor of safety (FOS)	23	48	118

In the thigh link, maximum Von Mises stress ranged from 21.22 MPa to 21.29 MPa this is well above the yield strength as seen in Table 11. This stress occurs at the outer corner of the obtuse angle formed by the slope and the vertical. High stress can also be seen in the top axial hole, where the *encastor* boundary condition was applied. FOS which is the lowest for aluminium is well above the general standard of 2 to 4. The FOS is based on the maximum Von Mises stress and material yield stress (refer to Table 7). Little to no stress is found around the motor/actuator housing and the very top of the link, above the axial hole. Little to no deflection occurs on the top half of the link. Refer to Figure 36

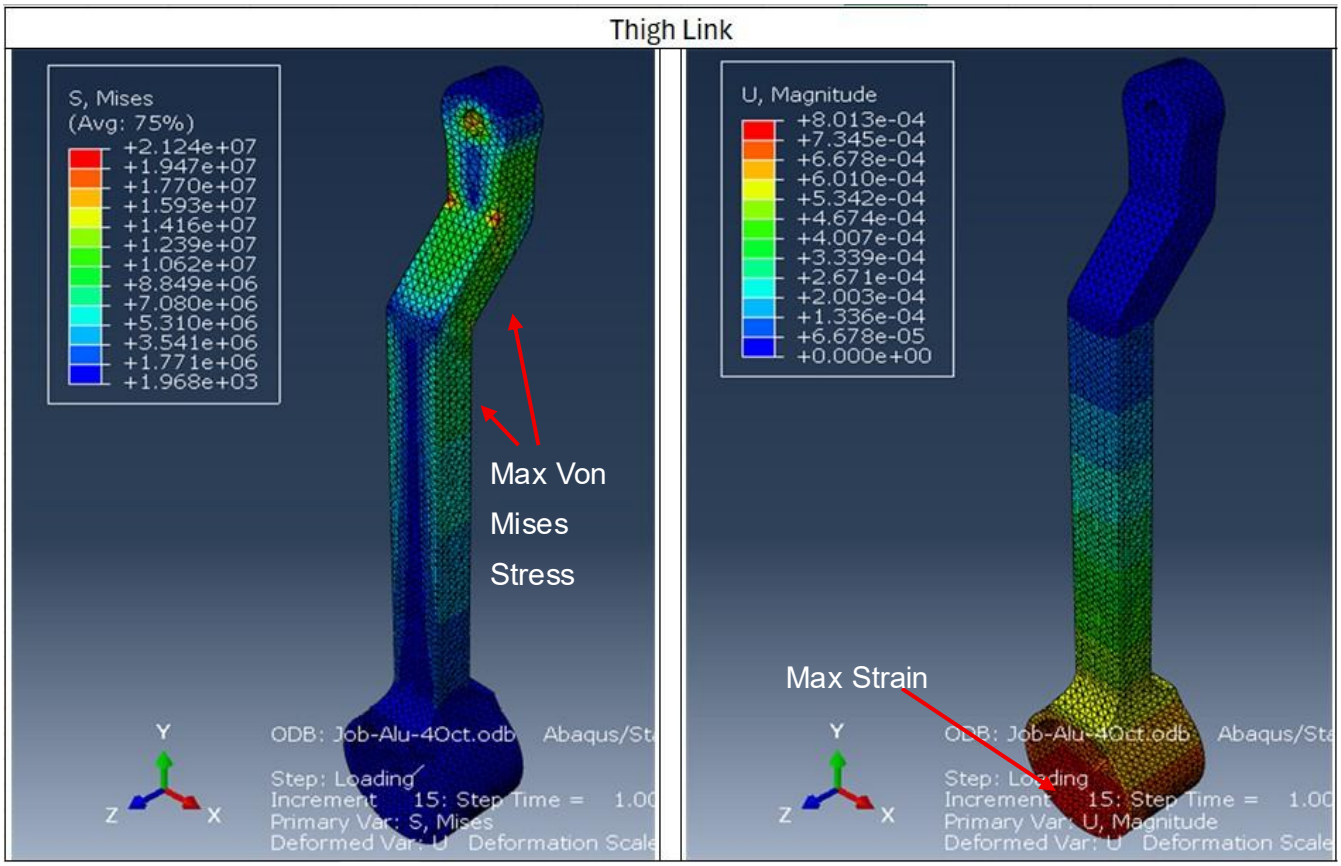

Figure 36: Thigh Link FEA Results

4.1.3. Shank Link

Table 12: Shank Link FEA Results

Shank Link	Aluminium AA7068	Titanium Ti-6Al-4V	CFRC
Max Von Mises Stress	19.45 Mpa	19.43 Mpa	19.51 Mpa
Max Deflection	$0.806e^{-3}$ mm	$0.536e^{-3}$ mm	$0.3885e^{-3}$ mm
Factor of safety (FOS)	25	45	128

Similar to the thigh link, the maximum stress occurs at the outer corner of the obtuse angle formed by the slope and the vertical. High stress can also be seen in the top axial hole, where the *encastor* boundary condition was applied. FOS was based on the maximum Von Mises stress and material yield stress (refer to Table 7). Similar to the thigh link, little to no stress is found around the large motor/actuator housing, as well as the top of the link above the axial hole. The deflection ranged between $0.806e^{-3}$ mm and 0.3885e-3 mm (refer to Table 12).

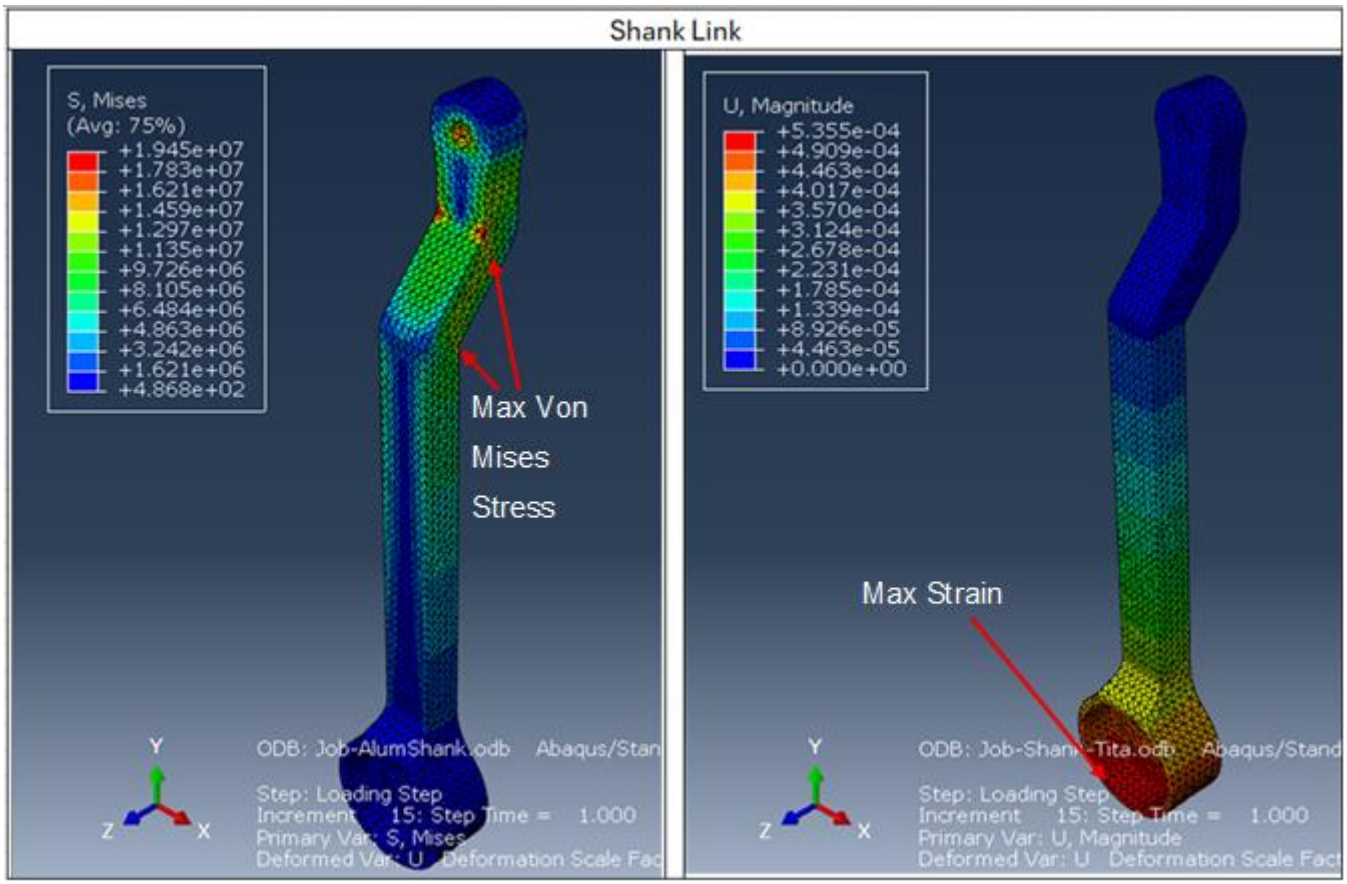

Figure 37: Shank Link FEA Results

4.2. Topology Optimisation

Two sets of topology optimisation simulations were run for the Thigh and Shank links components across aluminium AA7068 and titanium Ti-6Al-4V. See Figures 38 and 39.

CFRC are not considered in this section due to limited simulation capabilities and vast unpredictable variables. Although more isotropic behaviour could be achieved under ideal conditions, the ideal manufacturing processes to ensure this is achieved is very complex. Even if the laminate is quasi-isotropic globally, each ply has its own orientation and properties. There is also the risk of unknown dynamic behaviours or unknown forces active in the z-axis.

A suitable failure criterion for CFRC layup is still required. Where CFRC are brittle, and failure depends on fibre orientation, matrix strength, and shear interaction. The use of Von Mises stress to evaluate CRFC simulated as an isotropic material is a rough approximation of the potential of CRFC under ideal manufacturing conditions (as highlighted in section 3.3.2.1.), but this is not accurate enough data for designing a structural component. The design, simulation and manufacture of CFRC needs to be studied further.

The waist bracket, having the lowest FOS and maximum deflection in the material stress analysis, showed the least potential for weight reduction and is therefore not optimised further. The volume design response in the Abaqus optimisation set up was reduced by 10% for every iteration until system failure.

4.2.1. Thigh Link

Aluminium AA7068

Table 13: Thigh Link AA7068 TO Results

Thigh Link	Aluminium AA7068
Max Von Mises Stress	59.15 Mpa
Max Deflection	1.69e^{-3} mm
Factor of safety (FOS)	8
Volume percentage reduction	Volume reduced to 40% of the original model
New weight	0.628 kg

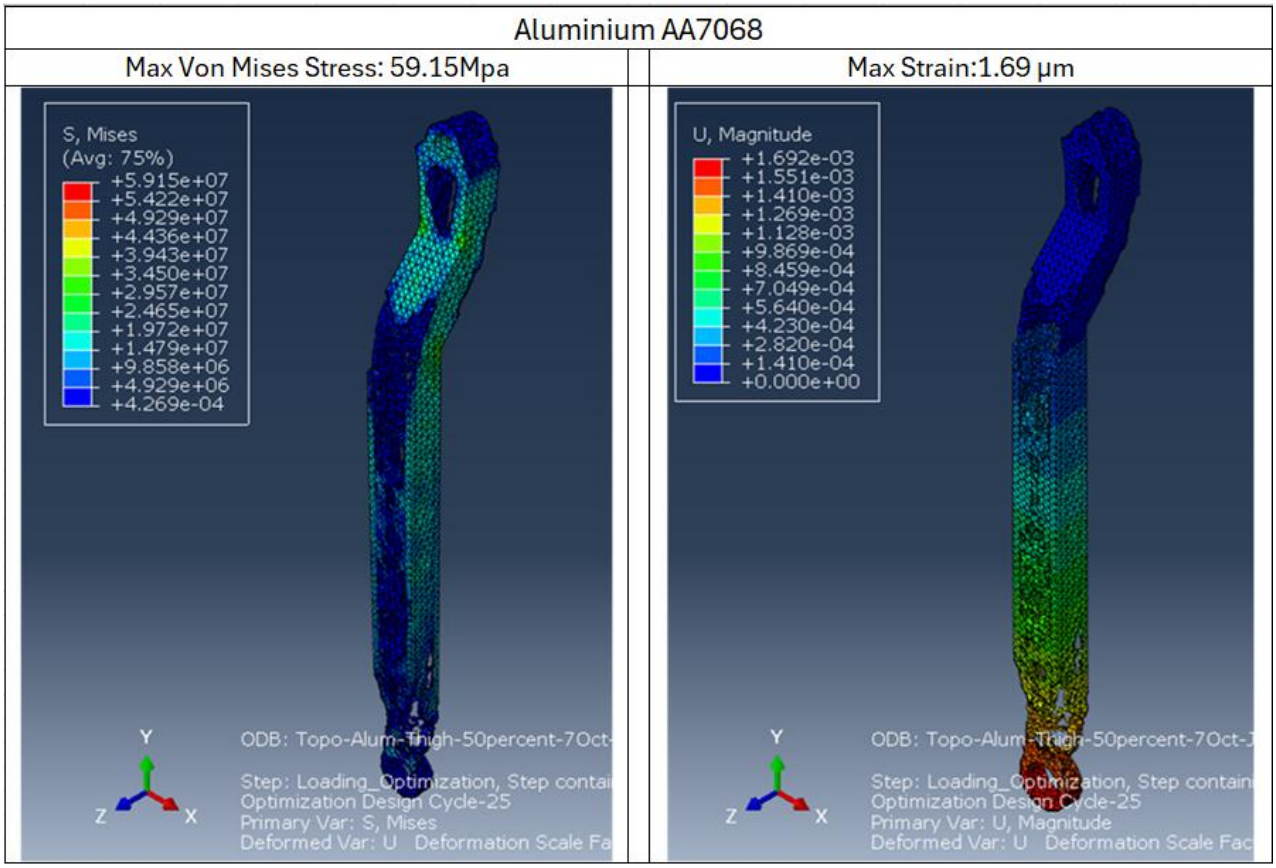

Figure 38: Thigh Link Aluminium Topology Optimisation Results

Results in Table 13 state that the volume was reduced to 40% of the original model. As can be seen in Figure 38, an organic topology/geometry was produced. The most weight/volume loss occurred around the bottom of the link/actuator housing, as well as the centre straight portion of the link. Maximum deflection still occurred at the load application point. The FOS of 7 is still very good, above the general FOS used for LLE and prosthetics.

Titanium Ti-6Al-4V:

Table 14: Thigh Link Ti-6Al-4V TO Results

Thigh Link	Titanium Ti-6Al-4V
Max Von Mises Stress	63.65 Mpa
Max Deflection	$1.38e^{-3}$ mm
Factor of safety (FOS)	14
Volume percentage reduction	Volume reduced to 30% of the original model
New weight	0.733 kg

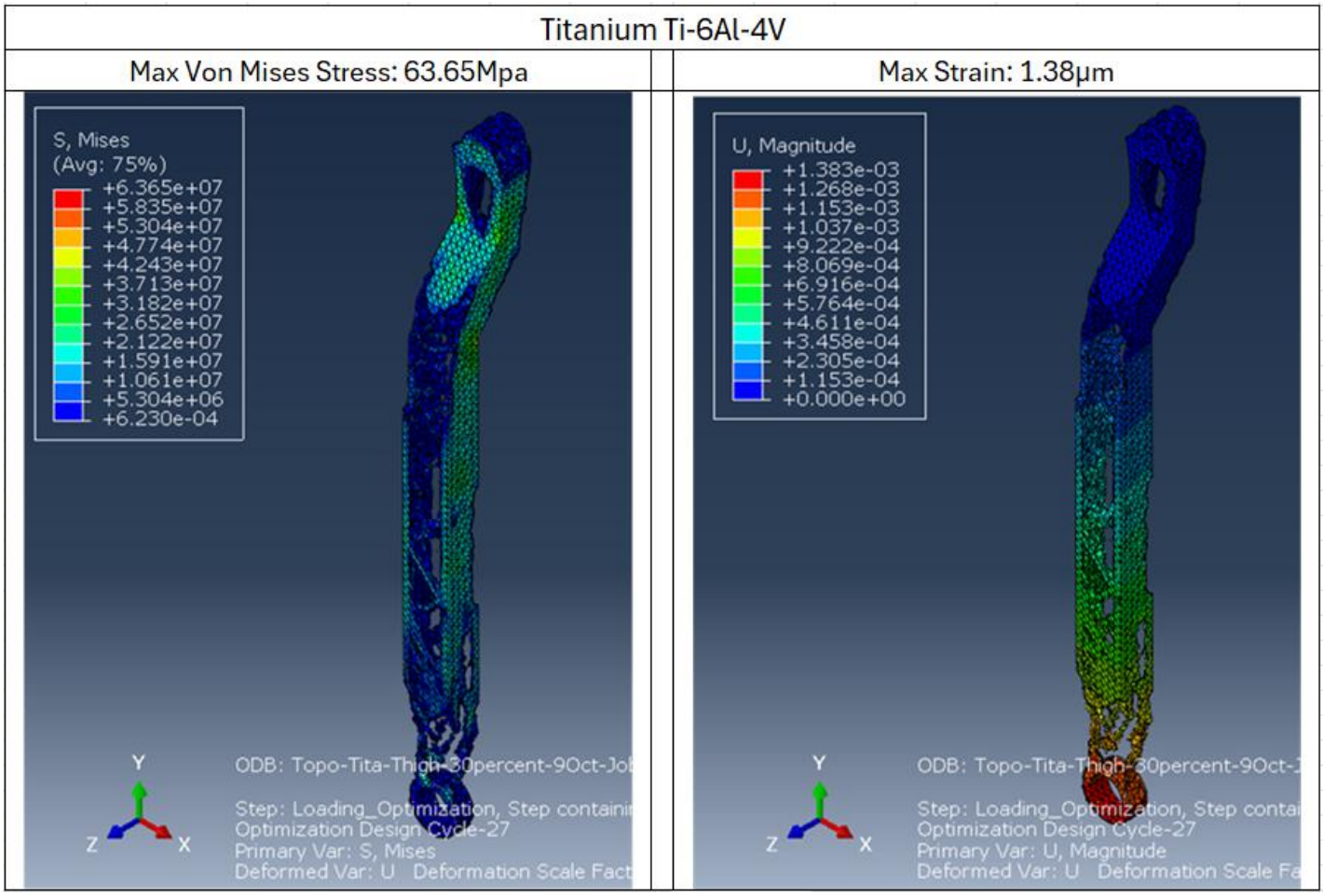

Figure 39:Thigh Link Titanium Topology Optimisation Results

The volume was reduced to 30% of the original model (refer to Table 14). An organic topology with most of the volume reduction occurring around the bottom of the link/actuator housing can be seen in Figure 39. The centre straight portion of the link has been hollowed out, creating a vertical truss-like zigzag pattern. Max deflection still occurs at the load application point, similar to the material stress analysis models.

4.2.2. Shank Link

Aluminium AA7068

Table 15: Shank Link AA7068 TO Results

Shank Link	Aluminium AA7068
Max Von Mises Stress	62.09 Mpa
Max Deflection	$1.82e^{-3}$ mm
Factor of safety (FOS)	8
Volume percentage reduction	Volume reduced to 50% of the original model
New weight	0.683 kg

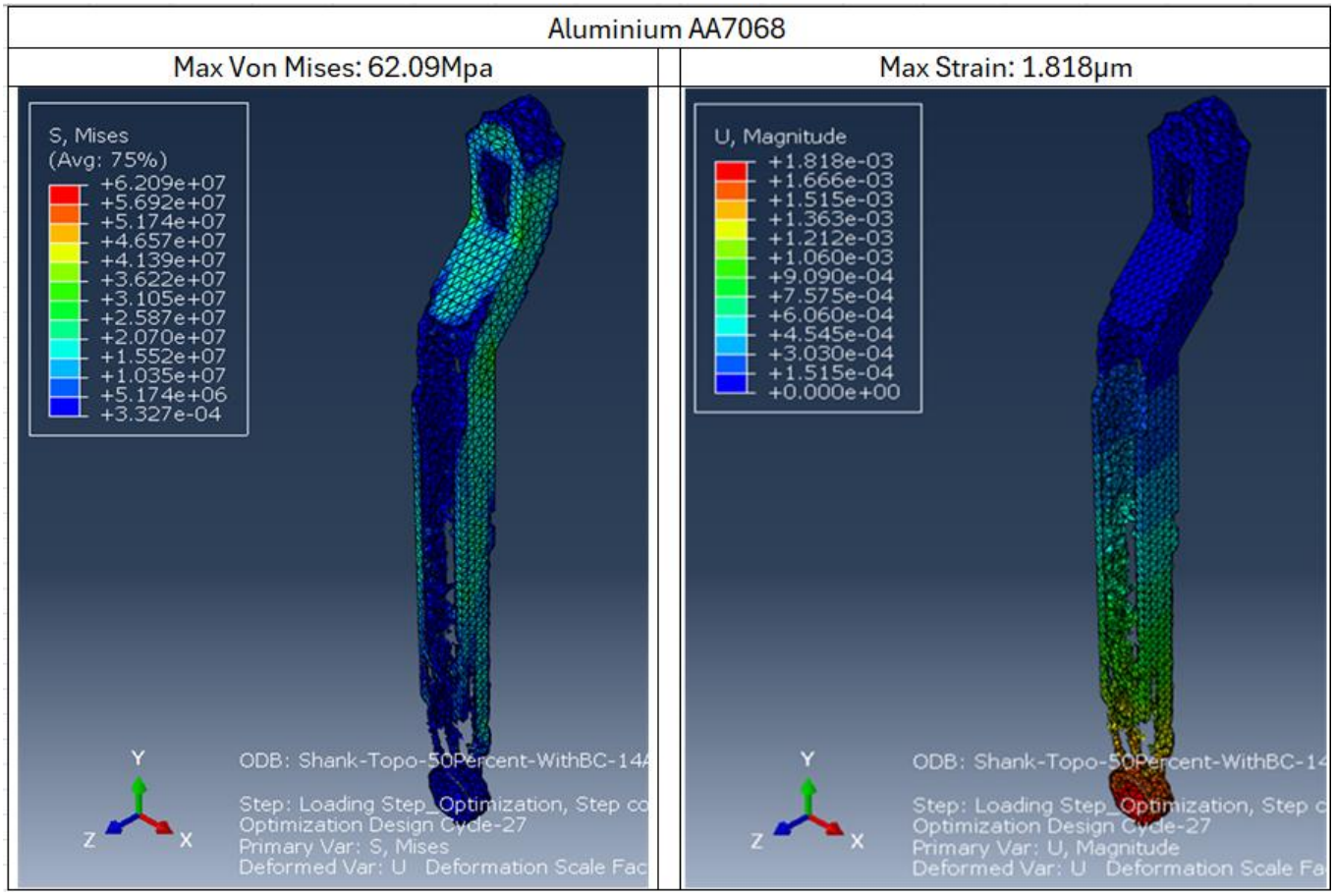

Figure 40: Shank Link Aluminium Topology Optimisation Results

Similar to the thigh link, Figure 40 displays an organic geometry with the most weight/volume reduction around the bottom of the link/actuator housing. 50% volume reduction was achieved. (Refer to Table 15). This volume reduction occurred in the centre straight portion of the link. Max deflection of $1.82e^{-3}$ mm occurred at the load application point, similar to the material stress analysis models. A maximum Von Mises stress of 62.09 MPa is found at the outer corner of the obtuse angle formed by the slope. The link maintains a good FOS of 8.

Titanium Ti-6Al-4V:

Table 16: Shank Link Ti-6Al-4V TO Results

Shank Link	**Titanium Ti-6Al-4V**
Max Von Mises Stress	68.71 Mpa
Max Deflection	$1.48e^{-3}$ mm
Factor of safety (FOS)	13
Volume percentage reduction	Volume reduced to 40% of the original model
New weight	0.849 kg

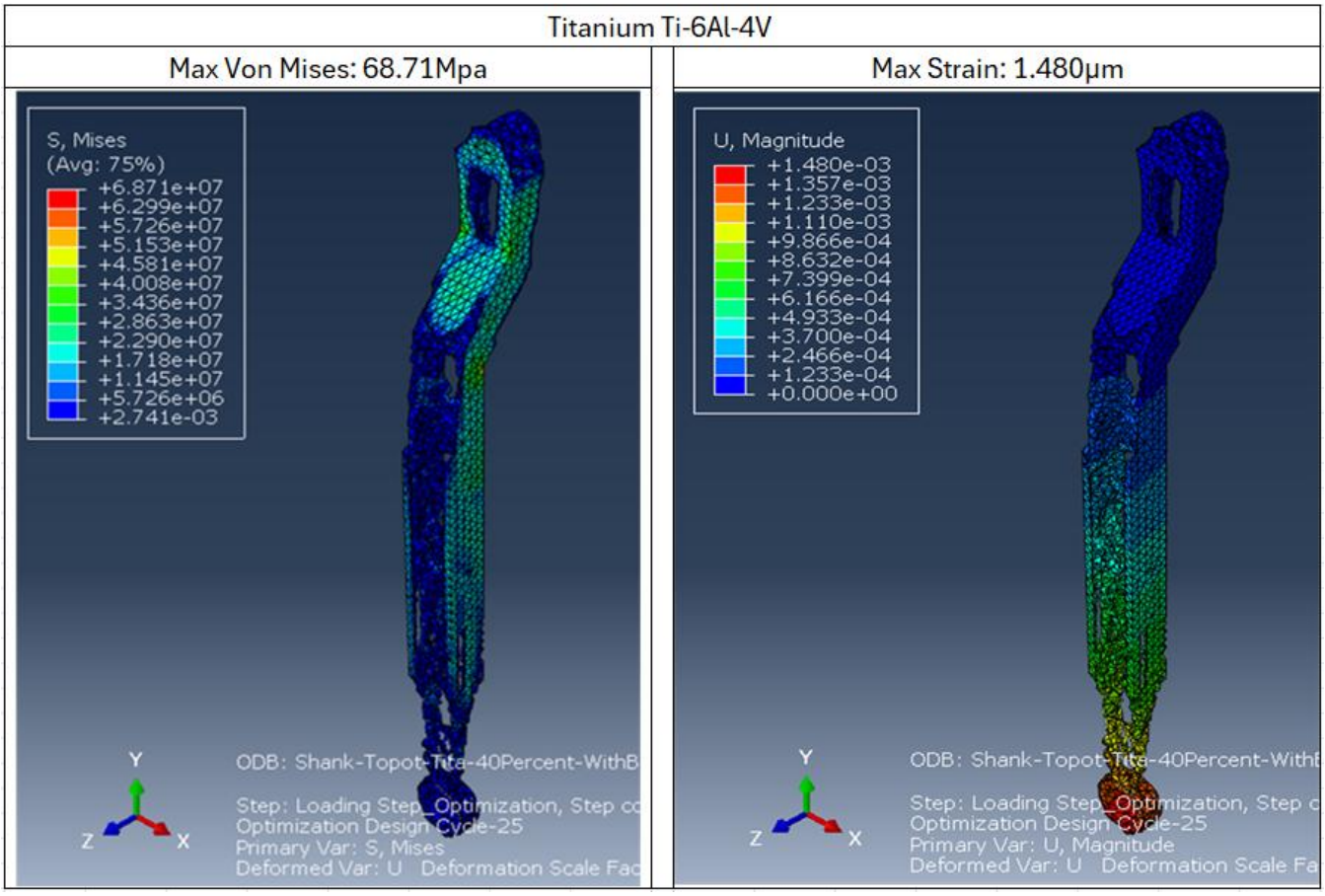

Figure 41: Shank Link Titanium Topology Optimisation Results

Similar to the thigh aluminium link, 40% volume reduction was achieved (see Table 16). A complex geometry with the most weight/volume loss occurring around the bottom of the link/actuator housing, as well as in the centre straight portion of the link (see Figure 41). Max deflection of $1.48e^{-3}$ mm occurs at the load application point, similar to the material stress analysis models. Location of max deflection has been consistent with the thigh links and the aluminium shank link.

The Abaqus simulations work by reducing volume. Table 10 summarises the weight reduction in kilograms of each model topology optimisation result.

Table 17: Structure weight change

	Original Design Weight (kg)	Optimised model weight Aluminium AA7068 (kg)	Optimised model weight Titanium Ti-6Al-4V (kg)
Waist Bracket	2.809	N/A	N/A
Thigh link	1.549	0.628	0.733
Shank Link	1.347	0.683	0.849
Foot	0.563	N/A	N/A
Total (for whole structure)	**9.727**	**6.557**	**7.099**

These results show that optimised aluminium AA7068 Structure provides a much greater weight reduction than titanium Ti-6Al-4V and is therefore the preferred choice. Although the titanium Ti-6Al-4V experienced more volume reduction, its greater density offsets the weight.

4.2.3. Topology Refinement

The raw optimised models produced by Abaqus were coarse and complexly shaped. An almost symmetrical pattern can be seen along the length of the links, two straight, parallel frames sandwiching what appears to be an intended crisscross triangular pattern, creating a vertical truss. Along this truss section of the links are some incomplete or floating features, which are impractical. Refer to Figure 42.

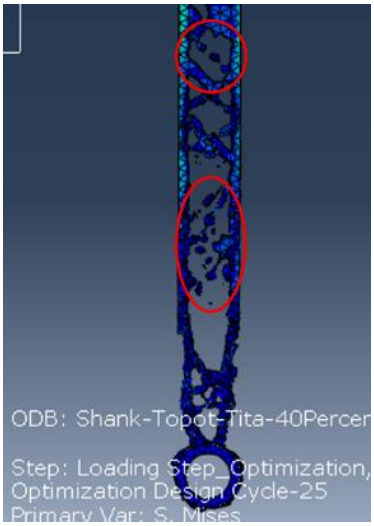

Figure 42: Topology Optimisation Incomplete Features

For both the thigh and shank link, a large amount of material was removed around the actuator housing, which indicates that this region carries much weight but is not needed for structural integrity. Therefore, the models can be refined to improve manufacturability and longevity. The refining process smoothens out surfaces and connects incomplete features. As aluminium AA7068 is the preferred material, it yields the greatest weight reduction. The aluminium AA7068 thigh and shank models were redrawn on SolidWorks following the pattern of the Abaqus topology optimisation model. Results can be seen in Figure 43.

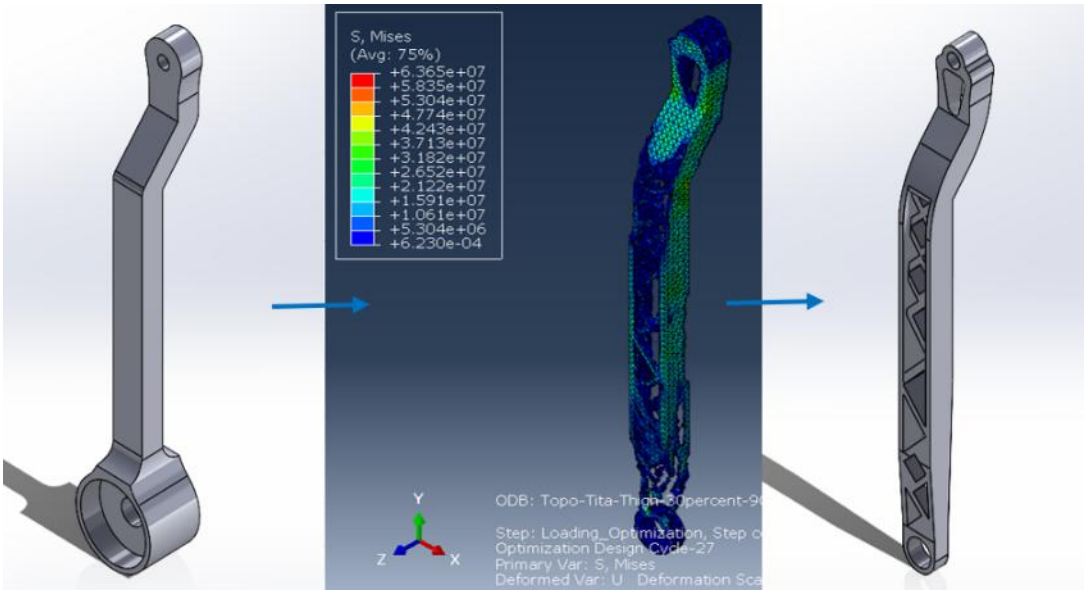

Figure 43:Refined Topology Optimisation

4.2.3.1. FEA Results of Refined Topology

Finite Element Analysis of the refined aluminium thigh and shank links was run using the same inputs. This was to evaluate the stress, deflection and FOS, ensuring that the model was not compromised in any way during the refining process. Results are shown in Tables 18 and 19. Maximum Von Mises stress of 8.49 MPa and 8.9 MPa appeared in the same regions as the raw topology optimised models, at the outer corner of the obtuse angle formed by the slope and the vertical. See Figure 44. An FOS of 56 and 54 was achieved for the thigh and shank link, respectively. This is well above any required standard and shows potential for further weight reductions.

Table 18: Refined Thigh Link FEA Results

Refined Thigh Link	**Aluminium AA7068**
Max Von Mises Stress	8.49 MPa
Max Deflection	$0.254e^{-3}$ mm
Factor of safety (FOS)	56

Table 19: Refined Shank Link FEA Results

Refined Shank Link	**Aluminium AA7068**
Max Von Mises Stress	8.90 MPa
Max Deflection	$0.269e^{-3}$ mm
Factor of safety (FOS)	54

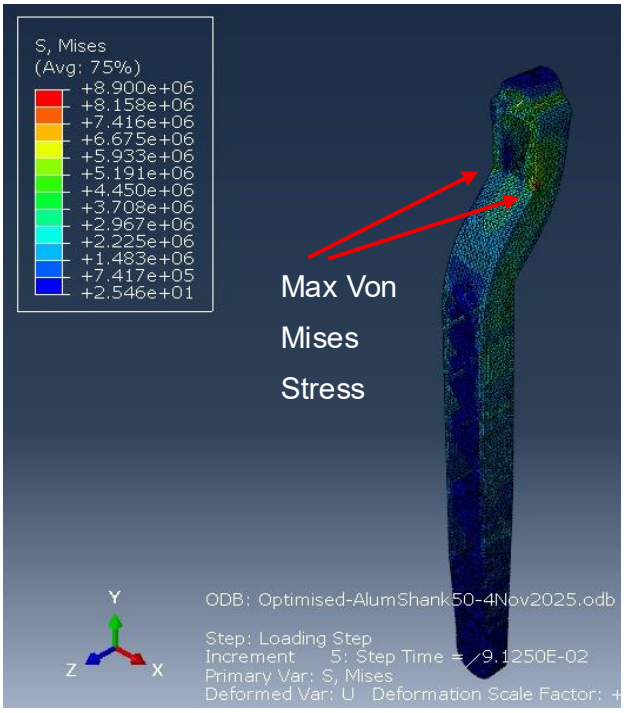

Figure 44: Refined Model FEA Results

4.3. New Weight and Gait Force Results

Table 11 shows summarised results of weight for the refined topology optimised aluminium models, compared to the raw optimised models and the original design.

Table 20: Weight Reduction Results

	Original Design Weight (kg)	Optimised model weight Aluminium AA7068 (kg)	Refined Optimised model weight Aluminium AA7068 (kg)
Waist Bracket	2,809	N/A	N/A
Thigh link	1,549	0,628	0,593
Shank Link	1,347	0,683	0,738
Foot	0,563	N/A	N/A
Total (for whole structure)	**9,727**	**6,557**	**6,5986**
Strength to weight ratio	**48MPa / kg**	**73Mpa / kg**	

Based on the weight of the refined optimisation models in aluminium, the forces acting during each gait phase were recalculated. This is an indication of the force/ motor torque requirement for the optimised LLE structure. The graphs in Figures 45 and 46 show force vs swing phase and force vs stance phase.

Table 21: Forces During Swing Phase

Forces During Swing Phase			
	Early swing	Mid swing	Late swing
Original Knee joint	-105	138	143
Original Hip joint	-369	508	515
Optimised Knee joint	-96	126	131
Optimised Hip joint	-332	457	463

Table 22: Forces During Stance Phase

	Forces During Stance Phase				
	Heel Strike (weight acceptance)	Foot flat (1st peak)	Mid Stance	Heel off (2nd peak)	Toe off (Push off)
Original structure	45	813	594	727	36
Optimised structure	43	782	571	699	35

Table 21 and 22 detail the forces acting during the gait phases, comparing the original structure and the new optimised structure. The peak force which occurs during the mid-swing and late-swing reduces by 51N and 52N respectively. The greatest reduction in stance phase occurs as a 32N drop at foot flat.

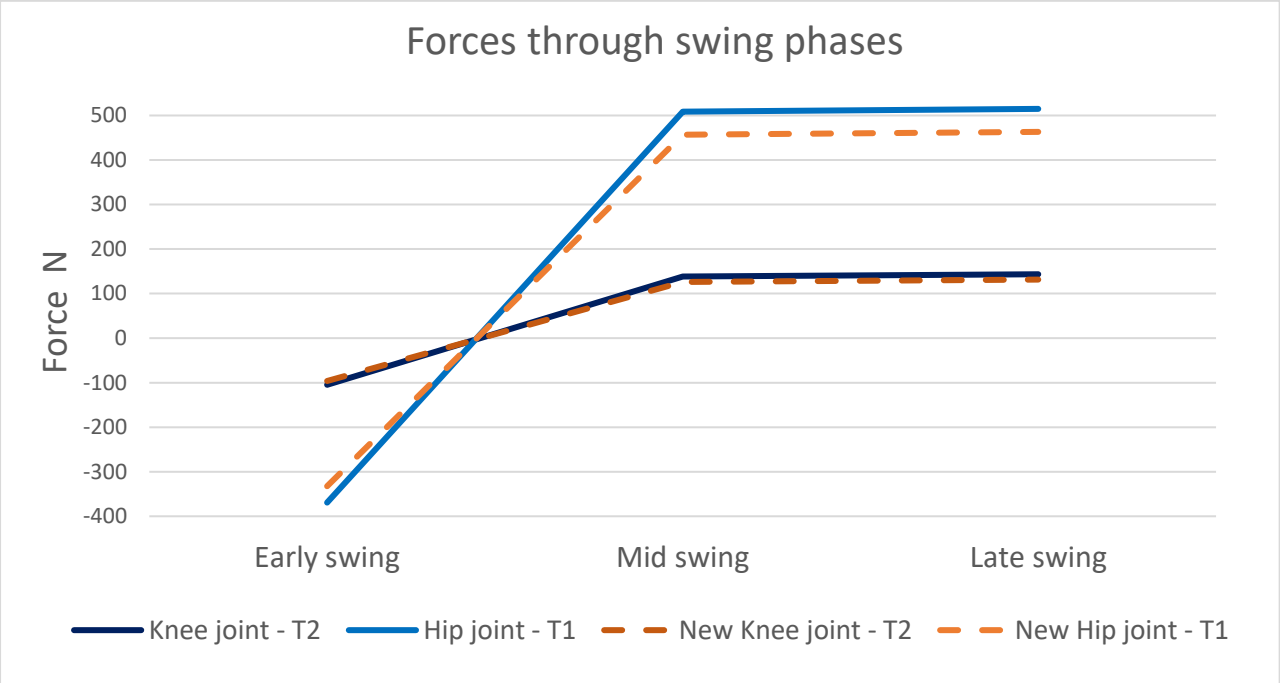

Figure 45: Force vs swing phase graph

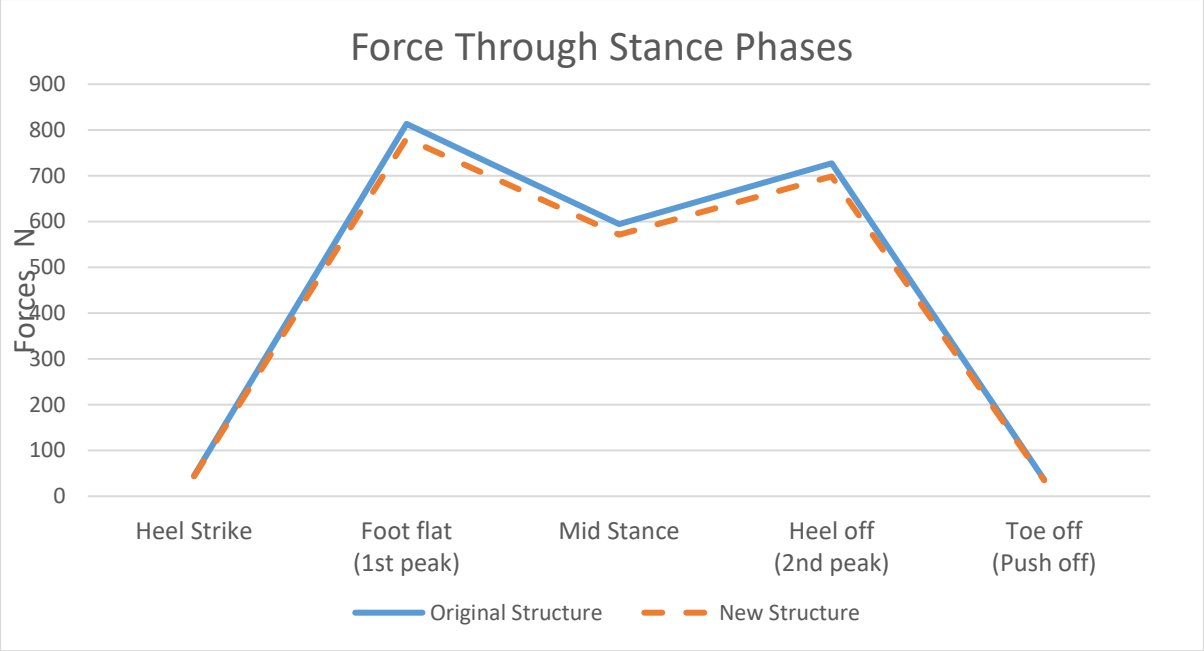

Figure 46: Force Through Stance Phase graph

5. DISCUSSION

In this section results of the Stress Analysis material selection and topology optimisation for the waist bracket, thigh link and shank link are discussed. For the material stress analysis across all three models, CFRC, having the highest material performance index in the material selection section, presented preliminary promising results in terms of max deflection and factor of safety. However, these results have no accuracy and must be taken as rough approximations. This is because CRFC was considered to have isotropic behaviour and only experience loading along the direction of the fibres, which only has the possibility of some accuracy/relevance under ideal manufacturing and loading conditions. Therefore, the topology optimisation models were only run in titanium and aluminium, due to the unreliability of the results that would be produced from running a topology optimisation simulation of CFRC as an isotropic material.

In the material FEA, the waist bracket yielded the highest max stress and max deflection across all three materials. It consequently presented the lower FOS compared to the thigh and shank, however this was still highly above the general standard used for LLE design. It can however be considered the weakest member of the LLE structure. The weakest point of the waist bracket was at the internal 90-degree folds of the frame. Therefore, the topology of the waist bracket was not optimised.

5.1. Material

In the material FEA, the thigh presented a max stress of 21.12MPa, less than a third that of the waist bracket. The max deflection ranged from $0.3867e^{-3}$ mm to $0.8013e^{-3}$ mm. This indicates low chances of bending failure across all three materials. The FOS were high, indicating great potential for weight reduction. The areas of maximum stress were the corners of the slope. The lowest stress appeared around the actuator housing.

Results for the shank link were very similar to those of the thigh link. This model displayed the lowest max stress and deflection across all three materials, as well as the highest FOS. However, there was lower potential for volume reduction than the thigh; this is mainly because a lot of the volume reduction for these two parts was around the actuator housing. For which the thigh link had a larger actuator housing. The weakest points identified on the thigh and shank links were the top-angled corners at the crease.

5.2. Topology

The Thigh link topology optimisation results correspond with this in that a great amount of material is removed from the actuator housing and the top of the link. Following topology optimisation, a 60% volume reduction was achieved with AA7068 and a 70% volume reduction with Ti-6Al-4V. This translates to 59% and 52% weight reduction, respectively. The max stress increased by 218% and 250% but the FOS remained above 5. With titanium, 10% more volume reduction was achieved over aluminium. However, because of the greater density of titanium, this did not translate into the titanium models weighing less than the aluminium ones the aluminium AA7068 resulted in a 32% weight reduction of the overall LLE structure, and a Titanium Ti-6Al-4V structure resulted in 27% weight reduction. The model was refined to eliminate impractical, incomplete features and to smooth our coarse surfaces. Doing so makes the components more manufacturing friendly. (Refer to Appendix D, Figures 64 to 67) This is a negligible weight increase from refining the optimised model. The Refined models were run in Abaqus again using the same set-up and force inputs. This yielded even better results than the material stress analysis simulations. Although weight was reduced by 50% to 60% for the shank and thigh links, the max Von Mises stress dropped to 8.9Mpa and 8.48Mpa, respectively meaning the material is operating well with its serviceability limits.. This translates into more than 100% increase in the FOS.

The topology optimisation results displayed the amount of material removed from the actuator housing and the top of the link. Following topology optimisation, a 50% volume reduction was achieved with AA7068 and a 60% volume reduction with Ti-6Al-4V. This translates to 49% and 37% weight reduction, respectively. The max stress increased by 218% and 250%, and the FOS remained above 7.

The new light weight LLE structure yields a 10.11% reduction in maximum motor forces of the hip joint and 2.35% at the knee joint, which can be seen occurring in the mid-swing phase.
To maximise on the potential energy savings, this, as some researchers propose this advocates for the use of the different actuators for the for the two joints. The reduced maximum torque requirement could lead to reduced power requirement and improved performance. Consequently, operating time could increase to 4% to 8%. The maximum GRF have also reduced by 3.92% reduced throughout the stance phase. This reduced impact could increase the life of the structure. The overall strength to weight ratio, which is calculated by weight of the structure divided by the yield strength of the material, improved from 48Mpa / kg to 73 MPa/kg

5.3. Manufacturing Process

For Titanium, Ti-6Al-4V, casting would be the more suitable manufacturing process. It is more cost-effective than additive manufacturing. However, similar to AM processes, porosity and inclusions may occur, resulting in lower mechanical properties than wrought material. This means post-manufacturing testing of components is critical.

However, for the selected material aluminium AA7068, machining would be the most suitable manufacturing process. With machining of aluminium, it is possible to achieve high precision and complex geometries as seen with the thigh and shank link. Machining, unlike casting and SLM, does very little to alter the material properties of the base material. This is important because it reduced unexpected changes to the material such as porosity. The manufactured product is expected to behave very similarly to the computer model which underwent FEA.

Machined aluminium AA7068 components also typically exhibit the best resistance to fatigue failure, which is an excellent feature for the cycling loading of gait the structure experiences. It is also more accessible and cost-effective than additive manufacturing processes. There is no bespoke tooling investment required and although there will be waste generated, the relatively low cost of AA7068 makes this less of a concern. The development of an LLE requires low-volume prototyping for which machining is the ideal manufacturing process. However, this thesis lacks in the manufacturing a physical testing of a prototype model. Therefore, manufacturing process and its impact on the structure cannot be fully validated.

5.4. Limitations

Although CFRC was not analysed for topology optimisation, it had the highest material performance index and displayed good potential in the FEAs across all three components, with FOS over three times greater than Ti-6Al-4V and AA7068. Unfortunately, these results are only an indication of the potential of CFRC. The use of CFRC comes with many challenges to design, simulate and manufacture. Particularly when considering complex-shaped components.

This has however been successfully done with bicycle frames (Anon, 2024). Also propelled by the demand for durable, lightweight, high-stiffness structures, the bicycle industry has been revolutionised by the introduction of CFRC (Zhang, 2024). The first carbon fibre bike was introduced to the Tour de France in 1989 by American cyclist Greg LeMond, who rode the Look TVT carbon fibre bike. This bike was about 1kg lighter than its aluminium counterparts. Today, almost all top cyclists in the Tour de France use CFRC bikes. The success of carbon fibre in this field can be attributed to years of research and development in materials science and manufacturing techniques (Anon, 2024). CFRC structures are made through an additive manufacturing process.

The layup is the main influencing factor of the mechanical properties of the end product. There are no predetermined or generic layups for optimum properties (Sineri et al., 2015). The best layup for every design must be established through a design development process involving trial and rigorous testing. This process can be so bespoke that in the bicycle industry, layup can be developed for a specific bike to match the individual rider’s weight and power output (Anon, 2018).

Drilling can lead to cracks around the hole, compromising the integrity of the component. Bolt holes can create stress concentration points where the material is more likely to experience stress and potential failure. Drilled holes are required to attach the motor/actuator to the links. The attachment method in this area would need to be redesigned. Optimal carbon fibre component design and engineering should be used to minimise the number of holes needed and optimise their placement to reduce the impact on structural integrity (Olliges, 2018). While carbon fibre is strong, it can be more prone to impact collisions compared to metals (Oomi, 2024). This sudden, abrupt failure of the LLE structure could be a serious safety concern.

Rigorous testing is conducted to ensure the component meets performance and safety standards testing and feedback loop is a crucial step in the design and development of a carbon fibre. (Zhang, 2024)

An alternative approach to still take full advantage of carbon fibres' great weight reduction would be to manufacture components of a combined material, where the straight portion is made out of CFRC, and the actuator housing is made of Aluminium or Titanium.

This analysis could be improved by the manufacturing of a prototype model to better validated the optimised design and analysis things like friction and material behaviour at joint interaction.

6. CONCLUSION

This thesis sought to establish what impact of weight reduction of an LLE have on the maximum motor torque requirement, strength, deflection and factor of safety. Overall, the reduced weight of the structure through material selection and topology optimisation reduced the peak motor torque of the requirement. Material integrity was not compromised as the max stress in the material was well within serviceability limits, the maximum deflection was below one micron and a high FOS of 54 was achieved.

It was key to confirm which materials can be used for the structure to provide a good weight-to-strength ratio. 15 different candidate materials were reviewed in a material selection process. From this aluminium AA7068 and titanium Ti-6Al-4V were found to be good alternative materials for LLE structures. Aluminium AA7068 was ultimately identified as the most suitable material providing the most weight reduction while maintaining strength and stiffness. Titanium Ti-6Al-4V outperformed Aluminium AA7068 in volume reduction, achieving up to 70% in the thigh link and 60% in the shank link. Although there was an increase in Von Mises stress post-optimisation, both materials retained high FOS values. Aluminium AA7068 yield the best results, achieving a 32% overall structure weight reduction as opposed to Titanium Ti-6Al-4V's 27% weight reduction. The stress analysis of the refined topology in Aluminium AA7068 resulted in a significant improvement in stress, deflection, and FOS. The overall weight reduction of the structure also presents slight improvements in gait forces, which is indicative of reduced joint torque requirements and consequently performance efficiency. Manufacturing considerations support the use of machining for an Aluminium AA7068 for structure, given its cost-effectiveness and fatigue resistance

The question of does reducing the overall weight of an LLE structure reduce the required motor torque to operate it. Is answered as the weight reduction in the LLE structure has yielded a reduction in the peak required motor torque which can be seen through reduced gait swing force. as well as the peak GRF. The optimised structure yielded reduction in maximum force experienced in the swing and stance phase. The 10.11% reduction in force in the swing phase translates to reduced motor torque requirement which subsequently reduces the power requirement and improve efficiency.

This paper also answers the question of how the design of LLE structures can be modified to reduce weight while maintaining structural integrity. Structural optimisation has been achieved by reducing the weight of a lower limb exoskeleton structure through material selection and topology optimisation, without compromising the structural integrity of the LLE. Modular 3D models of the LLE structure underwent stress analysis where the inputs/applied loads were calculated from human gait force. It was then subjected to topology optimisation in Abaqus. In

the FEA simulation, Von Mises stress, max deflection, FOS and areas of high stress were reviewed. This produced new 3D models of optimised and refined thigh and shank links of the LLE structure.

Limitations identified in this paper include the restrictions in running FEA of CFRC. In the material performance index, CFRC yielded promising results, displaying the potential for high factors of safety. However, its practical application is limited by simulation and manufacturing complexities. Future work should explore advanced simulation techniques and post-manufacturing/prototype validation to refine the design and enhance the safety and performance of the LLE.

A secondary limitation was the lack in construction and physical mechanical testing of a prototype model. The work was fully computer simulation based, it therefore lacks in validating manufacturability of the design or understanding the impact of joint interface behaviour.

Overall, this thesis demonstrated that through material selection and topology optimisation the weight of an LLE structure can be effectively reduced without compromising on structural integrity. This optimisation in this instance resulted in a 52% increase in the overall strength-to-weight ratio and a 10,11% reduction peak swing force requirement. Such improvements could improve the efficiency of LLE by reduced power consumption and increasing operating time.

7. RECOMMENDATIONS

In the gait phase analysis, the forces Fx, the mediolateral (ML) GRF component and Fy, the anteroposterior (AP) GRF component, were ignored. Although minor compared to the Fz forces, in future studies, these forces should be taken into account to have more accurate results. This is specifically important when deal with a composite material like quasi-isotropic CFRC where forces in the z-axis drastically affect stress analysis results.

CFRC, although promising, requires bespoke design and rigorous testing to ensure reliability, especially when working with organic/complex geometries. The development must involve a design, rigours stress analysis simulations, prototype manufacture and post/manufacture testing loop. The test work should be rigours, incorporate quasi-isotropic layering simulation and prototyping to understand the full mechanical behaviour of CFRCs in such complex shapes. A hybrid design combining CFRC for the simple straight portions of the links and metal for the complex joint portion is a good solution to explore. This was a method employed in the design of Indego, which is currently the lightest commercialised Locomotion assistance

LLE available. This solution may offer a good balance between weight reduction and manufacturability.

Gait forces were theoretically calculated in this thesis; however, to properly evaluate the effectiveness of this design, a prototype model of this design should be built and tested. Kinetics such as global torques, global forces, global power and ground reaction forces (GRF) should be practically measured. Lastly, to better evaluate the LLE design, life cycle fatigue testing should be conducted as the structure undergoes cyclic loading.

8. REFERENCES

Abdulgadir, M.M., M.AHMADI, A. & WaledY., B., 2019. Machinability of Titanium Grade-5 Alloy (Ti-6Al-4V) During Turning Processes: A Review. *International Research Journal of Engineering and Technology*, 6(10), pp.565-72.

Aires, R., Ferreira, L. & al., e., 2022. A New Multi-Criteria Approach for Sustainable Material Selection Problem. *Sustainability*, 14(18).

Al-Hayali, N.K., Chiad, J.S., Nacy, S.M. & Hussein, O., 2021. Investigation of Vertical Ground Reaction Force during Walking with the Exoskeleton for Patient with Unilateral Lower Limb Weakness. *EAI*.

Alves, M.A., Pilusa, S. & Mashola, M.K., 2023. The prevalence and profile of spinal cord injury in public healthcare rehabilitation units in Gauteng, South Africa. *The international Spinal Cord Society*, pp.9-15.

Andrei, M., 2014. *New alloy has record strength-to-weight ratio*. [Online] Available at: https://www.zmescience.com/research/materials/alloy-strong-material-11122014/ [Accessed 12 September 2021].

Annon, 2016. Powered Lower Limb Exoskeletons for spinal cord injury. *ISCRR Horizon Scanning*.

Annon, 2018. *The Ultimate Guide to Carbon Fiber Design and Application*. [Online] Available at: https://element6composites.com/a-comprehensive-guide-to-carbon-fiber-design-and-application/ [Accessed 2 October 2023].

Annon, 2020. *The Application Of Magnesium Alloy Materials In Lightweight Robots*. [Online] Available at: https://www.cncmachiningptj.com/article-305.html [Accessed 9 April 2024].

Annon, 2025. *Polyetheretherketone (PEEK): How to select the right grade?* [Online] Available at: https://www.specialchem.com/plastics/guide/polyetheretherketone-peek-thermoplastic [Accessed 1 August 2025].

Anon, 2018. *Black magic: How carbon fibre bicycle frames are made*. [Online] Available at: https://velo.outsideonline.com/road/road-gear/how-carbon-fibre-bicycle-frames-are-made/ [Accessed 2 October 2014].

Anon, 2022. *Selective Laser Melting – The Ultimate Guide*. [Online] Available at: https://facfox.com/docs/kb/selective-laser-melting-the-ultimate-guide [Accessed 4 June 2024].

Anon, 2024. *How carbon fibre revolutionised the Tour de France*. [Online] Available at: https://www.r-techmaterials.com/news-and-blog/how-carbon-fibre-revolutionised-the-tour-de-france/?form=MG0AV3 [Accessed 7 Febuary 2024].

Anon, 2025. *Isotropic Material vs Anisotropic Basics and Examples*. [Online] Available at: https://caeassistant.com/blog/isotropic-material/ [Accessed 14 November 2025].

Anon, 2025. *The Ultimate Guide to Carbon Fiber*. [Online] Available at: https://element6composites.com/carbon-fiber/ [Accessed 14 November 2025].

Arunkumar, S., Jayakumar, N. & al, e., 2024. A comprehensive review on lower limb exoskeleton: from origin to future expectations. *International Journal on Interactive Design and Manufacturing*.

Ashby, 2020. *Strength vs Density Chart Ansys Granta*. [Online] Available at: https://innovationspace.ansys.com/courses/wp-content/uploads/sites/5/2022/08/Materials-Selection-Ashby-Charts-Homework.pdf [Accessed 13 August 2025].

Assencio, D., 2014. *Double pendulum: Lagrangian formulation*. [Online] Available at: https://dassencio.org/33 [Accessed 10 August 2025].

Avialasha, B.G., D.S., R. & al., e., 2025. Design and analysis for weight reduction by topology optimization in various industrial applications. *International Journal on Interactive Design and Manufacturing*, 19, pp.7623 - 7636.

Balasubramani, T., Kumar, N.M., Aseer, J.R. & al., e., 2025. Additive Manufacturing of Ti-6 Al-4 V Alloys: Fabrication Techniques and Material Properties—Review. *Transactions of the Indian Institute*, 78.

Barela, A.M.F. et al., 2014. Ground reaction forces during level ground walking with body weight unloading. *Brazilian Journal of Physical Therapy*, pp.572 - 579.

Batkuldinova, K., Abilgaziyev, A. & Sheh, E., 2021. The recent development of 3D printing in developing lower-leg exoskeleton: A review. *Materials Today: Proceedings*.

Baunsgaard, C.B., Nissen, U.V., Brust, A.K. & al., e., 2017. Gait training after spinal cord injury: safety, feasibility and gait function following 8 weeks of training with the exoskeletons from Ekso Bionics. *PubMed*, 2, pp.106-16.

Bell, T., 2019. *Titanium Properties and Characteristics*. [Online] Available at: https://www.thoughtco.com/metal-profile-titanium-2340158.

Chang, S.R., Audu, M.L., Kobetic, R. & Quinn, R.D., 2015. Powered Lower-Limb Exoskeletons to Restore Gait for Individuals with Paraplegia - a Review. *ORTHOPAEDIC JOURNAL* , 12(1), pp.75-80.

Chen, B., Ma, H. & Qin, L.-Y., 2016. Recent developments and challenges of lower extremity exoskeleton. *Journal of Orthopaedic Translation*, 5, pp.26-37.

Choudhury, S., nd. *Titanium Alloys: Applications, Types, Grades, and Examples*. [Online] Available at: https://whatispiping.com/titanium-alloys/#google_vignette [Accessed 27 July 2025].

Churchwell, R., Hollander, K.W. & Theisen, 2016. The Use of Additive Manufacturing to Fabricate Structural Components for Wearable Robotic Devices., 2016. ASME.

Danylenko, M., 2018. Aluminium alloys in aerospace. *Aluminium International Today*, p.35. Available at: www.aluminiumtoday.com [Accessed 17 August 2023].

de Leva, P., 1996. Adjustments to Zatsiorsky-Seluyanov's Segment Inertia Parameters. *Journal of Biomechanics*, pp.1223-30.

Derlatka, M., Parfienuik, M. & al., e., 2023. Real-world measurements of ground reaction forces of normal gait of young adults wearing various footwear. *Scientific Data*, p.60.

Djadoudi, H., 2025. *Mastering Composite Materials in FEA: A Complete Guide for CFRP and GFRP Analysis*. [Online] Available at: https://www.worquick.com/post/mastering-composite-materials-in-fea-a-complete-guide-for-cfrp-and-gfrp-analysis [Accessed 2014 November 2025].

Duan, L., Li, D., Bao, C. & Qian, X., 2023. Structural Design and Dynamics Simulation of Lower. *Journal of Engineering Mechanics and Machinery*, 8(4).

Fereiduni, E., Ghasemi, A. & Elbestawi, M., 2020. Selective Laser Melting of Aluminum and Titanium Matrix Composites: Recent Progress and Potential Applications in the Aerospace Industry. *MDPI*, 7(6), p.77.

Flora-Unda, O., Casa, B., Fuentes, M. & et, a., 2023. Exoskeletons: Contribution to Occupational Health and Safety. *Bioengineering*, 10(9), p.1039.

Fryar, C. et al., 2021. *Anthropometric reference data for children and adults: United States, 2015–2018*. Maryland: National Center for Health Statistics.

George, M., 2014. *selection of materials and processes*. 4th ed. University of Technology.

Gruijicic, R., 2023. *Gait cycle - Kenhub*. [Online] [Accessed 1 July 2024].

Hasan, S., Alam, N. & al., e., 2025. Comprehensive Comparative Analysis of Lower Limb Exoskeleton Research: Control, Design, and Application. *Actuators*, 14(7), p.342.

Helmenstine, A.M., 2019. *Titanium Chemical & Physical Properties*. [Online] Available at: https://www.thoughtco.com/titanium-facts-606609 [Accessed 4 September 2023].

Helmenstine, A.M., 2020. *Aluminum or Aluminium Alloys*. [Online] Available at: https://www.thoughtco.com/aluminum-or-aluminium-alloys-603707 [Accessed 24 August 2023].

Herr, H., 2009. Exoskeletons and orthoses: classification, design challenges and. *Journal of NeuroEngineering and Rehabilitation*, 6(21).

Hong, T., Ding, F., Chen, F. & Zhang, H., 2023. Mechanical Properties of 6061 Aluminum Alloy under Cyclic Tensile Loading. *MDPI*, 13(8), p.1171.

Huo, W., Mohammed, S., Moreno, J.C. & Amarit, Y., 2016. Lower Limb wearable robots for assistance and rehabilitation: a state of the art. *IEEE Systems Journal*, 10(No. 3), pp.1068-78.

Hussain, F., Goecke, R. & Mohammadian, M., 2021. Exoskeleton robots for lower limb assistance: A review of materials, actuation, and manufacturing methods. *Journal of Engineering in Medicine*, pp.1-11.

Jaynes, E., 2024. *30 Facts About Ti 6Al-4V*. [Online] Available at: https://facts.net/earth-and-life-science/earth-sciences/30-facts-about-ti-6al-4v/ [Accessed 14 November 2025].

Jiamin, M. et al., 2019. Design and Implementation of a Lightweight Lower Extremity Exoskeleton. *MATEC Web of Conferences*.

Jianfeng, L. et al., 2015. Structure Design of Lower Limb Exoskeletons for Gait Training. *CHINESE JOURNAL OF MECHANICAL ENGINEERING*, 28(5), pp.878-87.

Jindal, K., 2023. *What is PEEK Material? | The Definitive Guide*. [Online] Available at: https://plasticranger.com/what-is-peek-material/#google_vignette [Accessed 23 October 2023].

Jones, B., 2023. *The Art of Carbon: How Carbon Fiber Transformed Road Bike Performance*. [Online] Available at: https://bicyclevolt.com/the-art-of-carbon-how-carbon-fiber-transformed-road-bike-performance/ [Accessed 2 October 2023].

Joseph, C., Scriba, E. & Wilson, V., 2017. People with Spinal Cord Inury in Repubilic of South Africa. *Ameriacan Journal of Physical Medicine & Rehabilitation*, 96(2), pp.S109 - S111.

Junk, S., KLERCH, B. & HOCHBERG, U., 2019. ADDITIVE MANUFACTURING OF A TOPOLOGY OPTIMIZED. In *International Conference on Simulation for Additive Manufacturing - Sim-AM 2019*. Offenburg, 2019. University of Applied Sciences Offenburg.

Kapelovich, A., nd. *Joint Range of Motion During Gait*. [Online] Available at: https://www.physio-pedia.com/Joint_Range_of_Motion_During_Gait?form=MG0AV3 [Accessed 10 August 2025].

Karthikeyan, S., Mohan, K. & al., e., 2024. redicting the Mechanical Properties of Friction-Stir-Welded AA7068-T6 Joints Using an Adaptive Neuro-Fuzzy Inference System. *Transactions of the Indian Institute of Metals*, 77, pp.4101-12.

Kiron, M.I., 2024. *Kevlar Fiber: Types, Properties, Manufacturing Process and Applications*. [Online] Available at: https://textilelearner.net/kevlar-fiber-types-properties-manufacturing/ [Accessed 17 August 2023].

Liang, R., Fu, H. & Wang, X., 2025. Structural Design and Analysis of Lower Limb Exoskeleton Rehabilitation Robots. Singapore, 2025. Lecture Notes in Mechanical Engineering. Springer.

Lindsey, J., Seplavy, T. & al., e., 2023. *10 Things You Didn't Know About Carbon Fiber*. [Online] Available at: https://www.bicycling.com/bikes-gear/g20029412/the-10-things-you-didnt-know-about-carbon-fiber/ [Accessed 3 September 2025].

Liu, F., Chen, M., Wang, L.W.X. & Lo, C.-H., 2021. Custom-Fit and Lightweight Optimization Design of Exoskeletons Using Parametric Conformal Lattice. Singapore, 2021. Proceedings of the 2021 DigitalFUTURES. CDRF 2021. Springer.

Lynch, K.M., Park, F.C. & al., e., 2017. *Modern Robotics: Mechanics, Planning, and Control*. Updated first edition ed. Cambridge: Cambridge University Press.

McClements, D., 2025. *Magnesium Alloy: Components, Types, and Uses*. [Online] Available at: https://www.thomasnet.com/articles/metals-metal-products/magnesium-alloy/?msockid=2d241d4850bb643f2a140c3b51f66551 [Accessed 29 July 2025].

Morrissey, J.R., Theodore, N. & et.al., 2005. Fatigue strength of Ti–6Al–4V at very long lives. *International Journal of Fatigue*, 27, pp.1608-12.

Munro, O., 2023. *The 16 Best Manufacturing Processes & Methods*. [Online] Available at: https://www.unleashedsoftware.com/blog/manufacturing-processes/ [Accessed 8 September 2023].

Najam, H., Bal, B. & Unal, R., 2018. MATERIAL SELECTION FOR KNEE EXOSKELETON FRAME. In *The Internatinonal Conference on Materials Science, Mechanical and Automotive Engineerings and Technology*. Kayseri, 2018.

Nasr, A., Inkon, K. & McPhee, J., 2024. Safety in Wearable Robotic Exoskeletons: Design, Control, and Testing Guidelines. *Journal of Mechanics and Robotics*, 17(5), p.12.

Nelson, J., 2024. *Exoskeleton Technology Shines at Paris Olympics*. [Online] Available at: https://decrypt.co/241745/robotic-exoskeleton-olympics-paraplegic-wandercraft [Accessed 20 October 2024].

Ning, M. et al., 2016. Theory analysis and structure optimization design of powered gait orthosis. *Advances in Mechanical Engineering*, 8(3).

Okorie, O., Perveen, A., Talamona, D. & Kostas, K., 2023. Topology Optimization of an Aerospace Bracket: Numerical and Experimental Investigation. *MDPI*, 13(24).

Olliges, 2018. *The Good, Better and Best Ways to Drill Carbon Fiber*. [Online] Available at: https://www.elevatedmaterials.com/drilling-carbon-fiber/ [Accessed 9 May 2024].

Oomi, E., 2024. *What is Carbon Fiber? The Advantages and Disadvantages of Carbon Fiber*. [Online] Available at: https://www.apzomedia.com/what-is-carbon-fiber-the-advantages-and-disadvantages-of-carbon-fiber/ [Accessed 16 November 2024].

Orme, M.E., Michael, G., Michael, F. & Ivan J., M., 2017. Additive Manufacturing of Lightweight, Optimized, Metallic. *JOURNAL OF SPACECRAFTAND ROCKETS*, 54(5), pp.1050-61.

Pinto-Fernandez, D., Torricelli, D. & Sanchez-Villamanan, M.d.C., 2020. Performance Evaluation of Lower Limb. *IEEE TRANSACTIONS ON NEURAL SYSTEMS AND REHABILITATION ENGINEERING*, 28(7), pp.1573-38.

Poggensee, K.L., Collins, S.H. & al., e., 2024. Lower limb biomechanics of fully trained exoskeleton users reveal complex mechanisms behind the reductions in energy cost with human-in-the-loop optimization. *Frontiers in Robotics and AI*, 11.

Rasheed, M., 2022. *Manufacturing processes for selection in mechanical design*. [Online] Available at: https://www.school-mechademic.com/blog/manufacturing-processes-for-selection-in-mechanical-design [Accessed 8 March 2025].

Rodriguez-Fernandez, A., Lobo-Prat, J. & Font-LLagunes, J.M., 2021. Systematic review on wearable lower-limb exoskeletons for gait training in neuromuscular impairments. *Journal of NeuroEngineering and Rehabilitation*, (18), p.22.

Rupal, B.S., Rafique, S. & Singla, A., 2017. Lower-limb exoskeletons: Research trends and regulatory guidelines in medical and non-medical applications. *International Journal of Advanced Robotic systems*, (November - December).

Saboori, A. et al., 2017. An Overview of Additive Manufacturing of Titanium Components by Directed Energy Deposition: Microstructure and Mechanical Properties. *MDPI*, 7(9), p.883.

Sanchez-Villamañan, M.d.C. et al., 2019. Compliant lower limb exoskeletons: a comprehensive review on mechanical design principles. *Journal of NeuroEngineering and Rehabilitation*, 16(55).

S, P., FG, E. & T, A., 1983. Anatomical data for analyzing human motion. *Research Quarterly for Exercise and Sport* , pp.169-78.

Shippee, E., 2017. *What is ultra-high molecular-weight polyethelene (UHMWPE)?* [Online] Available at: https://www.servicethread.com/blog/is-ultra-high-molecular-weight-polyethylene-uhmwpe-right-for-your-product [Accessed 17 October 2023].

Shi, D., Zhang, W., Zhang, W. & Ding, , 2019. A Review on Lower Limb Rehabilitation Exoskeleton Robots. *Chinese Journal of Mechanical*, 32(74).

Shi, D., Zhang, W., Zhang, W. & Ding, X., 2019. A Review on Lower Limb Rehabilitation Exoskeleton Robots. *Chinese Journal of Mechanical* , 32(74), pp.1-11.

Sicetsha, A., 2018. *Ekso Suit: The Capetonian quadriplegic has the chance to walk again*. [Online] Available at: https://www.thesouthafrican.com/video/ekso-suit-capetonian-quadriplegic-chance-walk-again/ [Accessed 14 July 2025].

Sineri, G., Ferdinando, A. & Scalet, G., 2015. *Finite Element Formulations for Isotropic and Anisotropic Materials: a comparison between different approaches*. Pavia: UNIVERSITA DEGLI STUDI DI PAVIA FACOLTA DI INGEGNERIA.

Tang, X., Wang, X., Ji, X. & Zhou, Y., 2022. A Wearable Lower Limb Exoskeleton: Reducing the Energy Cost of Human Movement. *Micromachines*, 6(13).

Thesleff, A..A.B..A.J.e.a., 2021. Design of a stepwise safety protocol for lower limb prosthetic risk management in a clinical investigations. In *Proceedings of the Annual International Conference of the IEEE Engineering in Medicine and Biology Society*. Virtual Conference, 2021. IEEE.

Thorat, S., nd. *What is Casting process | Advantages , Disadvantages and Application*. [Online] Available at: https://learnmech.com/what-is-casting-process-advantages-disadvantages-and-application/?form=MG0AV3 [Accessed 16 August 2024].

Tian, Y.-T., Chen, C.-J., Wu, X.-J. & al., e., 2025. A Rigid-Flexible Coupled Lower Limb Exoskeleton for Enhancing Load-Bearing Ambulation. *Biomimetics*, 10(11), p.767.

Van Herpen, F.H.M. et al., 2019. *Case Report: Description of two fractures during the use of a*. Case Report. The International Spinal Cord Society.

Vaughan, C.L., Davis, B.L. & O'Connor, J.C., 1992. *Dynamics of Human Gait*. Cape Town: Kiboho Publishers.

Vaverka, F., Elfmark, M., Svoboda, Z. & Janura, M., 2015. System of gait analysis based on ground reaction force assessment. *Acta Gymnica*, pp.187-93.

Wang, S., 2015. Design and Control of the MINDWALKER Exoskeleton. *IEEE Transactions*, Available at: https://www.semanticscholar.org/paper/Design-and-Control-of-the-MINDWALKER-Exoskeleton-Wang-Wang/b6e3ab7d4b11f141418183e3bd14f93125d87d31 [Accessed 6 May 2025].

Wong, P., 2025. *How to Effectively Machine Titanium Grade 5 (Ti-6Al-4V)*. [Online] Available at: https://www.ptsmake.com/how-to-effectively-machine-titanium-grade-5-ti-6al-4v/ [Accessed 29 September 2025].

Woodford, C., 2023. *Kevlar®*. [Online] Available at: https://www.explainthatstuff.com/kevlar.html [Accessed 10 October 2023].

Yadav, A., 2019. Review of Optimization Aspects for Weight Reduction. *International Research Journal of Engineering and Technology*, pp.1596-601.

Yadav, M., Asim, T., Vishwas, D. & Nitesh, P.Y., 2025. Exploring the Impact of Drilling Parameters on Damage. *Journal of Materials Engineering and Performance*, 34(9), pp.7371-85.

Yang, X. et al., 2024. Design and Optimization Analysis of an Adaptive Knee Exoskeleton. *Chinese Journal of Mechanical Engineering*, 37.

Youssefa, K.M. et al., 2014. A Novel Low-Density, High-Hardness, High-entropy Alloy with Close-packed. *Materials Research Letters*, 3(2), pp.95-99.

Zhang, D., 2024. *Understanding the Strength and Modulus of Carbon Fiber in Bicycle Frames: A Tideacebike Perspective*. [Online] Available at: https://tideacebike.com/blogs/news/understanding-the-strength-and-modulus-of-carbon-fiber-in-bicycle-frames-a-tideacebike-perspective [Accessed 9 November 2023].

Zouh, T., Li, T., Zouh, H. & al., e., 2025. Review of Lower-Limb (Quasi-)Passive Exoskeletons for Human Augmentation. *IEEE*, 13.

Appendix A: FEA Model Set Up

Property: Material property set up. Setting density and elastic properties (Young's Modulus and Poisson's ratio)

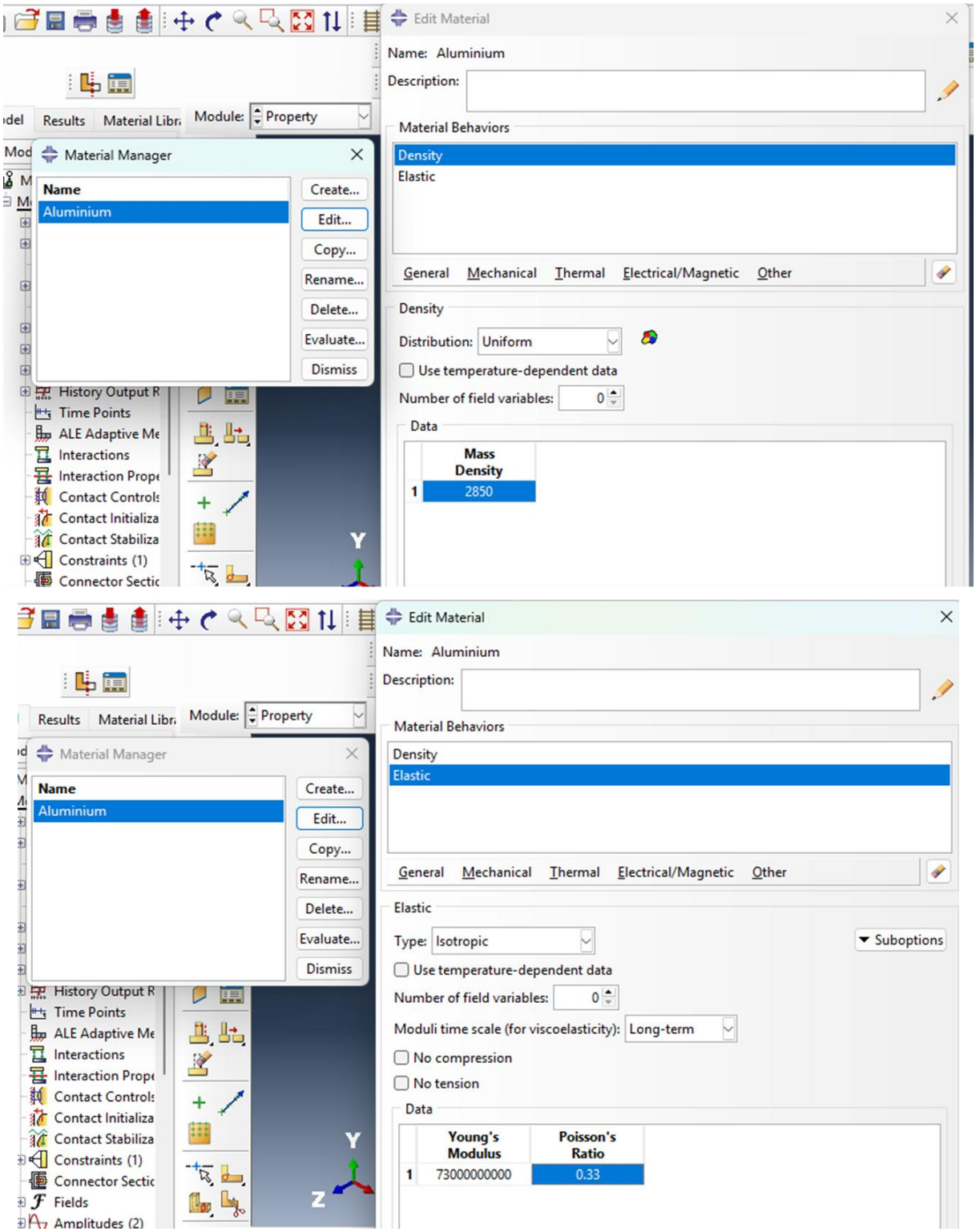

Figure 47: Abaqus material property set up

Solid homogeneous material section for the whole model.

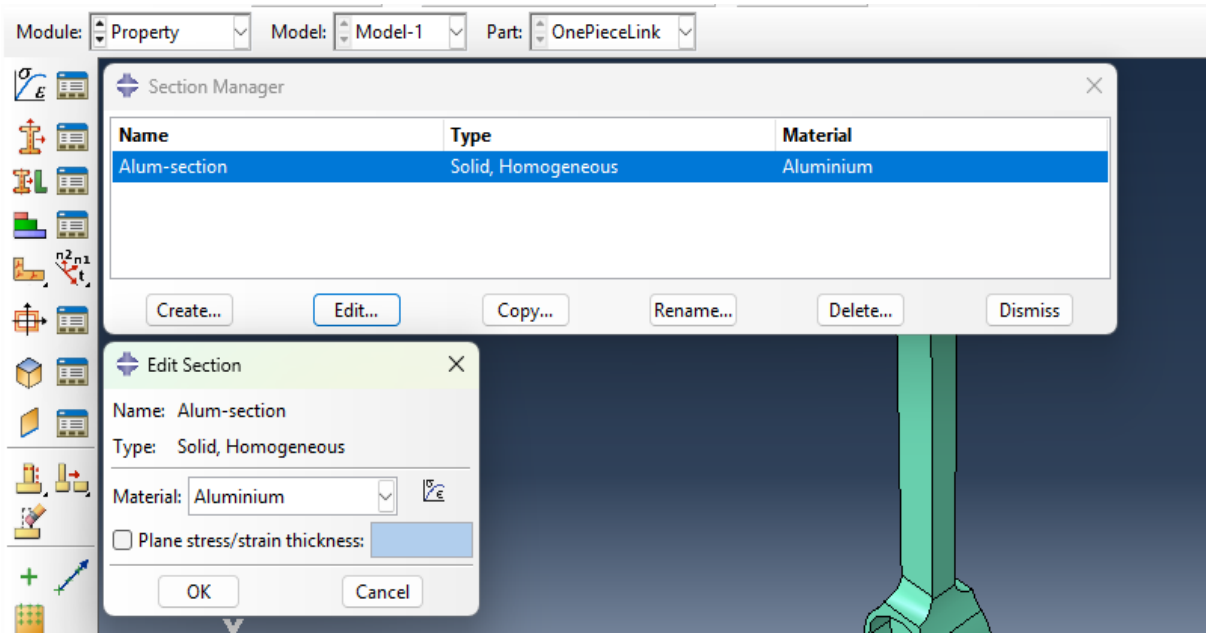

Figure 48: Abaqus material section set up

Interaction: Create a rigid body constraint to the reference point of the joint hole

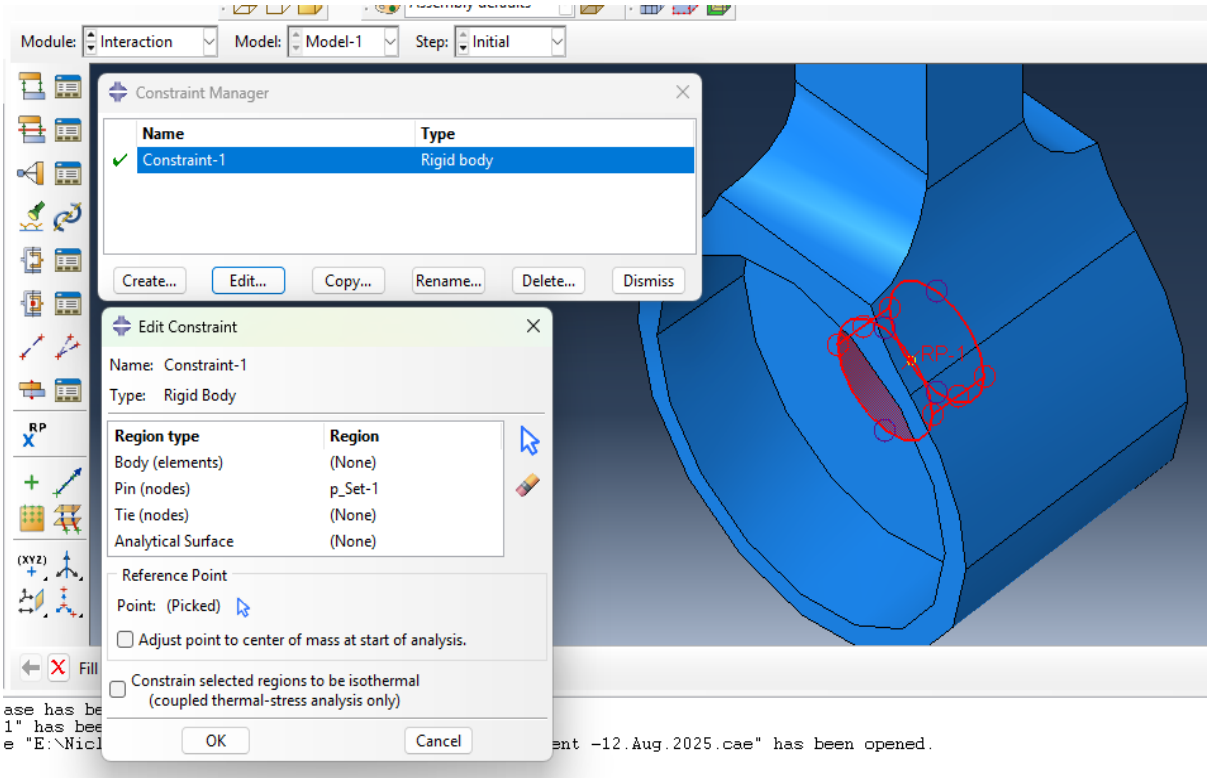

Figure 49: Abaqus interaction

Boundary Conditions: Create displacement/rotation at load application joint hole. For the opposite fixed end, create an encastre boundary condition.

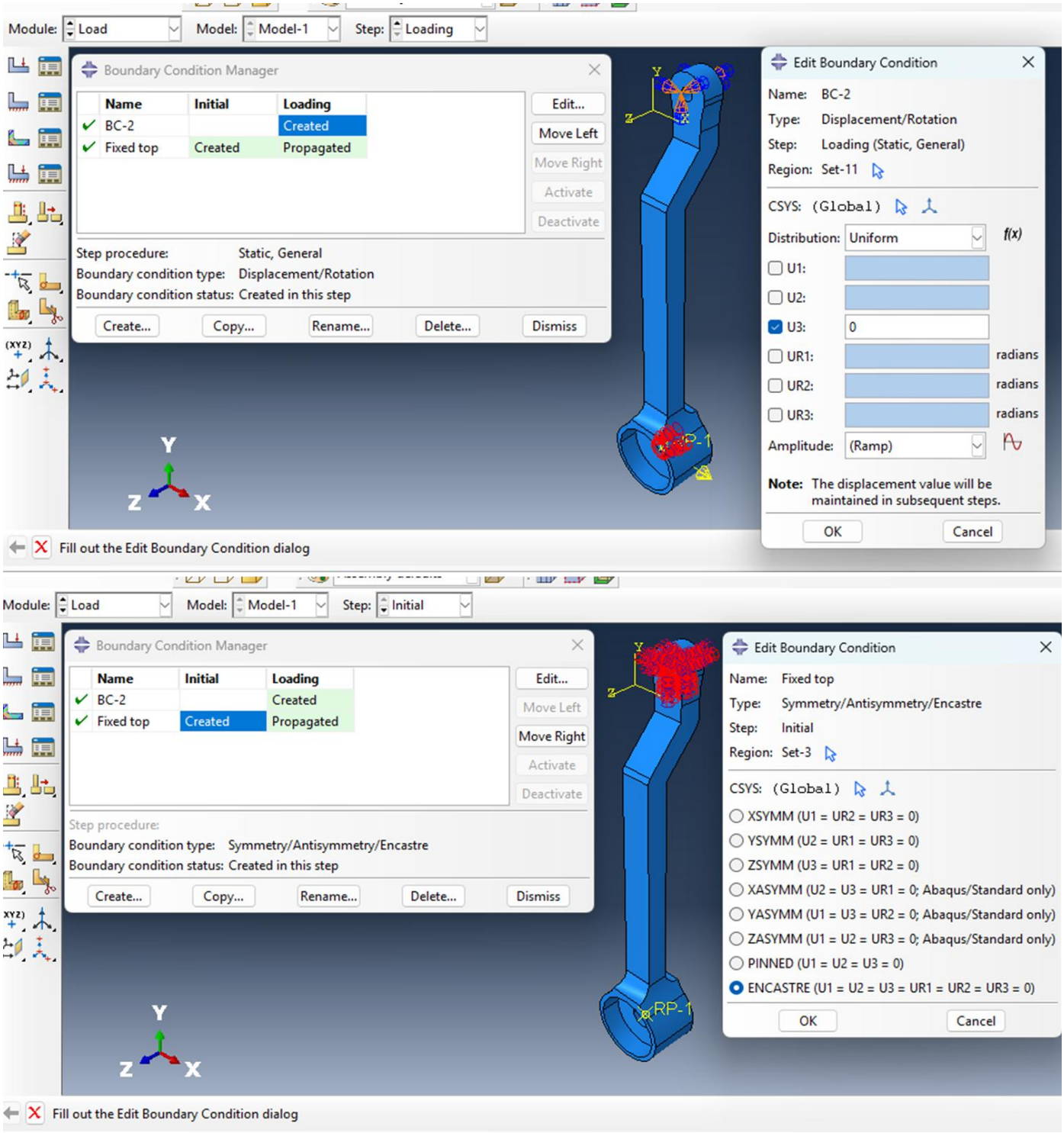

Figure 50: Abaqus boundary conditions

Loads: Amplitude for ground reaction loads applied in the y axis. Amplitude for swing loads applied along the x-axis.

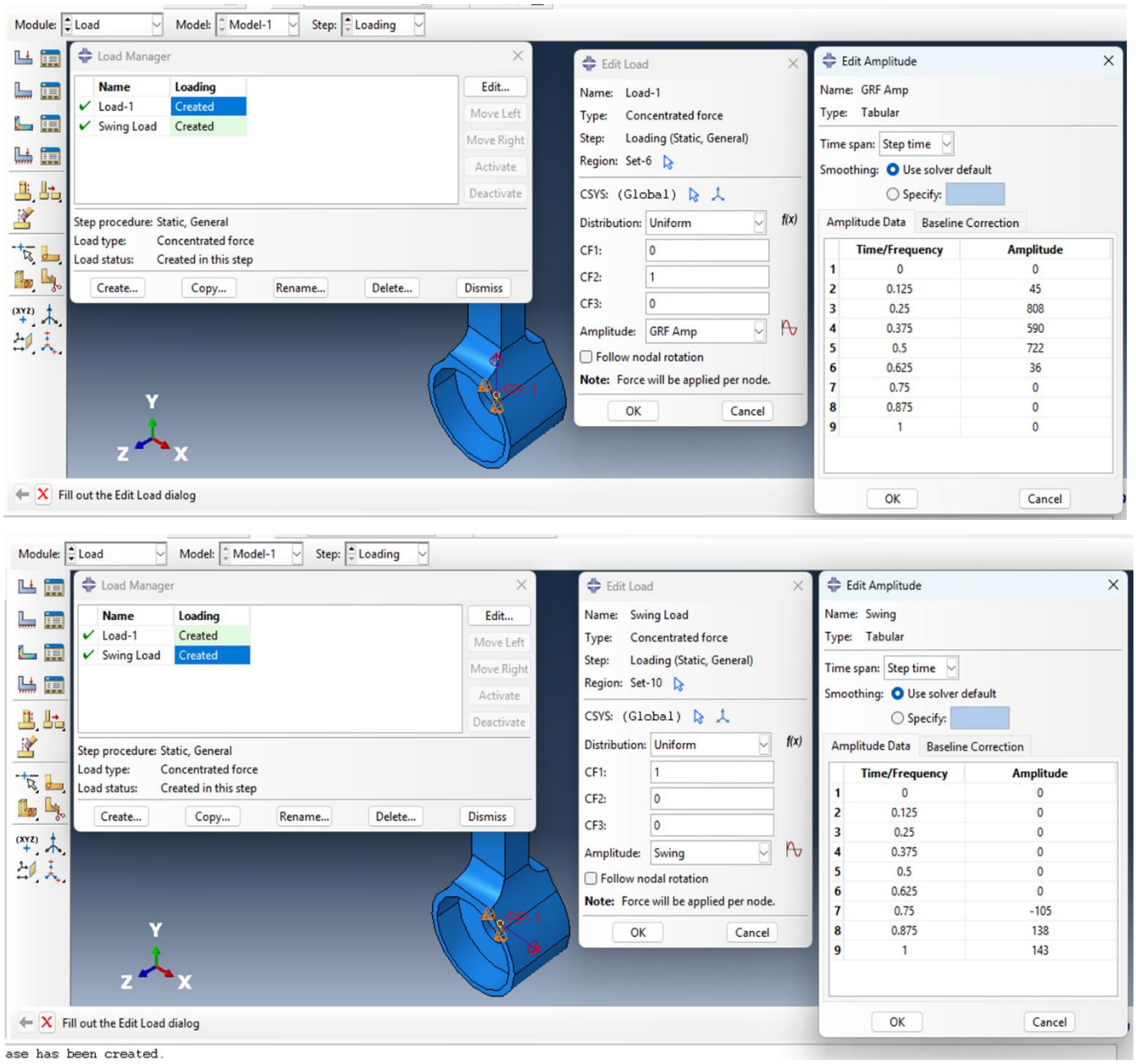

Figure 51: Abaqus loads

Meshing: Global seeding of 0.005 size with curvature control.

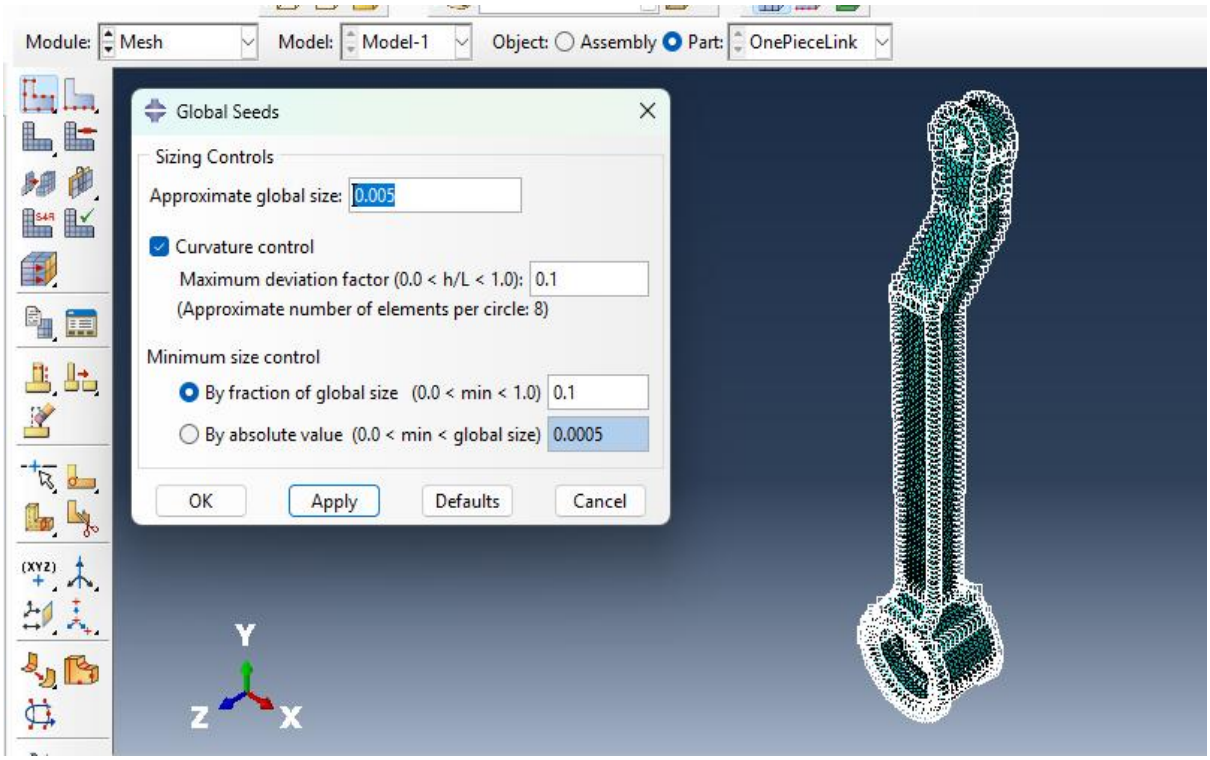

Figure 52: Abaqus seeding

Meshing: Mesh controls set to *Tet* element shape using default algorithm.

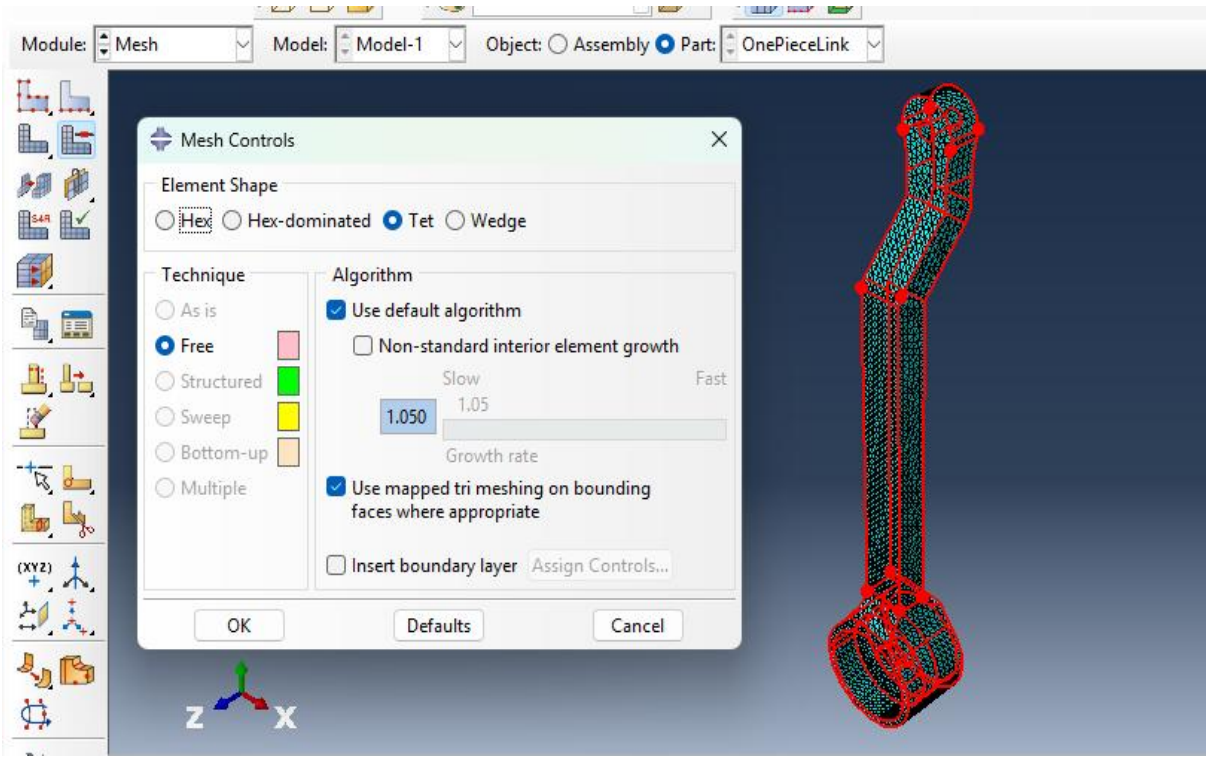

Figure 53: Abaqus mesh controls

Meshing: Standard element library, quadratic geometric order.

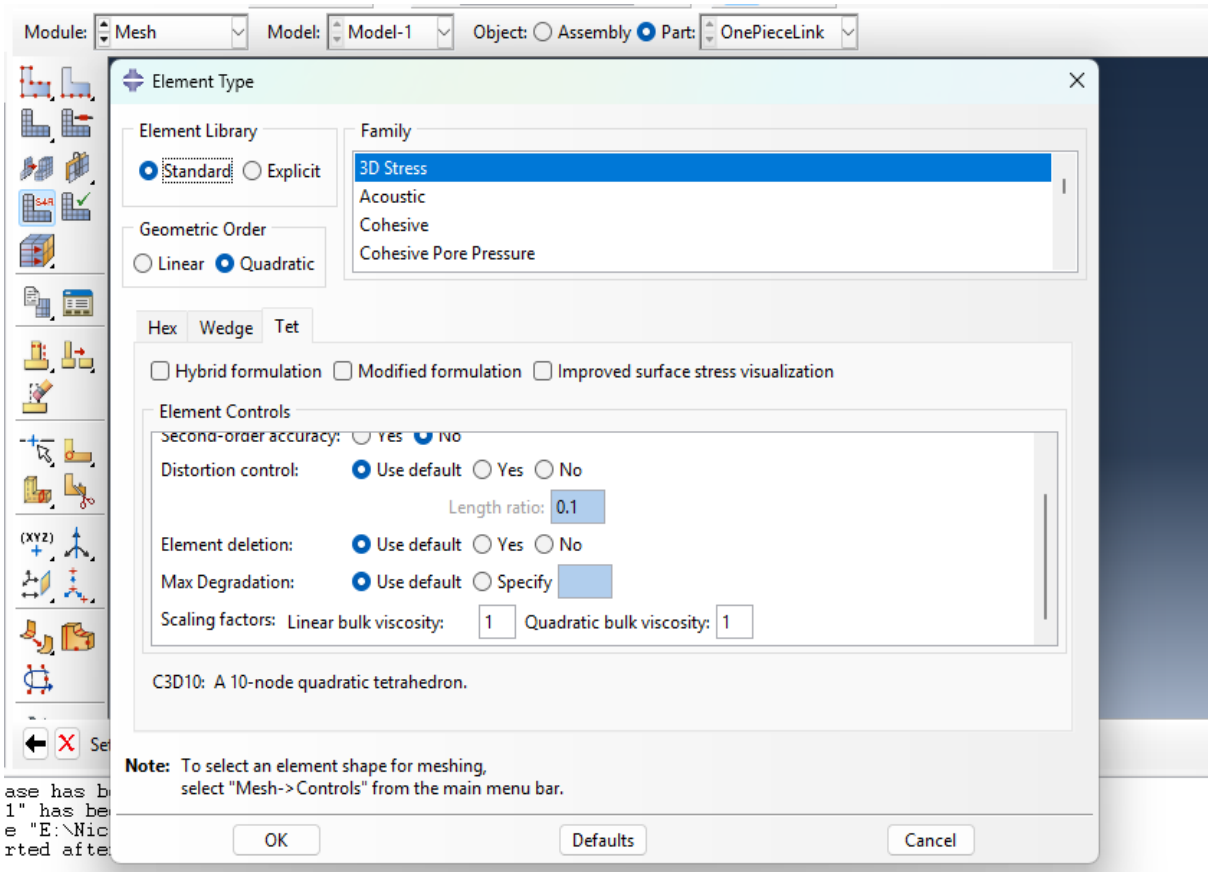

Figure 54: Abaqus element type

Meshing: Thigh link mesh.

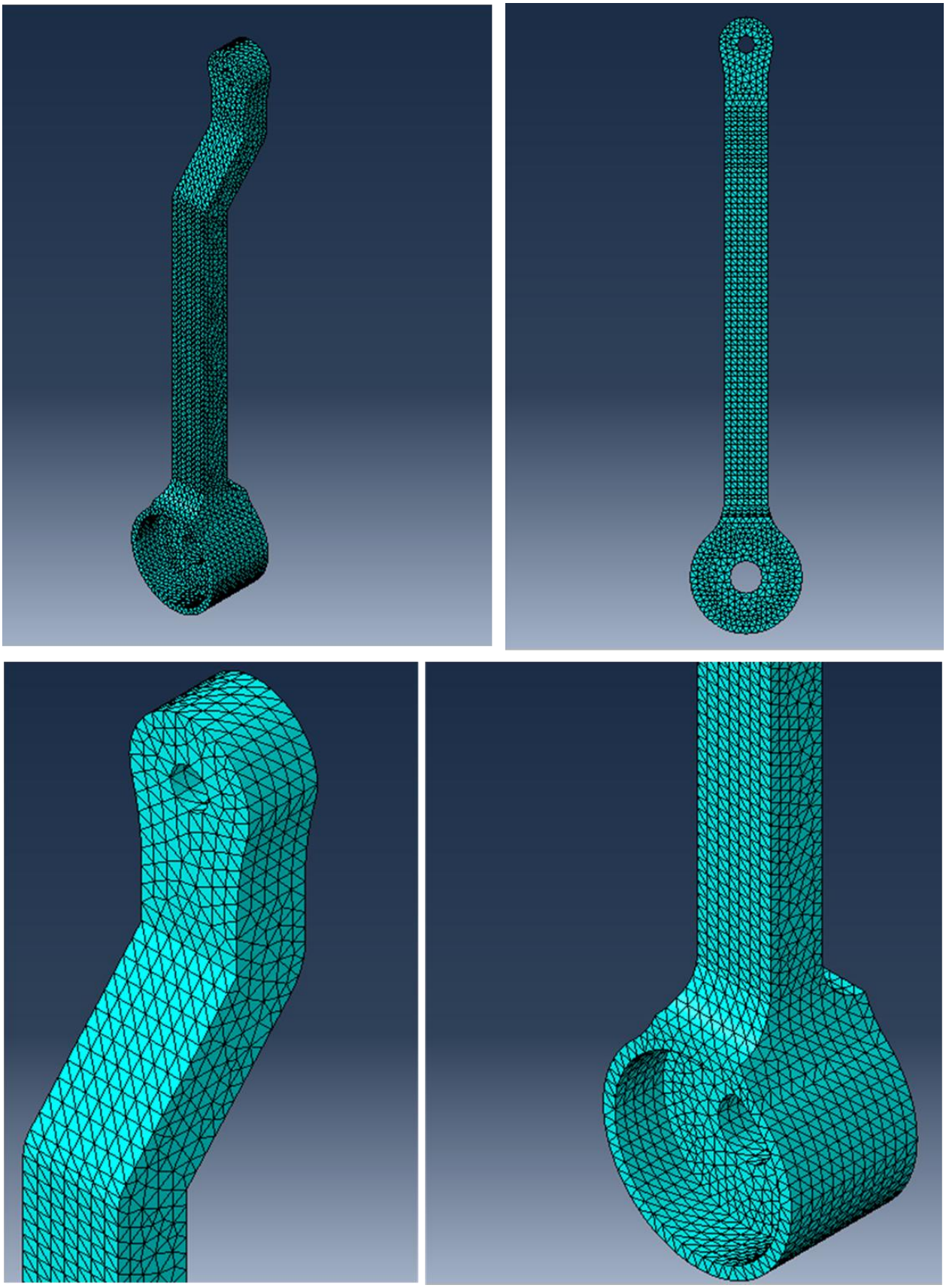

Figure 55: Thigh link meshing

Meshing: Waist bracket meshing

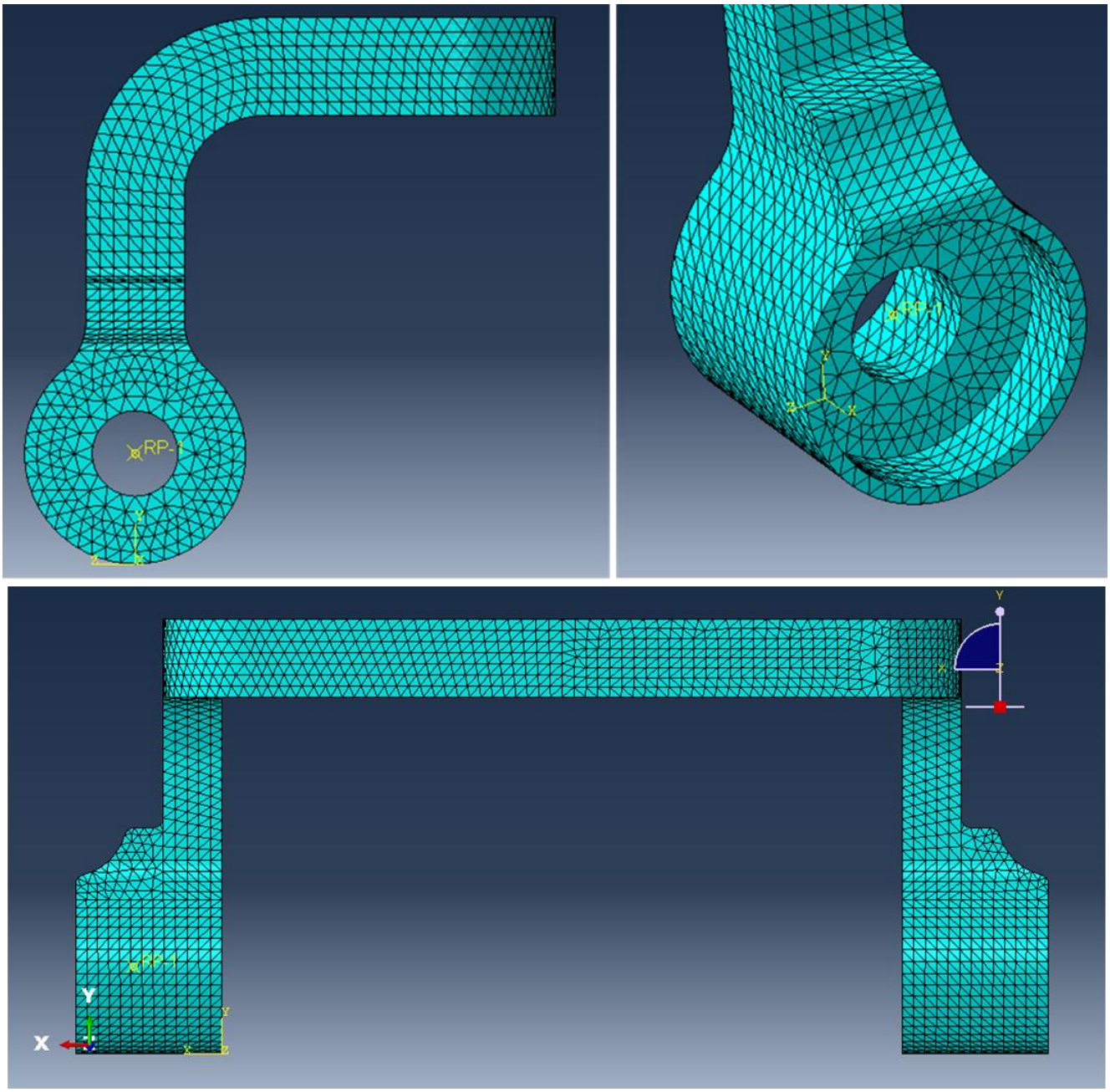

Figure 56: Waist bracket mesh

Meshing: Shank link meshing

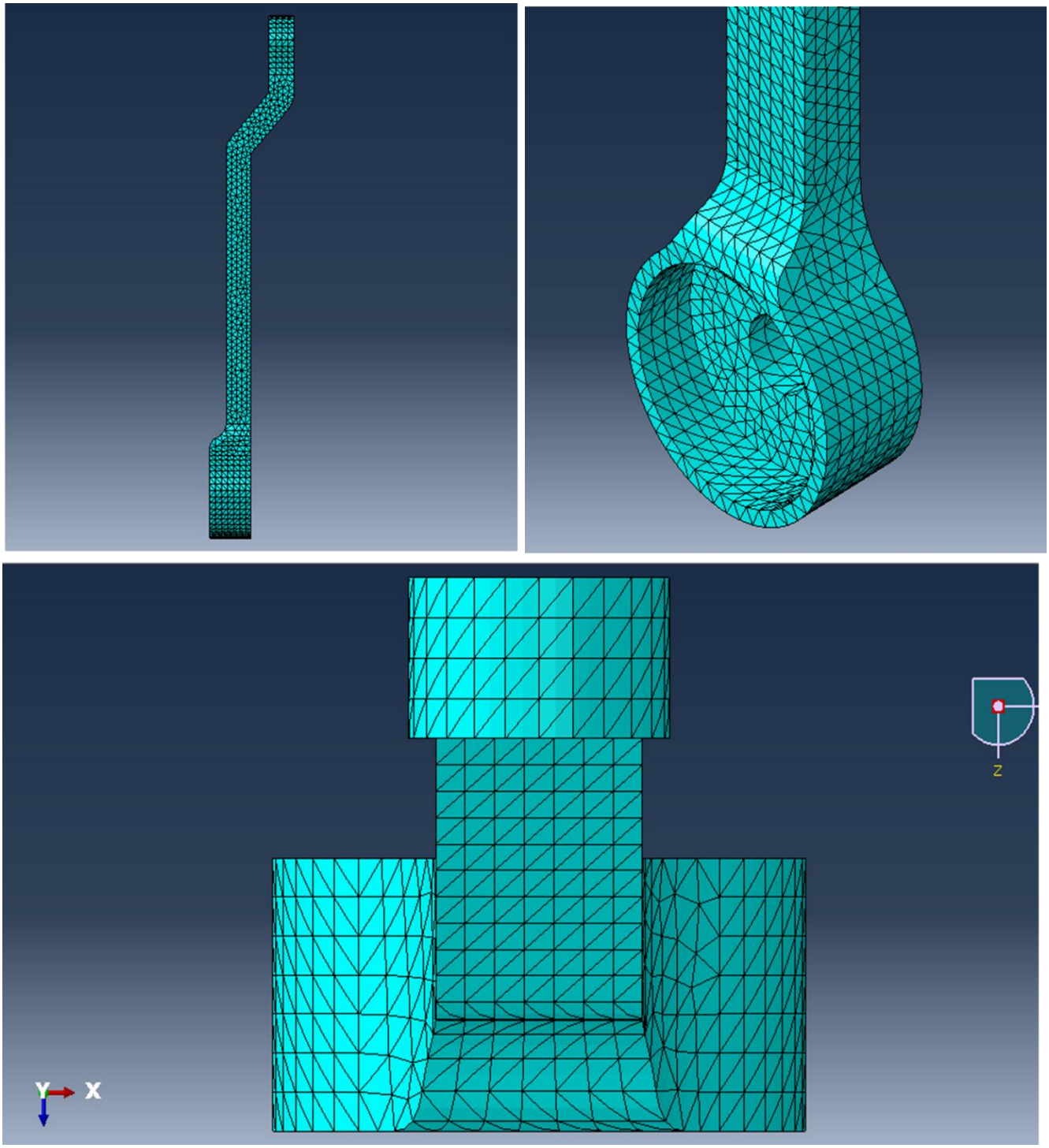

Figure 57: Shank link meshing

Appendix B: Topology optimisation model set up

Optimisation task: Select the whole model, feed load regions and boundary condition region.

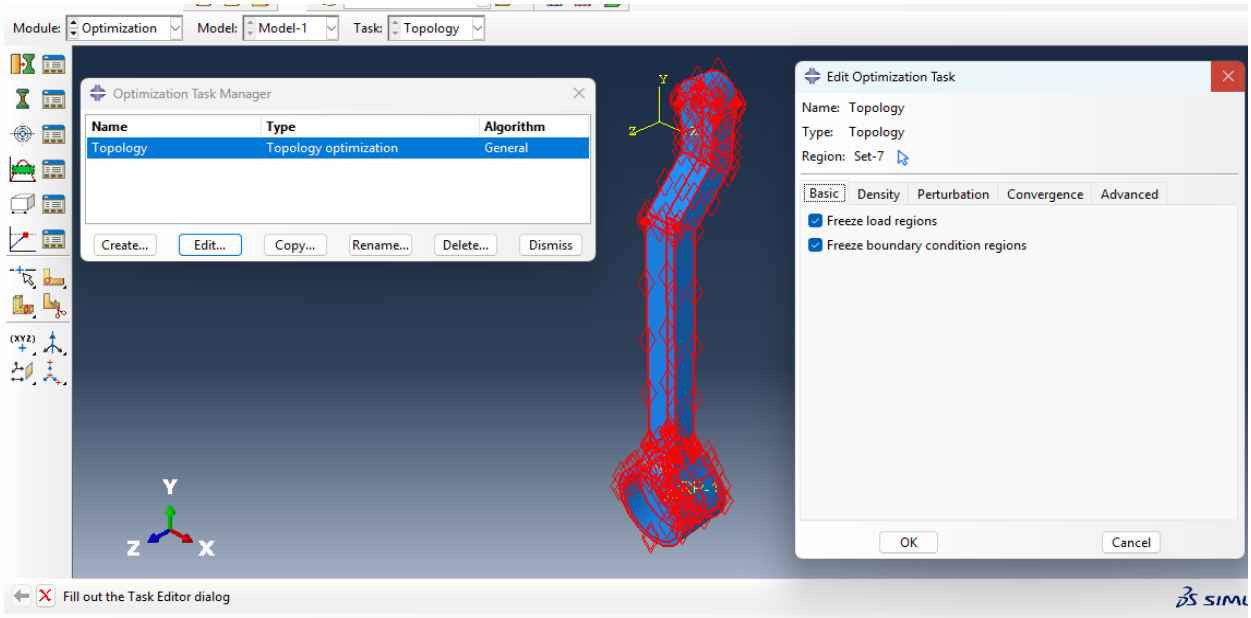

Figure 58: Optimisation task

Design response: Create one volume and one strain energy design response. Select the whole model for both.

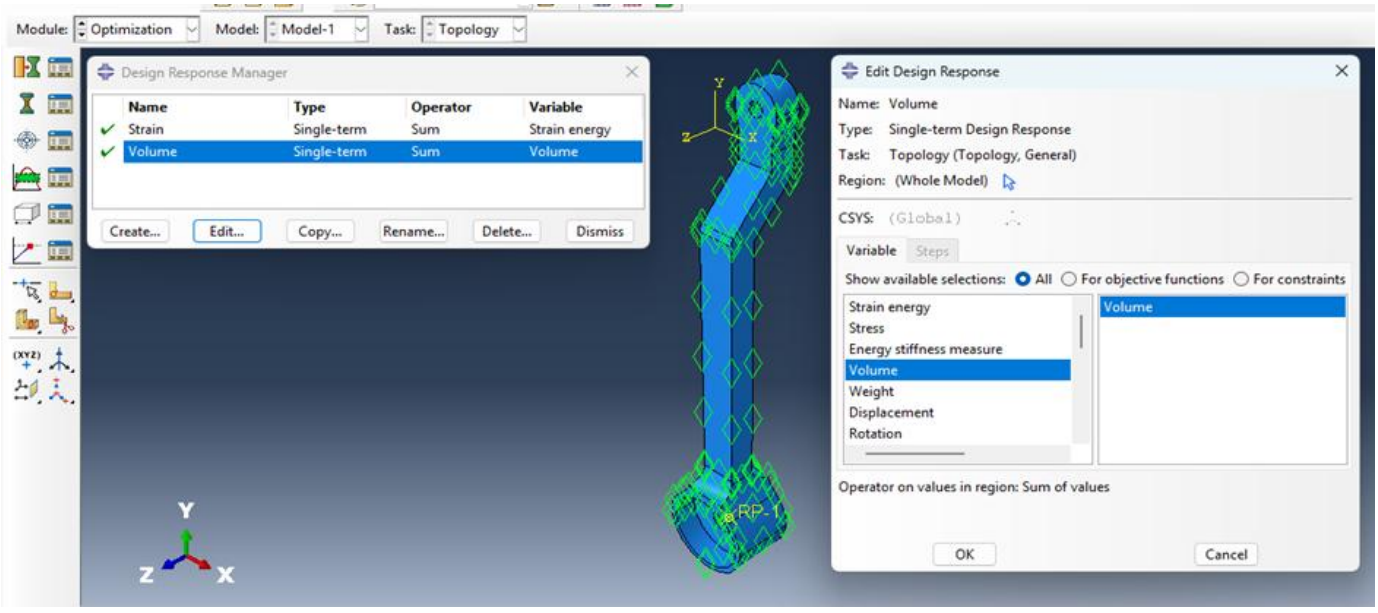

Figure 59: Abaqus design response

Objective function: Create an objective function selecting both response model. Set target to minimise design response values.

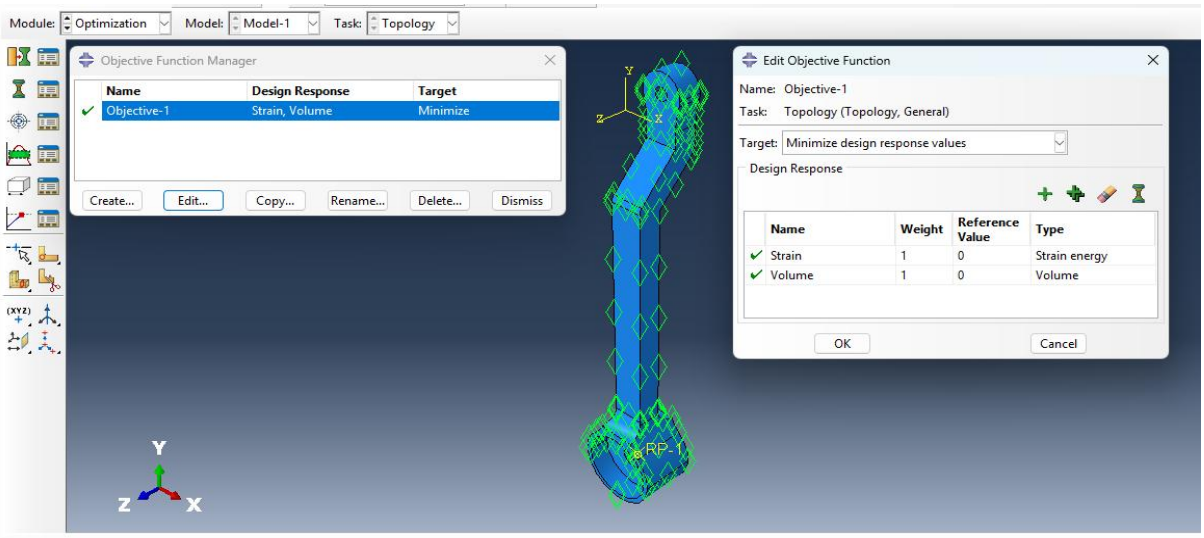

Figure 60: Abaqus objective function

Optimisation constraints: Select the volume design response and set the constraint response to less than or equal to the targeted percentage volume reduction.

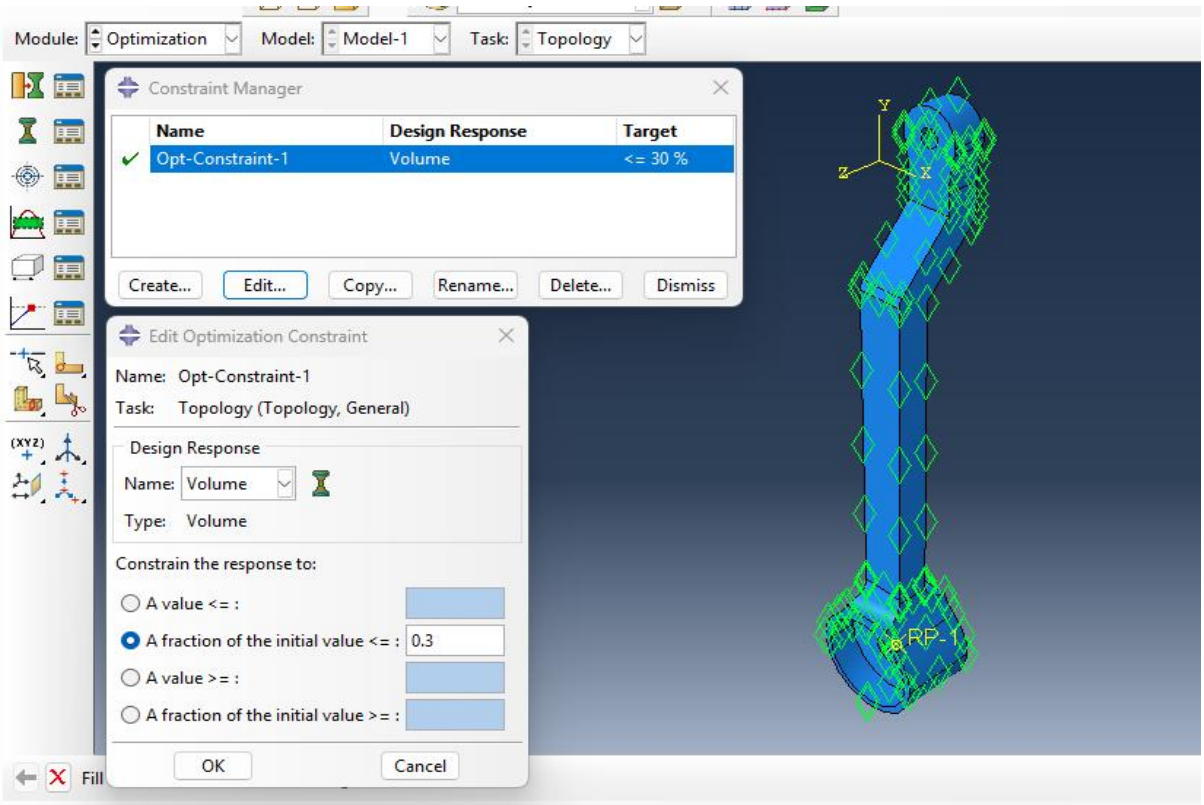

Figure 61: Abaqus constraint

Appendix C: Current LLE Structure

3D CAD of the original LLE structure

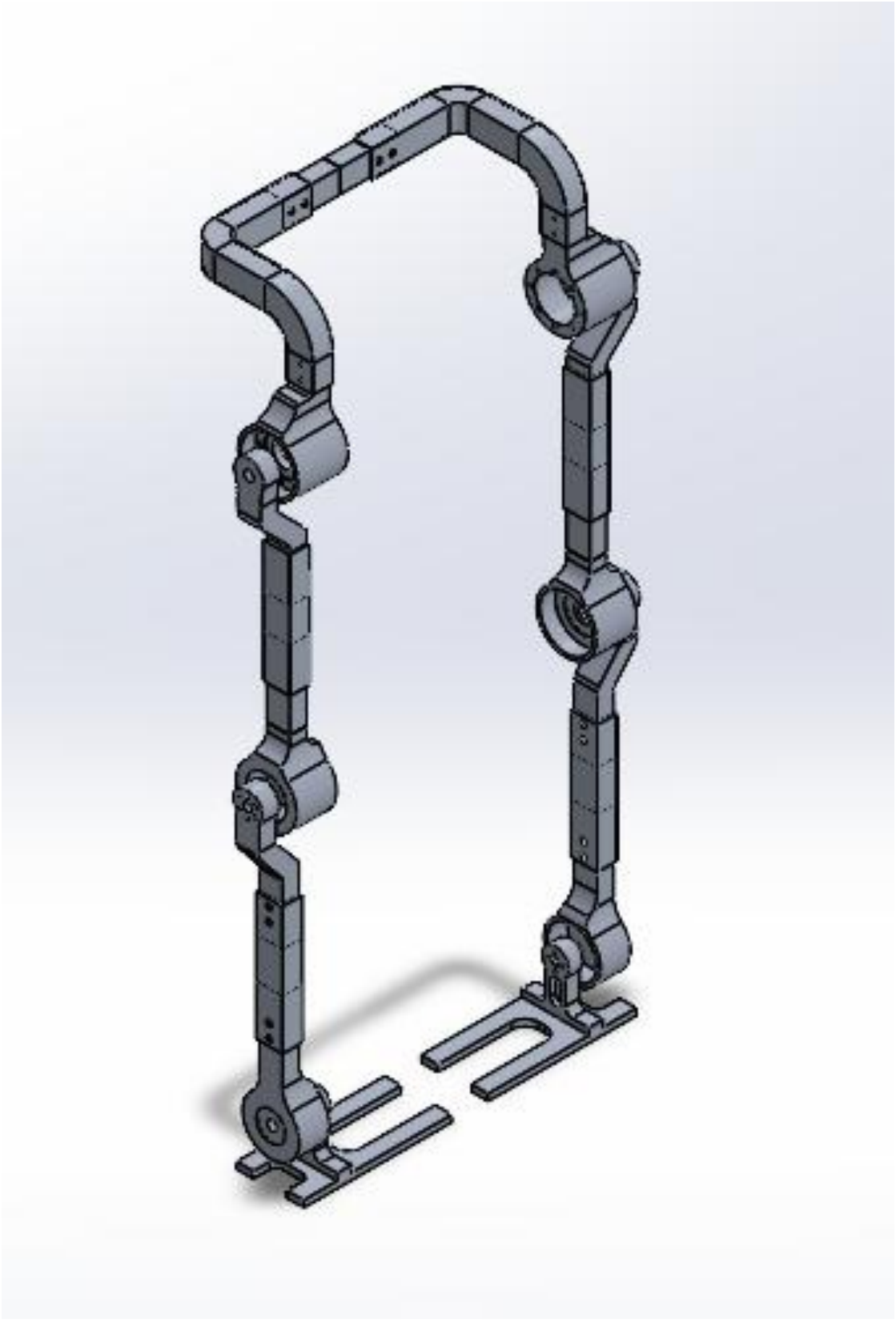

Figure 62: Current LLE 3D CAD drawing

3D CAD of the original LLE structure

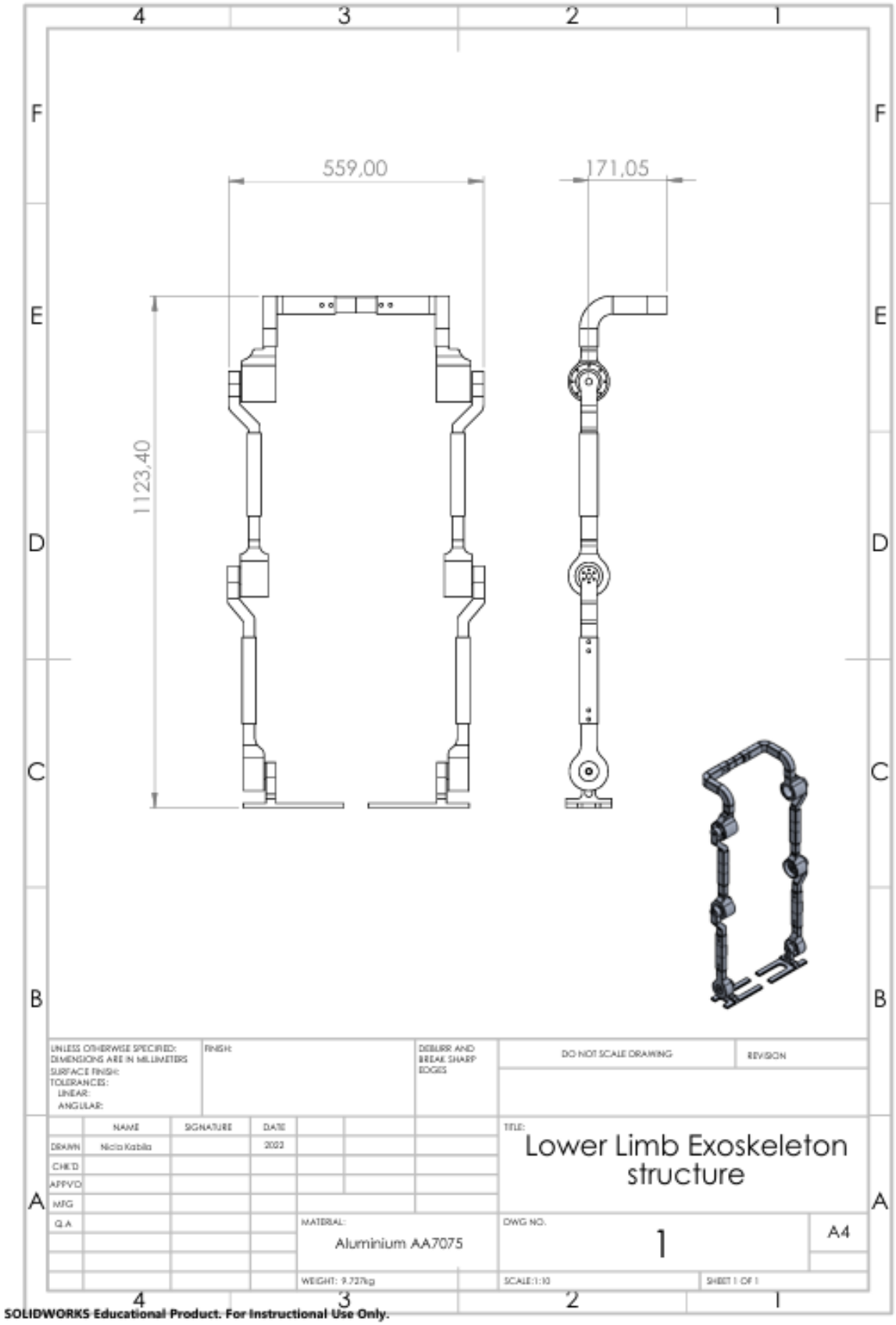

Figure 63: 2D drawing of the original LLE structure

Appendix D: Optimised and Refined Links

3D drawing of optimised and refined thigh Link

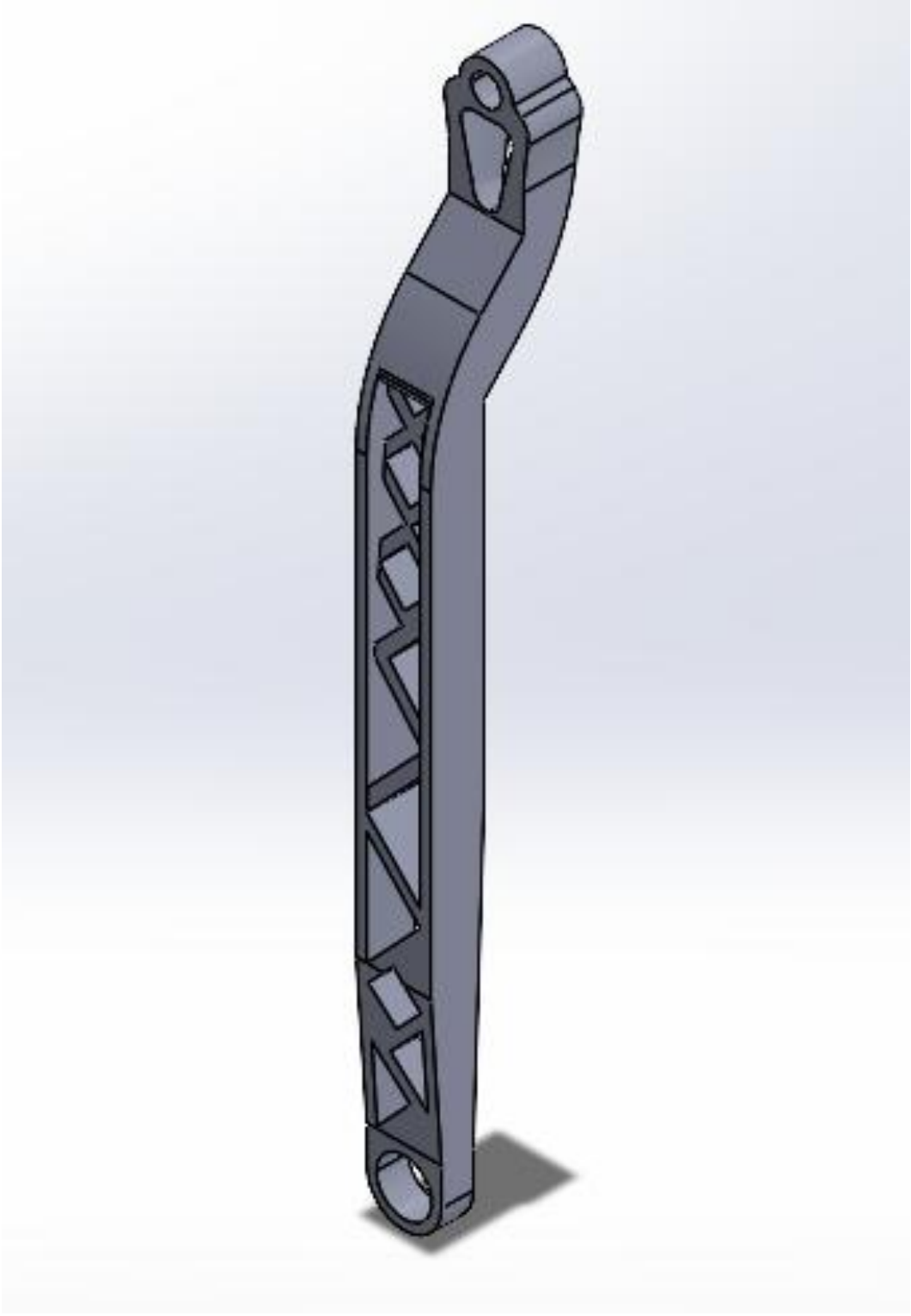

Figure 64: 3D CAD drawing of optimised and refined thigh link

2D drawing of optimised and refined thigh Link

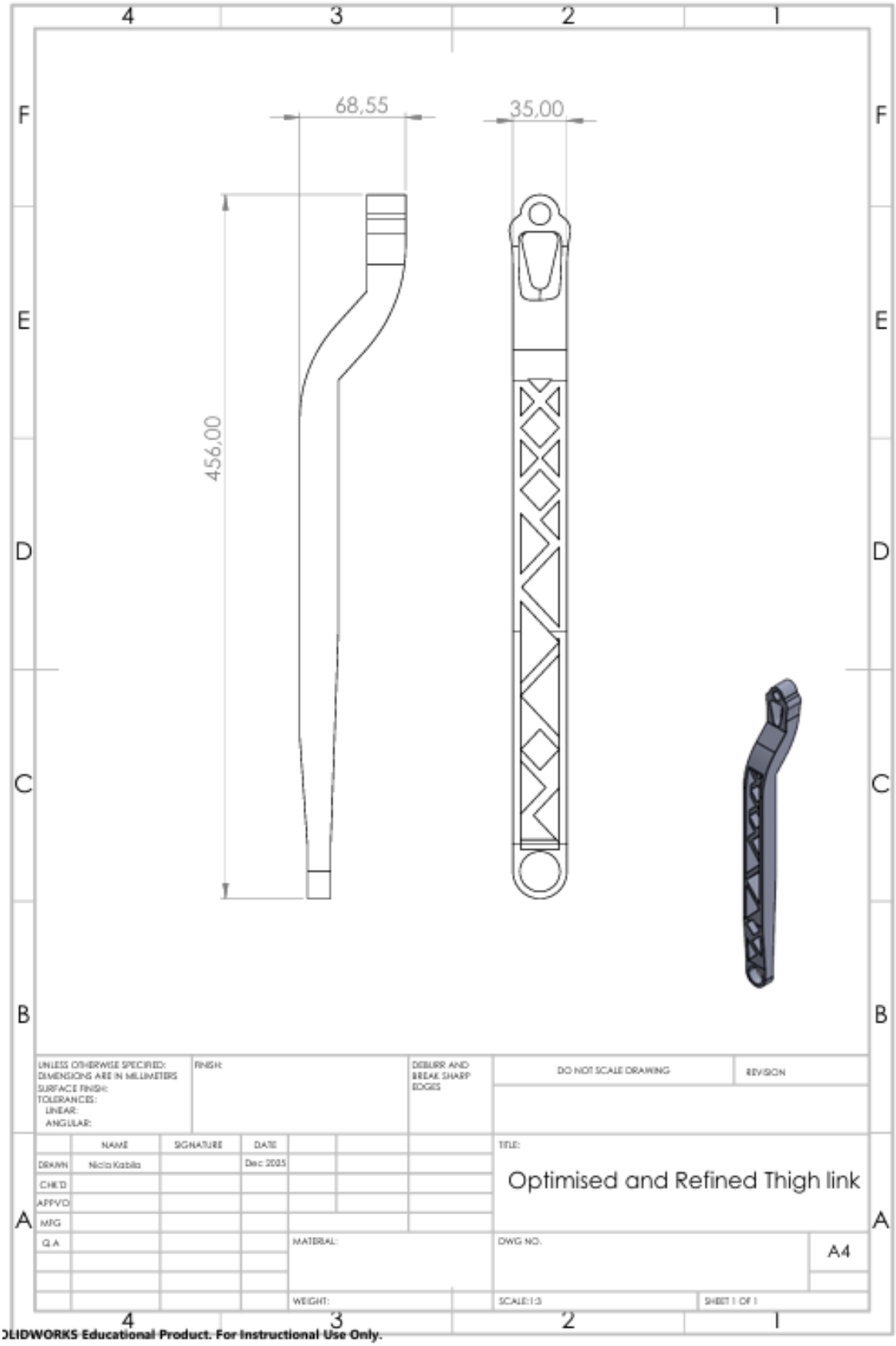

Figure 65: 3D CAD drawing of optimised and refined thigh link

3D drawing of Optimised and refined Shank Link

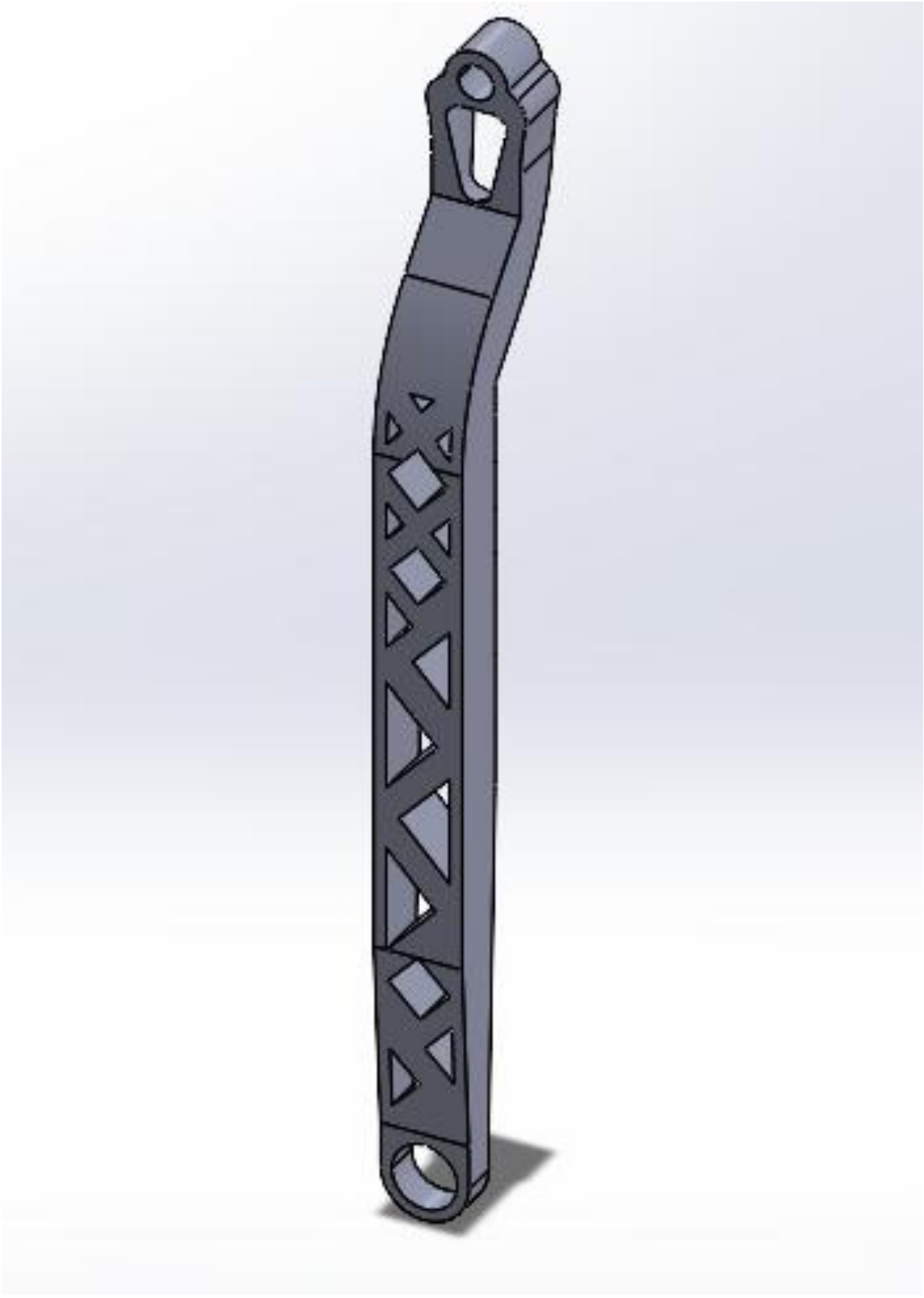

Figure 66: 3D drawing of optimised and refined shank link

3D drawing of Optimised and refined Shank Link

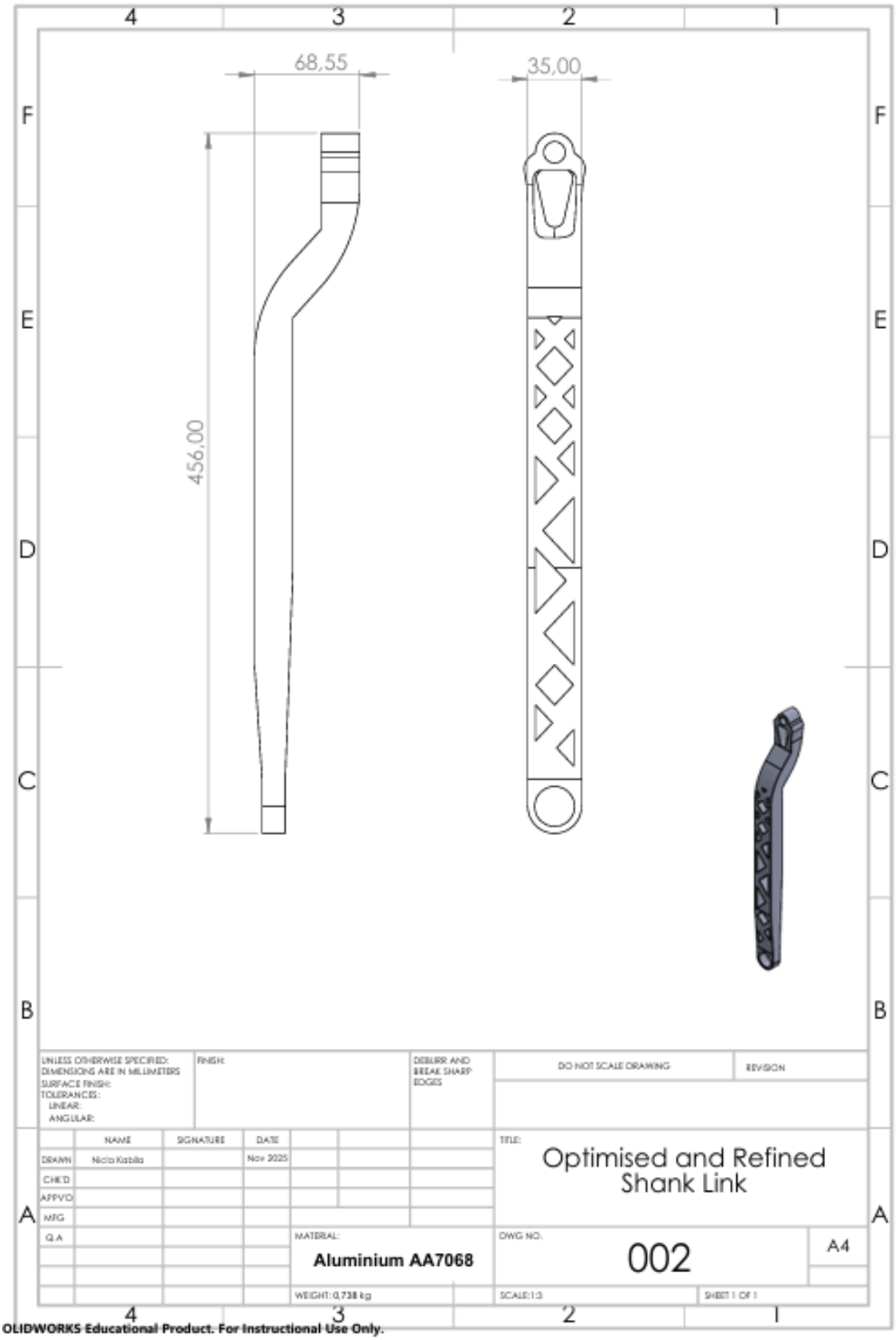

Figure 67: 2D drawing of optimised and refined shank link